UNIVERSITY OF BIRMINGHAM

Mechanochemical Finishing – Developing a mechanical finishing process to form tribologically superior surfaces

by

James Jonathan Firth

A thesis submitted to the University of Birmingham

for the degree of DOCTOR OF PHILOSOPHY

Department of Mechanical Engineering

University of Birmingham

December 2021

Abstract

Both mechanical and chemical finishing process are regularly used to reduce frictional losses and improve the wear resistance of components within mechanical systems like internal combustion engine cylinders and fluid pumps. Coatings often require highly specialised equipment and are usually expensive in comparison to mechanical processes. In many applications, both mechanical finishing and chemical coatings are applied to component surfaces in order to achieve a surface with all the desired properties. This thesis applies tribofilm forming research when using particular nano-additives to mechanical finishing processes in order to mechanochemically generate a tribologically superior surface through a simple, single stage operation.

Cast iron plates were honed against grit paper with dry Cu_2S microparticles causing a reduction reaction in the particles for sulphur to then react with the iron in the plates. Energy Dispersive Spectroscopy (EDS) revealed a huge increase in the quantity of copper in the cast iron caused by the mechanochemical honing. X-ray Photoelectron Spectroscopy (XPS) did suggest a small quantity of iron sulphides had formed. While the honing process did successfully reduce the copper sulphide, a lot of the sulphur was lost in the process while the copper sintered into the surface. Lubricated friction tests at a variety loads showed a small reduction in friction with the copper honed samples.

In order to better understand mechanisms for tribofilm formation and discover any synergistic behaviours between nano-MoS_2 and ceramic nanospheres, SiO_2 was tested with MoS_2 as lubricant additives in a variety of High Frequency Reciprocating Rig (HFRR) tests. At high load and 50 °C the two nanoparticles on there own could not improve friction or wear but when used together, the SiO_2 improved the conditions for MoS_2 to chemically react with the steel contacts forming a protective tribofilm. This was characterised through a combination of EDS and Hard X-Ray Photoelectron Spectroscopy (HAXPES). Attempts to recreate these results in the TE 77 High Frequency Friction Machine (TE 77) low load adapter were unsuccessful.

Keeping lubricant additives successfully dispersed is a well documented issue. To get

round this, Cu_2S and Al_2O_3 microparticles were mixed with a base grease whose viscosity was great enough that once dispersed the particles could not settle. The formulated greases were put under very high load (920 N) in line contact in the TE 77 to generate a tribofilm style layer that was then tested with point contact wear in a base lubricant. The formulated greases were tested against a commercial grease containing MoS_2. At low loads, only the MoS_2 treated surface produced lower friction than the untreated plate. In 50 °C tests at a higher load, all the treated surfaces slightly reduced friction compared to the untreated plate and the hybrid Cu_2S, Al_2O_3 surface had the lowest friction. MoS_2 produced the shallowest scar with a tribofilm similar to that generated with the hybrid lubricant in the previous chapter.

This thesis introduces a proof of concept for two mechanochemical finishing processes as well as developing understanding for the synergistic behaviour of Transition Metal Dichalcogenides (TMDC) and ceramics as nano-additives in lubricants. The potential scope for this research is huge as the finishing processes could be beneficial to any mechanical system where there are sliding metal contacts. A large amount of work is still needed to bring this work from its concept stage to full realisation in a commercial setting.

To my son, Jonathan

- In the hope that sutainable research leads to a planet you are able to enjoy.

Acknowledgements

I would first like to thank my supervisors, Prof. Karl Dearn and Prof. Thanos Tsolakis for your guidance over the last four and a bit years. Karl, in particular, thank you for all your ideas and advice, both academic and parental.

My thanks go to Dr Iestyn M.N. Stead and Dr David G. Eckold for all the technical support and equipment training you have given me, without you, little of the testing or analysis I have done in this thesis would have been possible. Also, all the other members of the Mechanical Innovation and Tribology Group, thank you for your support and keeping me company during long hours in the lab.

I want to express my appreciation to the Henry Royce Institute for the funding that enabled my access of XPS and HAXPES facilities with Royce@Manchester. In particular, thank you to Dr. Ben Spencer, who trained me how to operate the HAXPES remotely as the pandemic prohibited travel and helped me understand and interpret the results. I'm very happy with what we were able to achieve in such difficult circumstances. Additionally, I would like to thank Dr. Christian Burton, who, when at Aston University, helped me with XPS analysis when I had little understanding of the machine's operation and limitations.

To all my friends that I have played and trained with at University of Birmingham Ultimate, thank you for giving me such an enjoyable outlet outside of the office. You provided many a distraction for me and allowed me to switch off from work for a weekend or 50. I don't think I would have made it this far without you.

Thank you to my family and your unfailing support. To Alison for always being up for a chat even across continents; Joanna, who always knows what big news I have before I tell you; Matthew, who has experienced all this already and offered advice as well as

enjoyable relatability; and my parents, with always a free bed and warm meals for a complete get away and detox, as well as a sanity check when I was sure I was missing something obvious in an idea or calculation.

And finally I'd like to thank Olivia, for always believing I could achieve this, keeping me fed in the last few months and helping me see how many huge life events I could cram into the time it took to do a PhD.

Contents

List of Figures

List of Tables

Acronyms

AES Auger Electron Spectroscopy.

BDC Bottom Dead Centre.

BSE Back Scatter Electrons.

CEMS Conversion Electron Mössbauer Spectroscopy.

COF Coefficient Of Friction.

DI Deionized.

DLC Diamond-Like Coating.

DLS Dynamic Light Scattering.

EDS Energy Dispersive Spectroscopy.

EHL Elastohydrodynamic Lubrication.

HAXPES Hard X-Ray Photoelectron Spectroscopy.

HFRR High Frequency Reciprocating Rig.

HRTEM High-Resolution Transmission Electron Microscopy.

HSD High Speed Data.

IF Inorganic Fullerene-like.

LLA Low Load Adapter.

MoDTC Molybdenum dialkyl dithiocarbamate.

NCB Nano-Calcium Borate.

PAG Polyalkylene Glycol.

PAO Polyalphaolefin.

PIBS Polyisobutyleneamine Succinimide.

rGO reduced Graphene Oxide.

SDBS Sodium Dodecyl Benzene Sulfonate.

SEM Scanning Electron Microscopy.

TDC Top Dead Centre.

TE 77 TE 77 High Frequency Friction Machine.

TEM Transmission Electron Microscopy.

TMDC Transition Metal Dichalcogenides.

Tukey's HSD Tukey's Honestly Significant Difference.

WSD Wear Scar Diameter.

WSW Wear Scar Width.

XPS X-ray Photoelectron Spectroscopy.

XRD X-Ray Diffraction.

ZDDP Zinc dialkyldithiophosphates.

Chapter 1

Introduction

Tribology was a officially coined as a term by H Peter Jost in 1966 (Jost, 1966) and is defined as "the study of interacting surfaces in relative motion and the practices related thereto". It focuses on the interactions of materials, surfaces and lubricants that determine wear and frictional properties (Adams, 2010).

Improving the tribological properties of components in mechanical systems will reduce energy lost through friction, usually in the way of heat, and improve the life of those components. Reducing frictional energy losses will result in the burning of less fuel and components that last longer will result in the requirement for replacement parts being reduced which also saves energy. Jost (1966) estimated that more than £500 M could be saved annually through the adoption of more advanced tribological practices.

Metal mechanical finishing processes encompass a wide range of operations, usually designed to reduce surface roughness or to achieve a certain texture to get desired friction behaviour. Some operations can also increase the fatigue life of components. Roughness reducing processes typically involve fine abrasives or abrasive surfaces interacting with the component to remove very small quantities of material resulting in a reduced height and depth of asperities. These processes include polishing, honing/grinding and abrasive blasting. Burnishing uses pressure that exceeds the yield strength of the component material to plastically deform asperities into the surface and reduce roughness (Zhmud et al., 2014). Shot-peening introduces beneficial residual compression stresses that improve the fatigue strength of the material (Webster and Ezeilo, 2001). This is achieved by a high velocity bombardment of small metal balls at the surface. With the possible exceptions of shot-peening and abrasive blasting, mechanical finishing processes are generally cost effective, using tools and machinery that are readily available.

Coating is another type of finishing process that can introduce desirable tribological and thermal properties to a metal substrate. This includes electroplating, conversion coating, cladding and chemical vapour deposition (Gray and Luan, 2002). Each of these introduces a thin layer of a material that is different to the substrate or chemically changes the surface in order to get the desired tribological and thermal resistive properties of the coating while also keeping the required yield strength and/or density of the bulk material.

These coating mechanisms usually require a chemical reaction to bond the surface material to the bulk. These processes are often expensive and require highly specialised equipment.

For the greatest improvement in friction and wear resistance, many components would require a combination of mechanical and chemical finishing processes. This requires an expensive multistage operation using highly specialised equipment and expertise. Some lubricant additives have been shown to chemically bond to material surfaces through the purely mechanical movement of sliding contacts wearing against each other (Tannous et al., 2011). This occurs because the heat and pressure generated in the wear process is enough to cause a chemical reaction. Mechanical finishing processes are capable of producing a similar environment to that of a severe wear regime. With the simple addition of the right additives, mechanical finishing processes can generate a chemical change in material surfaces (Varenberg et al., 2016; Zhmud et al., 2014), doing the job of both mechanical and chemical processes in a single work stage and reducing the need for specialised equipment.

This thesis focuses on improving the understanding of how lubricant additives create chemically bonded protective surfaces and starts the development of two mechanochemical finishing processes for tribologically superior surfaces in a single stage operation.

Thesis Structure

Figure 1.1 outlines the structure of the thesis looking to mechanochemically induce superior trichological surfaces on metal contacts.

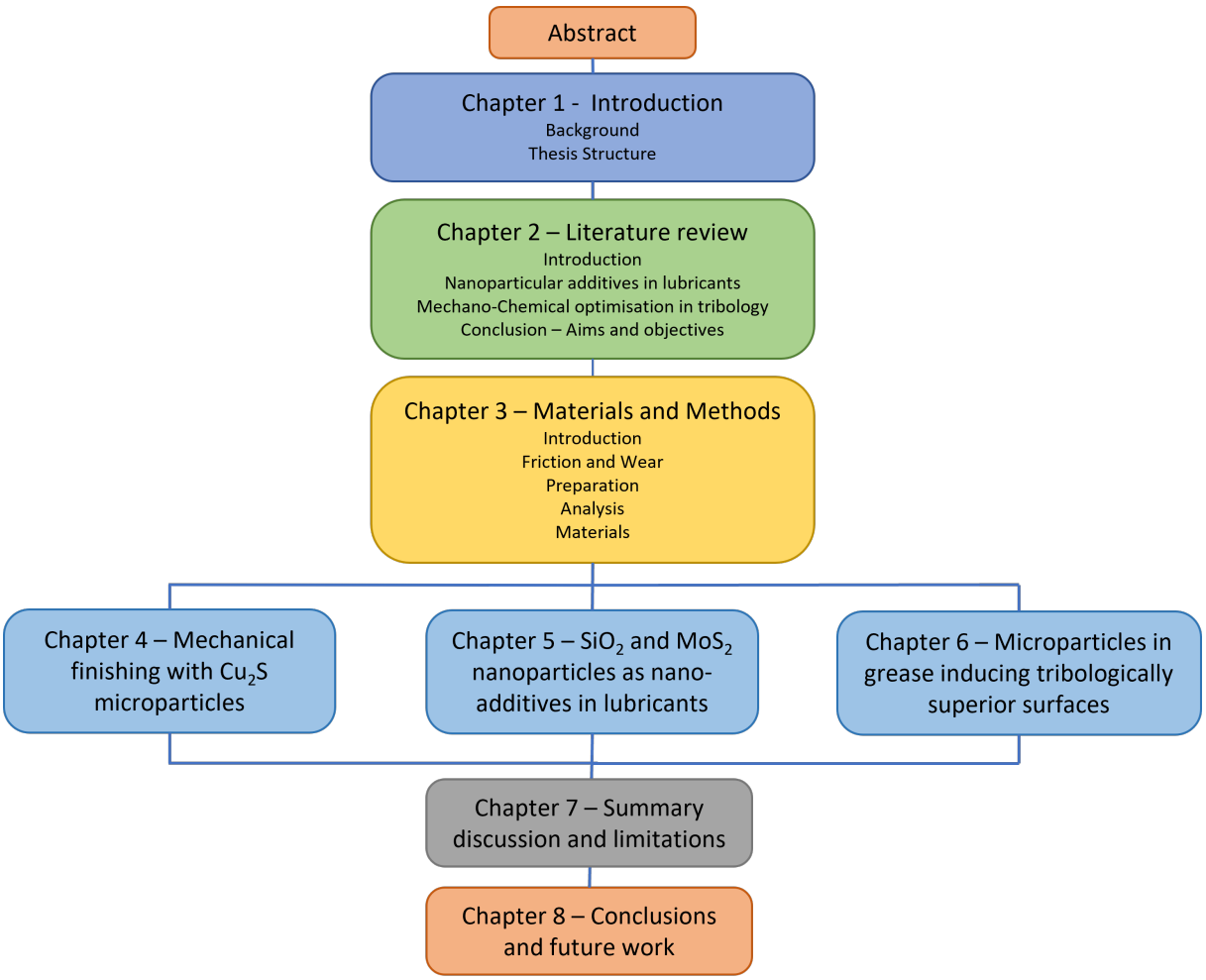

Figure 1.1: The structure of the thesis.

Chapter 2

Literature Review

Frictional losses have been shown to be responsible for up to 28 % of the total fuel energy in a passenger car (Holmberg and Erdemir, 2015) and friction is a major source of mechanical losses in all systems with interacting moving components. In order to reduce these losses and improve the efficiency of mechanical systems, a good understanding of how lubricants and interacting surfaces affect the tribological performance of a system is needed. This understanding will aid the development of superior fluids and surface treatments enabling the longer lifespan of components and less wasted energy.

2.1 Lubricated friction

General "rules of thumb" for the relationship between normal load and friction force have been described as the "laws of friction" (Hutchings and Shipway, 2017) and read as follows:

1. The friction force is proportional to the normal load
2. The friction force is independent of the apparent area of contact
3. the friction force is independent of sliding velocity.

A form of the first two were initially written in a notebook of Leonardo da Vinci's in around 1493 (Hutchings, 2016), they were stated as laws by Guillaume Amontons in 1699, with the third added by Couloumb in 1785 (Popova and Popov, 2015). These laws are generally applicable in dry friction between two solid surfaces in normal air or particular fixed lubricant conditions, but there are many exceptions for all three.

When lubricants such as oils, greases or even water are used, the first and third laws do not hold true, and a different relationship is needed. If the lubricant is able to fully support the normal load with no contact between two linearly sliding surfaces then full-film or hydrodynamic lubrication is the active regime. In this case friction will be very low (a Coefficient Of Friction (COF) of <0.002 (Hamrock et al., 2004)) and wear will be negligible (Hutchings and Shipway, 2017). Elastohydrodynamic Lubrication (EHL) is

a development of hydrodynamic lubrication and occurs when the film is thin enough to cause elastic deformation in asperities on the surfaces without the asperities of each surface directly contacting each other. Wear will still remain minimal (Dowson and Higginson, 1977). As the lubricant film gets thinner still, asperities of opposing surfaces will start to contact and mixed lubrication or partial EHL is the regime. Here friction and wear will both be higher. When contact pressure is very high or the entrainment velocity is very low, the hydrodynamic forces in the lubricant are insufficient to separate the surfaces and they will come into contact and most of the lubricant is squeezed out (Hutchings and Shipway, 2017). This is called boundary lubrication and is the most severe of the regimes.

Stribeck curve

In a simple lubricated regime with linearly sliding contacts, the relationship between COF and lubrication regime can be represented using the Stribeck curve (Wang and Wang, 2013). This curve, shown in Figure 2.1, is a model for how friction changes through the full range of lubrication, from boundary to full hydrodynamic lubrication. Stribeck (1902) discovered through extensive research of friction with bearings that there was a minimum COF in any set up of geometry and lubricant. The same year that Gumbel was able to summarise Stribeck's results in a single curve (Wang and Wang, 2013), Hersey (1914) showed that the COF was a function of $\frac{\mu N}{P}$ (where μ, N and P are viscosity, revolutions per unit of time, and average normal load respectively) in bearings with similar geometries that were similarly loaded and lubricated. In other applications N can be translated to sliding speed v.

Further experimentation has led to the understanding that the Stribeck curve can also be plotted as the COF against the λ-ratio (Johnson et al., 1972):

$$\lambda = \frac{h_{min}}{\sigma^*} \tag{2.1}$$

where h_{min} is the minimum lubricant film thickness and σ^* is the r.m.s roughness of the two contacting surfaces by:

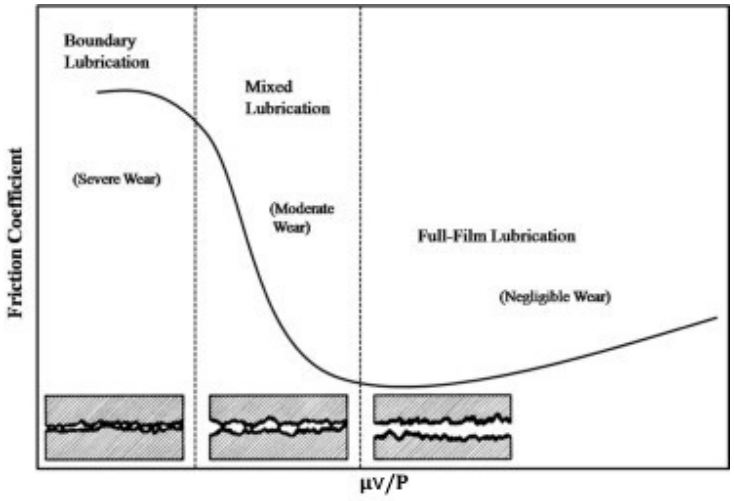

Figure 2.1: Stribeck curve and lubrication regimes. This image was adapted from Choi et al. (2009). μ: kinematic viscosity; v: Sliding speed; P: normal force

$$\sigma^* = \sqrt{{Rq_1}^2 + {Rq_2}^2} \tag{2.2}$$

If $\lambda > 3$ then full fluid film exists, if $\lambda < 1$ then it is boundary friction and anything in between is mixed lubrication.

Many real world applications use reciprocating motion, such as engine piston cylinders and water pumps. This leads to a more complicated system of lubrication as the sliding speed v is a function of $sin(t)$. Hersey's formula shows that as v tends towards 0, boundary lubrication becomes the prevalent regime as the hydrodynamically-generated film collapses, then as v gets larger, the friction moves along the Stribeck curve towards the hydrodynamic lubrication region. This means that in reciprocating motion, the lubricating regime is boundary at the ends of the stroke but moves through mixed and often into full hydrodynamic lubrication when v is maximum at the centre of the stroke. Lubricants in reciprocating motion must be effective across much of the Stribeck curve if significant gains in efficiency and component life are to be achieved.

2.2 Nanoparticles as lubricant additives

There have been great advances in nanoparticle technology in recent decades. From cancer treatment and drug delivery to lithium batteries and low energy lighting (Abe et al., 2018), the applications for nanotechnology are wide ranging. In the area of tribology, nanoparticles are being increasingly studied, both as solid lubricants and additives in liquid lubricants. There has been particular focus on their effectiveness in boundary lubrication (Vanossi et al., 2018). This section will look at nanoparticles and their uses as additives in lubricants, specifically between metal contacts.

Overview

The recent extensive coverage of nanoparticles in tribology include two main groups that will be discussed in this literature review. The first is 2D nanoparticles such as the graphene family (Singh et al., 2021), Transition Metal Dichalcogenides (TMDC) and α-zirconium phosphate (Guo et al., 2021). The second is metal oxides which include SiO_2 (Hao et al., 2021) and Al_2O_3 (Ali et al., 2016). These nanoadditives can have a variety of friction and wear modifying mechanisms; viscosity modifiers (He et al., 2014) to surface polishing and nano-bearing effects (Hao et al., 2021). As asperities in typical metal surfaces are in the micro scale, nanoparticles are able to fill the micro valleys and provide surface healing effects which can reduce the COF (Seyedzavvar et al., 2020). Finally, and most relevant to the research undertaken in this thesis, some nanoparticles chemically bond with the contacting surfaces, creating protective tribofilms that significantly reduce wear (Uzoma et al., 2020). A tribofilm is defined as a thin solid film that is generated due to sliding contacts. They are adhered to the substrate worn surface but have differing chemical composition, structure and tribological behaviour to that surface (Luo, 2013). They work as a third body and affect both friction behaviour and wear performance. A diagram of an example tribofilm formed with the use of WS_2 nanoparticle additives in a lubricant between steel contacts is shown in Figure 2.2. Understanding how these tribofilms are formed will aid the development of mechanochemical finishing processes

that improve the tribological properties of components.

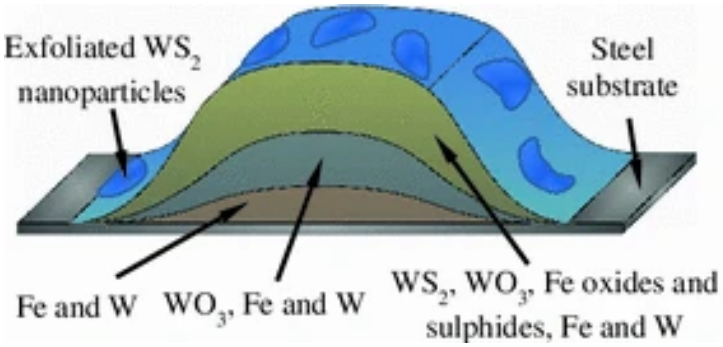

Figure 2.2: Diagram of tribofilm formed with WS_2 nanoparticles and steel substrate (Ratoi et al., 2013)

Graphene family

Graphene is a 2D material that consists of a single layer of carbon atoms in a honeycomb lattice (Peres and Ribeiro, 2009). It is relatively simple to make in small quantities through the micro-mechanical exfoliation of pure graphite until a single layer is present. Graphene is known for its very high strength with a Young's modulus of 1 TPa and intrinsic strength of 130 GPa. Due to pure graphene's chemical inertness, good dispersion in solvents is difficult (Zhai et al., 2017). The graphene family also includes graphene oxide which is also constructed of single layers of carbon with some attached to oxygen and sometimes hydrogen. The exact monolayer structure of graphene oxide (often abbreviated to GO) is not completely known, partly due to differences between samples (Dreyer et al., 2010), however, its individual layers are highly hydrophilic (Pei and Cheng, 2012) which give then good dispersed stability as a water based lubricant (Song and Li, 2011).

Graphene and graphene oxide can reduce the COF by at least 50 % in certain regimes as additives in Polyalphaolefin (PAO) (Zheng et al., 2016) and pure water (Elomaa et al., 2015) respectively though these papers also highlight the vast range in results for COF and wear depending on the base lubricant, mating surface materials and test parameters. Due to the 2D planar nature of graphene, the main friction reduction mechanism as a lubricant is considered to be easy sliding between graphene layers and the material surfaces (Eswaraiah et al., 2011). Graphene oxide nano-additives are occasionally shown

to produce a tribofilm-like layer (Kinoshita et al., 2014; Song and Li, 2011), these layers are through adsorption of the GO to the surfaces. Due to the very stable nature of pure graphene, it is unable to form a chemically bonded tribofilm though through the compacting of nano-sheets into the wear track, graphene can sometimes create a protective layer on the material (Piątkowska et al., 2018). The protective layers prevent the sliding metal surfaces from directly contacting and reduce wear. Nano-graphene has shown good synergistic behaviour with other additives such as Zinc dialkyldithiophosphates (ZDDP) (Zhao et al., 2021) and MoS_2 (Xu et al., 2015) where the graphene nanosheets are incorporated into the tribofilms enhancing their durability.

While the graphene family have promising characteristics as nanoadditives in lubricants, as they do not aid the mechanochemical creation of a tribofilm, they will not be focused on through the remainder of this thesis. Future development of mechanochemical finishing may be able to incorporate some of its synergistic friction reduction mechanisms when part of a chemical tribofilm once an effective process has been developed.

Transition Metal Dichalcogenides (TMDCs)

TMDCs consist of metal atoms (M) in a hexagonal layer between two layers of chalcogen atoms (X) in the form MX_2 (Hasan et al., 2019). A diagram of the TMDC molecular structure is shown in Figure 2.3. The M-X bonds are typically covalent and each sandwich layer is coupled by weak van der Waals forces, meaning individual layers are easily separated (Parvez, 2019).

Two examples of TMDCs commonly researching in tribology are MoS_2 and WS_2 (Guo et al., 2021). Their weak van der Waals interactions between layers mean easy sliding which leads to lower friction, similar to the graphene family. Unlike graphene, TMDCs have good adherence to many materials and can chemically react with the sliding surfaces. These reactions create tribofilms (Krishnan et al., 2019) similar to the diagram in Figure 2.2 and significantly reduce wear.

As well as in their 2D forms, they are also tested in Inorganic Fullerene-like (IF) forms

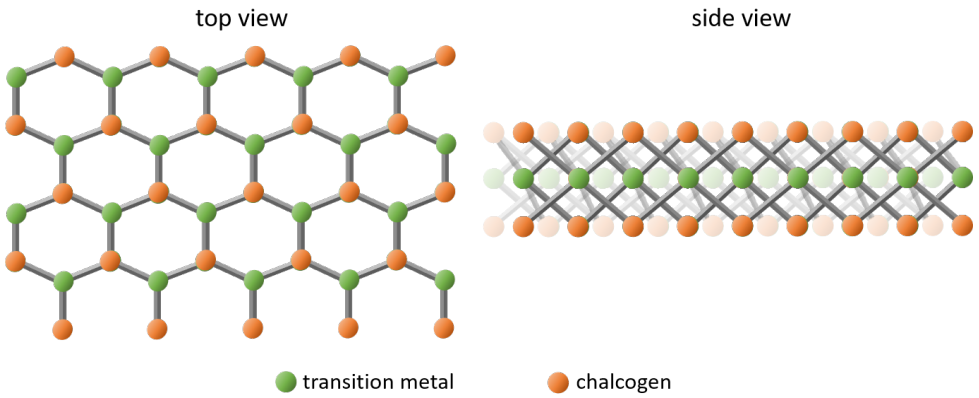

Figure 2.3: Diagram of molecular structure of TMDCs

(IF-MoS_2 and IF-WS_2) and nanotubes (Kalin et al., 2012; Rapoport et al., 2005). IF-nanoparticles are near-spherical arrangements of nanosheets; nanotubes are simply the cylindrical arrangement. These structures enable the particles to roll into the contact and once there, get exfoliated into nanosheets by the shear forces caused by the sliding surfaces. The nanosheets then remain in the contact often already attached to the surfaces. The more crystalline the IF-MoS_2 structures, the poorer the lubricating film stability as the particles are harder to exfoliate and get pushed out of the contact area (Rabaso et al., 2014b). Lahouij et al. (2014) were able to observe this exfoliation *in situ* between silicon and a diamond tip, and images from the recording are shown in Figure 2.4.

X-ray Photoelectron Spectroscopy (XPS) is a useful tool for understanding chemical species in the top few nanometres in the surface of a material. In tribology it can be used to give evidence for mechanisms of tribofilm formation. How it works is discussed in chapter 3. Hard X-Ray Photoelectron Spectroscopy (HAXPES) is XPS but capable of using higher energy X-rays (above 2 keV) which can penetrate deeper into the material than normal "soft"-XPS (Kalha et al., 2021). Mantovan et al. (2018) performed HAXPES on 2D-MoS_2 for reference and then again following 11 nm of iron deposition.

Figure 2.5a shows the peaks expected from pure MoS_2 with an S^{2-} peak at ≈226.5 eV and an Mo^{4+} doublet at ≈229 eV. After the deposition, in Figure 2.5b, the peaks attributed to MoS_2 have greatly reduced and a pure metallic Mo^0 doublet at ≈228 eV and a smaller S^{6+} sulphate peak are prevalent instead. Mantovan et al. (ibid.) believed the Mo^0

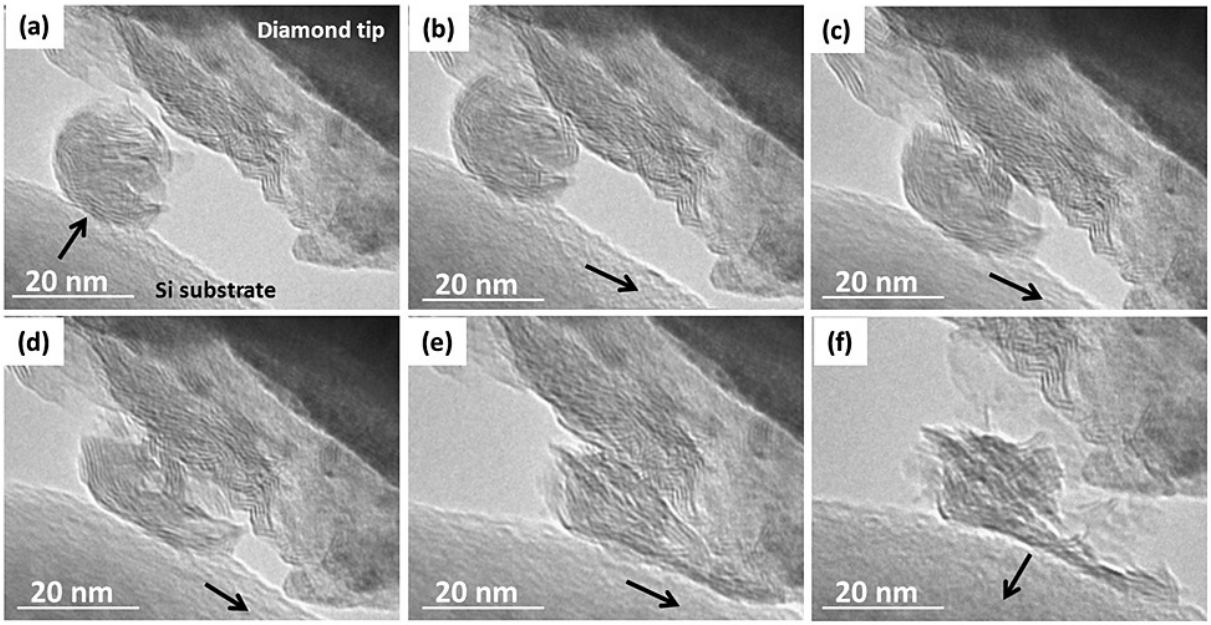

Figure 2.4: *In situ* exfoliation of IF-MoS_2 in sliding contacts (Lahouij et al., 2014). Each image is a displacement step. As the arrows show, the Si substrate moves to the right, rolling the IF-MoS_2.

peak was a result of alloying between Mo and Fe with the S^{6+} attributed to $FeMo_2S_4$. These results backed up previous Conversion Electron Mössbauer Spectroscopy (CEMS) analysis.

Tannous et al. (2011) studied the mechanisms by which IF-MoS_2 reduces friction in PAO in a boundary lubrication regime. The wear test was pin-on-flat and compared the coefficient of friction over time for steel, a Diamond-Like Coating (DLC) and alumina. Post-test analysis determined the mechanisms of wear. The readings taken during the test showed that for steel, the COF dropped from around 0.1 to 0.03 with the introduction of 1 wt% MoS_2 with much greater stability, whereas for the DLC and Alumina tests, very little change in COF was noticed and for alumina especially, the stability was much worse with MoS_2. For the steel, Transmission Electron Microscopy (TEM) images of a cross section of the surface (see Figure 2.6) and depth profiling using Auger Electron Spectroscopy (AES) showed that a tribofilm incorporating the molybdenum and sulphur with the iron, carbon and a small amount of oxygen had been formed on the surface at 5 nm to 10 nm depth. XPS showed the presence of some iron-sulphur bonds suggesting that the MoS_2 had reacted with iron in the surface. The presence of MoS_2 reduced the

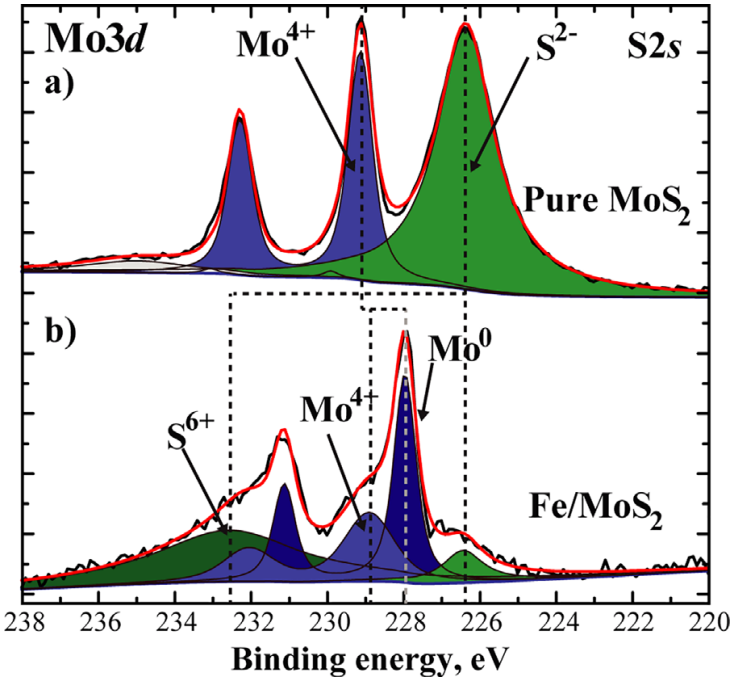

Figure 2.5: XPS Mo 3d/S 2s core level spectra of (a) 2D-MoS_2 sample before and (b) after Fe deposition (Mantovan et al., 2018)

wear scar diameter in the pin. AES images of the DLC samples found only carbon, so no tribofilm was formed and for alumina, large agglomerates of MoS_2 were found at the edge of the wear track but Energy Dispersive Spectroscopy (EDS) images of the wear track itself found no molybdenum or sulphur.

A great deal of analysis was also performed in order to understand the tribofilm formation using 2H-WS_2 nanoparticles between steel contacts in PAO 6 (Ratoi et al., 2013). The 2H- form of the nanoparticles was confirmed using X-Ray Diffraction (XRD). Sharp peaks at (002) and (101) indicated the larger crystal size, broader peaks would be expected for smaller crystal sizes (Fang et al., 2011), like those in IF-WS_2. Ratoi et al. (2013) showed, through Raman spectroscopy, that the nanoparticles contained few stacked layers. This was inferred from the relatively small A_{1g} peak in the Raman shift (around 419 cm^{-1}), where only the sulphur atoms vibrate (between layers) as opposed to the much larger E^1_{2g} peak where the metal atoms vibrate with the sulphur atoms within layers (Dumcenco et al., 2010). A graphical explanation of this can be seen in Figure 2.7.

The tribological tests were performed between a 19 mm⌀ ball and 46 mm⌀ disc both made of AISI 52100 steel with a slide-roll set up. Two 180 min tests were performed,

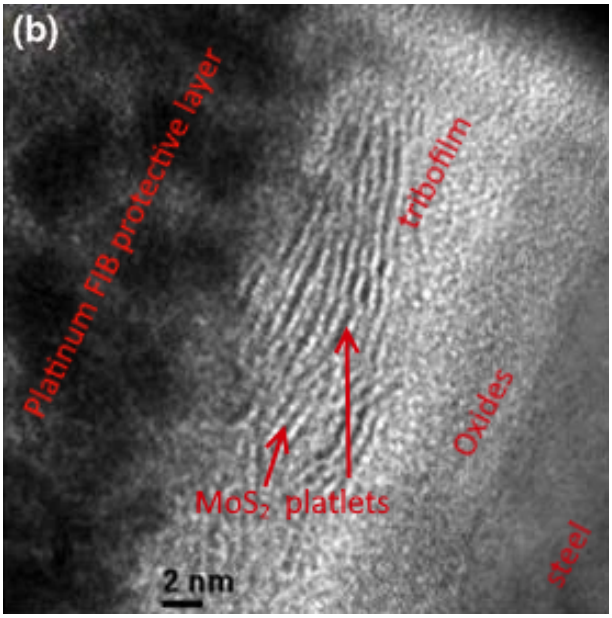

Figure 2.6: TEM image of a cross-section of steel surface and MoS_2 tribofilm. The cross-section was made with a Focused Ion Beam (FIB). This figure was adapted from an image in the paper by Tannous et al. (2011).

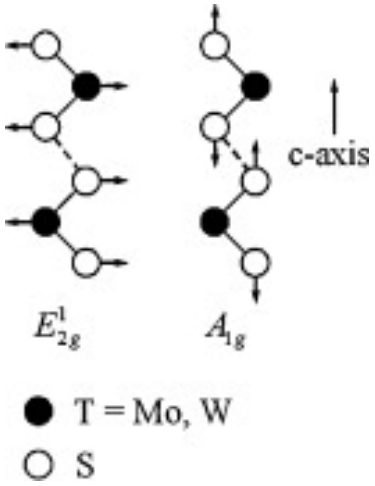

Figure 2.7: Diagram of atom vibration for TMDCs at E^1_2g and A_1g peaks in Raman spectroscopy (Dumcenco et al., 2010)

at 40 °C and 100 °C with varying sliding speeds from 1500 mm s^{-1} down to 10 mm s^{-1} to generate results across the Stribeck curve. The applied load was 30 N. A concentration of 1 wt% for the nanoparticles were dispersed in the PAO using a probe sonifier.

The friction coefficient along the Stribeck curve for the 40 °C tests did not produce superior results with WS_2 mixtures, however, at 100 °C, they produced significantly lower friction results at the lowest speeds (boundary lubrication) throughout the 180 minutes. This produced a very different Stribeck curve (Figure 2.8) to the expected one seen in

Figure 2.1.

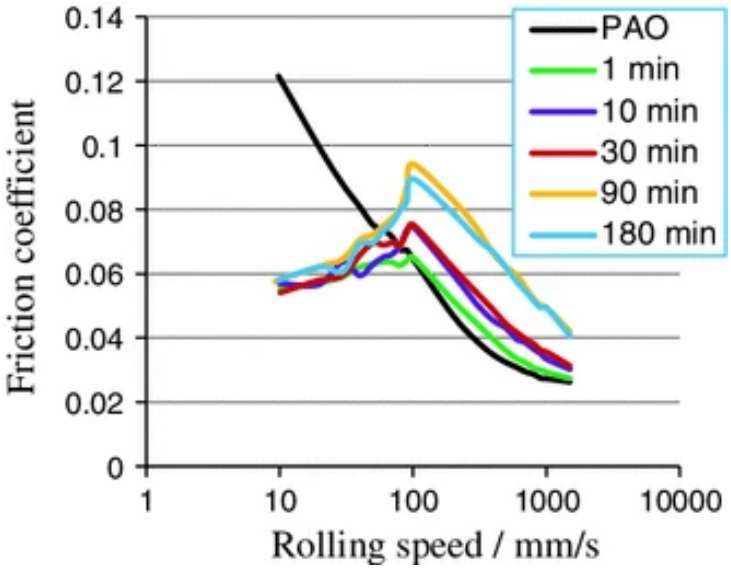

Figure 2.8: Stribeck curves for 1 wt% WS_2 NPs in PAO at 100 °C after 1, 10, 30, 90 and 180 min of rubbing (Ratoi et al., 2013)

A variety of surface analysis methods were performed to characterise the tribofilm formed in the 100 °C test. According to the depth profiling performed by XPS, sulphur was found in the top 50 nm and tungsten beyond 200 nm. The composition of the formed tribofilm at the surface according to EDS showed there to be around 10 × as much sulphur as tungsten, suggesting that chemical reactions had occurred between the WS_2 nanoparticles and the steel substrate and some of the sulphur had bonded with other elements in the surface. The tungsten much deeper in the surface was shown to be elemental, becoming purer the further in it was analysed suggesting that tungsten separated from the sulphur and sintered deeper into the steel. The XPS results, combined with Secondary Ion Mass Spectroscopy (SIMS) analysis, were employed to come up with the likely tribofilm composition shown in Figure 2.2.

Similarly to the earlier Tannous et al. (2011) paper, research by Kalin et al. (2014) has also compared the effectiveness of MoS_2 between steel contacts and DLC contacts. There were some key differences in the test set up though. This paper used MoS_2 nanotubes as opposed to IF-MoS_2 and a slide/roll ball-on-disc setup instead of pure sliding pin-on-disc. Kalin et al. (ibid.) started and ended each test with a speed decrease from

3.2 to 0.002 $\mathrm{m\,s^{-1}}$ in order to get a Stribeck curve for the lubricant with a 2 h constant mean contact velocity test at 0.05 $\mathrm{m\,s^{-1}}$ between the two. As expected, the COF was significantly lower than the base oil in boundary lubrication, particularly for the steel, but not at EHL. MoS_2 had less effect on the DLC surfaces but the nanotubes still improved the COF slightly. The Scanning Electron Microscopy (SEM) images in both surfaces showed many nanotubes that had not been exfoliated. This could be down to a more crystallised structure than typical IF-MoS_2 nanoparticles used in tribological testing as discussed in Rabaso et al. (2014b). SEM and EDS did show patches in the wear track with high concentrations of Mo and S. These areas were analysed under XPS but the authors did not think any Fe-S bonds had been formed in the tribofilm as the XPS peaks for DLC and steel were very similar in the S (2-) area of the S 2p spectra. They believed these peaks were purely down to embedded MoS_2 with some Mo-S-O species. The paper did not look in detail at the Fe 2p spectra for the steel surface. Looking at the ratio of oxidised iron to metallic could indicate possible iron sulphides, especially when compared to the base oil. This would provide further evidence for the authors' hypothesis.

For MoS_2 to have commercial prospects as a nano-additive in lubricants, the issue of keeping the particles evenly dispersed without agglomeration must be overcome. In laboratory conditions, the nanofluid can be agitated through stirring and ultrasonic shaking immediately prior to testing. However, when applied to intermittently used machines with an internal lubricant system, additives could form a sediment between uses, reducing the lubricant's effectiveness and perhaps increasing friction and wear (Rabaso et al., 2014a). MoS_2, like graphene, is hydrophobic which makes dispersion in water difficult, therefore it has limited effectiveness as a water-based additive (Wang et al., 2019). There are two methods for improving the suspension stability of a particular set of nanoparticles in any given lubricant. Either modify the particles, or mix a dispersant into the suspension.

Some methods of obtaining 2D-MoS_2, including liquid exfoliation leave some defects in the 2D sheets which include sulphur vacancies (Chou et al., 2013). Thiols (–SH bonded to an organic compound) can be bonded to the MoS_2 through the vacancies to improve their dispersion in water. This can be done through mixing MoS_2 in dilutes of certain

acids such as L-cysteine. Under 20 N point contact load in reciprocating motion, these modified nanoparticles in water can significantly reduce both friction and wear as well as form a tribofilm on the steel contacts when the un-modified particles fail to make any improvements over pure water (Wang et al., 2019).

Dispersants are a form of surfactant. Surfactants reduce the surface tension between two phases of matter, and dispersants specifically improves the separation of particles within a suspension to prevent them from agglomerating or settling. Dispersants are made of molecules that have two distinct groups. If they are used to disperse oil in water then one of these groups will be oleophilic/hydrophobic (often referred to as the head) and the other hydrophilic/oleophobic (the tail) (Cressey, 2010). The oleophilic head attaches itself to the oil molecules leaving the hydrophilic tail in the water preventing attachment of the oil molecule to others. For dispersing nanoparticles in oil, different surfactant molecules are needed. The anchoring group (head) are adsorbed to the particles and the solvent group (tail) is attracted by the oil, preventing attachment to other particles (Gao and Luo, 2016). A diagram of MoS_2 with different quantities of Polyisobutyleneamine Succinimide (PIBS) surfactant is shown in Figure 2.9.

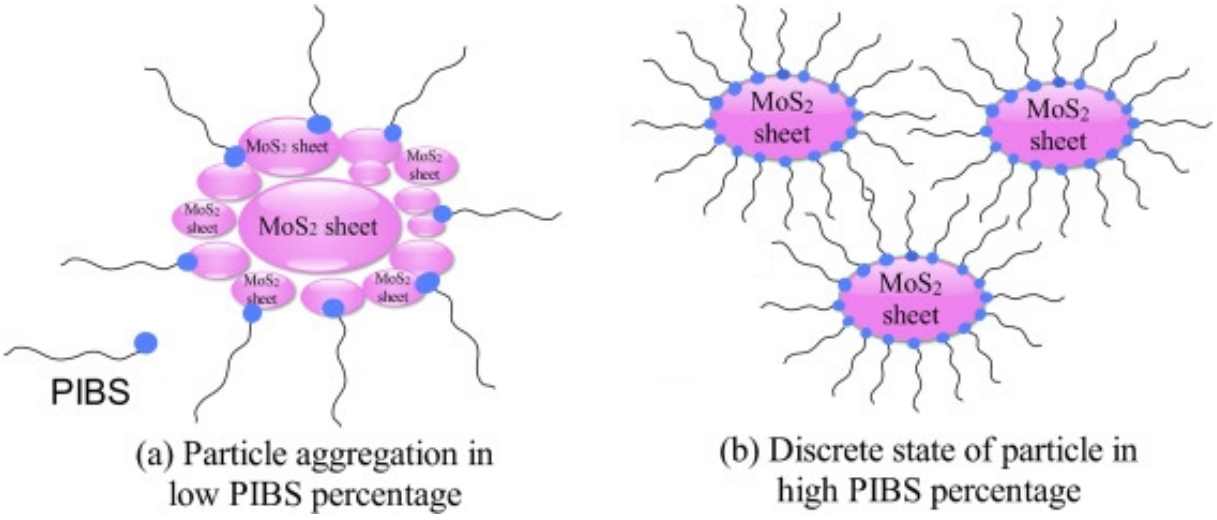

Figure 2.9: MoS_2 dispersed with PIBS. (a) With insufficient dispersant to completely prevent agglomeration. (b) Full dispersion achieved. Image adapted from Wu et al. (2017).

Using dispersants with MoS_2 has been explored by a number of authors but it appears to interfere with its friction and wear reducing mechanisms. Adding IF-MoS_2 to a fully

formulated gearbox oil in a High Frequency Reciprocating Rig (HFRR) set up, has very little effect on the COF between steel contacts. When used at 1 wt% with PAO base oil in the same conditions, the COF reduced from 0.2 to 0.06 (Rabaso et al., 2014a). The commercial oil contains dispersants to prevent debris build up when in operation.

Rabaso et al. (ibid.) investigate mixing a succinimide-based dispersant with IF-MoS_2 nanoparticles in PAO. In the initial tests, concentrations of 0.5 and 5 wt% dispersant were mixed with both 0.5 and 1 wt% IF-MoS_2. The dispersant concentrations were based off commercial automotive oil quantities. Through use of Dynamic Light Scattering (DLS), the dispersant was shown to reduce the mean agglomerate size from 422 nm to 174 nm (approx. average nanoparticle size). In the HFRR testing, all the mixtures containing dispersant and IF-MoS_2 failed to reduce the COF when compared to the pure base oil. XPS showed little to no increase in molybdenum or sulphur in the worn surface when the dispersant was used, suggesting that any MoS_2 in the contact was removed with cleaning. TEM analysis of the dispersed nanoparticles after a friction test showed that the IF-nanoparticles had been exfoliated when passing through the contacts which is required for tribofilm formation but the chemical bonding needed for adhesion did not happen. The authors put this down to "excessive adsorption" of the dispersants to the steel surfaces or a complete coating of the exfoliated platelets preventing the chemical bonding between the molybdenum or sulphur to the iron oxides in the surface. Similar results occur when nano-MoS_2 sheets are mixed with ZDDP and 3 wt% PIBS (Wu et al., 2017). In this case, the authors believed the agglomerations of MoS_2 could be dragged into the contact and worn between the surfaces until a tribofilm was formed whereas the dispersed particles would simply flow around the sliding ball ineffectually.

As commercial oil dispersants must prevent agglomeration of wear debris over time, the quantity is deliberately excessive, but detrimental to the MoS_2. Rabaso et al. (2014a) proposed that reducing the dispersant quantity to be enough to fully cover the nanoparticles with zero excess could be effective. With this hypothesis, the concentration of dispersant was reduced to 0.05 wt% with 1 wt% IF-MoS_2. DLS showed the agglomerate size to be almost identical to the higher dispersant quantities. HFRR testing showed the

nanofluid with 0.05 wt% reducing friction compared to base oil by about half for the first 90 000 cycles, with an eratic COF before settling after 110 000 cycles to around 0.06, just higher than the MoS_2 lubricant without the dispersant. Post HFRR DLS testing showed that nanoparticles left in the oil were still well dispersed. The long run in period could have been due to small excess of dispersant still in the oil preventing adhesion. Wu et al. (2017) tested MoS_2 and ZDDP with PIBS content 0.05 wt% in their paper. Again, the mixture performed better than with the higher dispersant content but not as well as with the nanoparticles alone. These papers showed that IF-MoS_2 could be compatible with succinimide-based dispersants if only a very small quantity is used, but in commercial oils, an excess is needed to extend the life of the components it is lubricating.

Molybdenum dialkyl dithiocarbamate (MoDTC) is a lubricant additive that is commonly used in fully formulated lubricants, often alongside ZDDP (Garcia et al., 2021). Its chemical structure can be seen in Figure 2.10. The friction reducing mechanism of MoDTC is known to be the formation of 2D MoS_2 nanosheets when the chemical bonds rupture under sever tribological conditions. These nanosheets then form a part of the tribofilms generated on the component surfaces enabling friction and wear reduction.

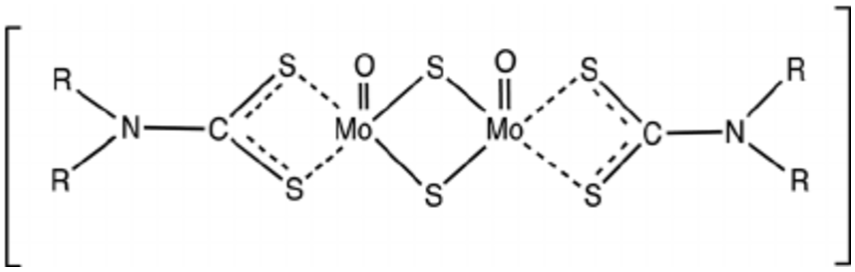

Figure 2.10: Planar representation of the chemical structure of MoDTC (De Feo et al., 2015)

Vaitkunaite et al. (2022) added different concentrations (0.1 wt%, 0.3 wt%, 0.5 wt% and 0.7 wt%) of MoDTC to a fully-formulated low-visocity oil that contained ZDDP for cast iron engine cylinder/piston interactions. At 0.3 wt% and above, significant reductions in friction were observed particularly when the piston was close to Bottom Dead Centre (BDC). The friction reduction correlated to increased quantities of MoS_2 found with Raman Microscopy; at 0.5 wt% MoDTC, MoS2 could be found in 72 % of the cylinder

liner surface at BDC, whereas it could only be found in 9 % at Top Dead Centre (TDC). The reduced coverage at TDC was proposed to be because of a combination of lubricant starvation and the influence of combustion to the conditions, such as gas pressure, sludge production and the presence of unburnt fuel. The MoS_2 present in the surface were part of a tribofilm that contained much higher concentrations of zinc, which was a result of the degradation of ZDDP in the contact.

MoDTC is an example of an additive that allows MoS_2 to form part of a tribofilm in a lubricated regime using fully-formulated oil. However, without ZDDP, MoDTC is unable to form an MoS_2-based tribofilm (Sutton et al., 2007). It has also been observed, that excess MoDTC can lead to oxidative degradation of engine oil (Wang et al., 2013) at which point the beneficial effect of the additive is negligible. There are additional concerns over its contribution to unwanted deposits in other powertrain components such as turbochargers (Howard, 2014). Further research is still needed for MoS_2 to be used beneficially and consistently in real world applications.

TMDCs have excellent tribofilm forming capabilities and the formation mechanism of wear resistant sulphide/sulphate tribofilms typical of MoS_2 and WS_2 is a mechanochemical process. Due to the challenge of good dispersion, more research is needed before they can be used effectively in most real world applications. However, a mechanical finishing process with sulphide additives could produce a similar protective layer on the surface of machine components without the need for nanoparticles in the lubricant.

Metal oxides

Metal oxides (also known as ceramics (Fan, 2009)) are hard and brittle materials. A vast range of metal oxide nanoparticles have been studied in tribology research including SiO_2 (Peña-Parás et al., 2015), Al_2O_3 (Kotia et al., 2019), ZnO (Wu et al., 2016), SnO_2 (Tao et al., 2018) and many more. They are known for enhancing heat transfer in base fluids (Wang et al., 2022) and are often in spherical form (see Figure 2.11). They can act as nano-bearings converting sliding friction into rolling as well as separating the interacting

surfaces (Luo et al., 2014; Sayuti et al., 2014). Their high hardness can also lead to beneficial surface polishing effects (Kotia et al., 2019), where the nanoparticles quickly smooth the contacting surfaces by removing asperities leading to reduced friction (Bao et al., 2017).

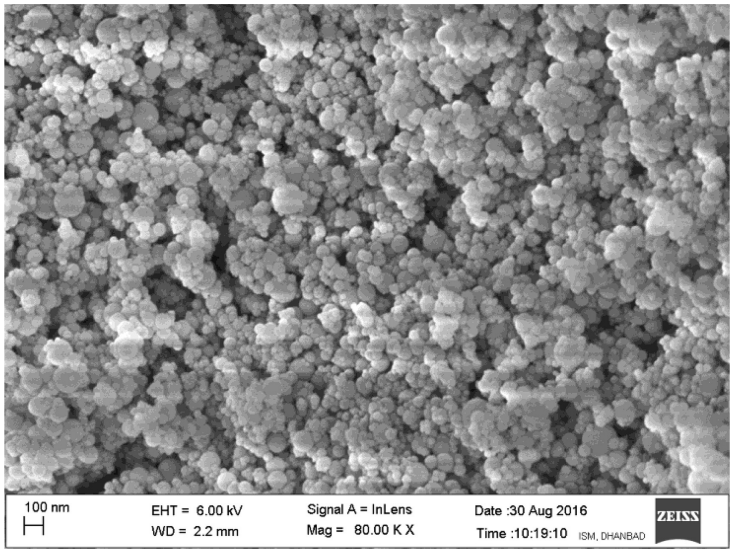

Figure 2.11: A Field Emission SEM image of Al_2O_3 nanospheres (Kotia et al., 2019).

As the nanoparticles are much harder than the metal surfaces they are acting between, in the wrong conditions their positive attributes can easily become negative. In some cases where the lubricant film becomes thinner than the size of the nanoparticle (Xie et al., 2016a) or if a high concentration of the particles are used forming agglomerates (Tao et al., 2018), then the spheres can become highly abrasive and increase wear due to their being very difficult to deform (Kotia et al., 2019). The nanoparitcles produce deep furrows in the softer metal surfaces which also leads to a much rougher surface and worse friction (Bao et al., 2017) (see Figure 2.12).

Luo et al. (2014) used a silane coupling agent, KP-560 to surface treat Al_2O_3 during their fabrication which hydrolysed the nanoparticles leading to improved dispersion and reduced agglomeration in a lubricating oil. In a four ball tribotester, 0.1 wt% of surface treated Al_2O_3 in a base lubricating oil was able to reduce the COF by ≈18 % compared to the base oil. At 0.05 wt%, the nanoparticle concentration was too small to be effective. Any higher than 0.1 wt%, the excess of nanoparticles started to increase friction.

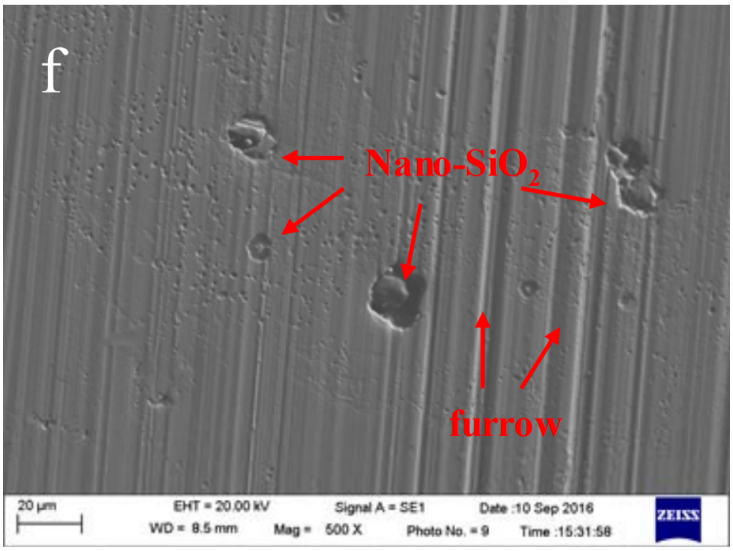

Figure 2.12: SEM image of furrows on a steel ring caused by excess SiO_2 (Bao et al., 2017).

Liu et al. (2017) believed that the beneficial friction and wear results using SiO_2 nanospheres in Polyalkylene Glycol (PAG) with reciprocating point contact was due to tribofilm formation; however, their reasoning for this is based on an EDS map of the worn surface showing patches of SiO_2. The metal oxide group of nanoparticles are usually quite stable making chemically bonded tribofilms quite unlikely, however, Tao et al. (2018) and Wu et al. (2016) discovered similar presence of the nanoparticles within the worn surface with SnO_2 and ZnO respectively and concluded that tribosintering had occurred. The pressures and temperatures generated during wear process had allowed the lose particles to be incorporated into the surfaces. If this occurs on both contacting surfaces then wear could be significantly reduced as the majority of the contact is between the hard metal oxides rather than the original substrate materials.

Metal oxide nanospheres are effective friction and wear modifiers as lubricant additives through purely mechanical means. The concentration and load has to be carefully considered, otherwise excessive wear can occur. The mechanical surface polishing mechanisms for reducing friction are very similar to ordinary mechanical finishing processes, so ceramics will be looked at in further detail to understand if they can aid the development of a mechanochemical method for improving the tribological properties of surfaces.

Hybrid nanofluids

TMDCs are effective in boundary lubrication, whereas, ceramics appear most effective when there is a small lubricant film. In terms of reciprocating motion they act on different areas of the stroke, with TMDCs at the change in direction and metal oxides in the stroke's centre. Combining the benefits of the two nanoparticles could lead to an ideal hybrid nanofluid that works across the entire stroke. Additionally, the mechanical mechanisms of the ceramics may increase the potential for chemical reactions to occur between TMDCs and the sliding surfaces.

The idea of combining metal oxides and TMDCs in a single nanofluid is quite new. Examples of the possible benefits are demonstrated in papers written by Xie et al. (2016a). When worn between a steel ball and a magnesium plate in EOT5# base oil, SiO_2 would reduce the COF by more than MoS_2 at lower loads (quoted p_o between 223 MPa and 312 MPa) but above 381 MPa the COF would be lower for MoS_2. The volume of wear was lower for MoS_2 throughout (Xie et al., 2016b). Individually, the optimum concentration for SiO_2 and MoS_2 was 0.7 and 1 wt% respectively, however, when combined, the optimum concentrations were found to be 0.25 wt% SiO_2 and 0.75 wt% MoS_2 for both friction and wear (Xie et al., 2016a) (see Figure 2.13).

In this synergistic regime, as the load increased, the COF decreased though at the highest loads tested, the hybrid fluid performed as well as 1 wt% MoS_2, suggesting that eventually the SiO_2 would have a negative effect. XPS showed that for the 312 MPa tests, more MoS_2 and molybdenum oxides were present in the hybrid scars than in the purely MoS_2 scars with a similar quantity of magnesium sulphides/sulphates detected in both. The authors' conclusion was that tribofilms were formed on both surfaces and did not suggest any new synergistic behaviour between the nano-particles rather both nanoparticles working independently but beneficially making a superior fluid.

A formulated Fe_3O_4–MoS_2 nanocomposite additive was able to reduce friction in steel-on-steel 50 N point contact tests better at 1 wt% than either MoS_2 or Fe_3O_4 could at a variety of concentrations. In fact, the Fe_3O_4 produced higher friction than the PAO4

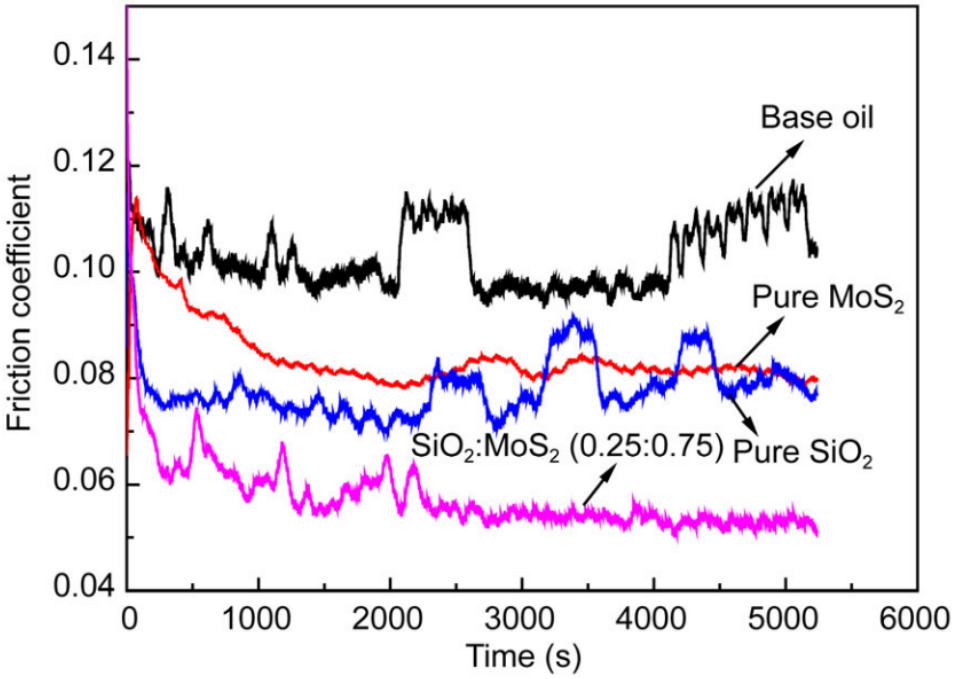

Figure 2.13: Friction coefficient of SiO_2, MoS_2 and hybrid lubricants at 8 N load (Xie et al., 2016a).

base oil (Xu et al., 2018). Both the pure MoS_2 and nanocomposite showed evidence of a tribolfilm containing iron sulphides and/or sulphates according to XPS, and EDS even showed more molybdenum and sulphur in the purely MoS_2 lubricated surface. The authors believe that the nanocomposite was more easily adsorbed to the friction surface giving a more even coverage and the magnetic core of Fe_3O_4 in the composite contributed to the optimal lubrication. On the other hand, the pure MoS_2 agglomerated easily, causing higher friction and a less effective tribolfilm. Evidence for these hypothesised mechanisms was not satisfactorily presented as the magnetic core did not aid the lubricant with only iron oxide in and there was no clear difference in the tribofilms between MoS_2 and the composite lubricant in the presented data.

The most recent research in this area combined various concentrations of SiO_2 and MoS_2 mixed into Deionized (DI) water (Meng et al., 2021). Also mixed into the lubricant was triethanolamine oleate (a dispersant), glycerin (to increase fluid viscosity) and Sodium Dodecyl Benzene Sulfonate (SDBS), a humectant to encourage the particles attachment to water and further dispersion stability. Another oleic acid based dispersant

similar to triethanolamine oleate used in this paper, oleylamine has been tested with MoS_2 previously (Chen et al., 2015). Like the succinimide dispersants discussed earlier, 0.5 wt% dispersant prevented 1 wt% MoS_2 from being as effective an additive than it was without the dispersant.

In Meng et al. (2021)'s paper, all the mixtures had very good dispersion. In a four ball tribotester, 0.3 wt% MoS_2 and the same concentration of SiO_2 together produced lower friction and a smaller Wear Scar Diameter (WSD) than 0.6 wt% of either particle on its own with MoS_2 producing lower friction than SiO_2. The authors did not state any friction and wear for if neither had been present in the lubricant with the same other additives. Based on previous papers analysed in this review, the MoS_2 could have been ineffectual throughout with the SiO_2 having a positive effect on the friction and wear at the lower concentration of 0.3 wt% but damaging the surfaces through excess wear at the higher concentrations. EDS did show significant quantities of MoS_2 in areas on both the hybrid and MoS_2 lubricated surfaces after cold rolling tests. The authors believed the MoS_2 had been adsorbed to the surface.

A number of papers have showed that there does appear to be a synergistic advantage when metal oxides and TMDCs are used together as lubricant nano-additives. It is not completely clear from the papers discussed if the advantage is due to the particles' separate beneficial mechanisms working at the same time or if there is a new behaviour that occurs when both are present. Further research in this area could provide a better understanding of the mechanochemical behaviour of TMDCs in metal contacts and if they can be improved by the introduction of ceramics.

Health risks

In recent years, more research has been done into the health risks of nanoparticles in our atmosphere. Many particulates were unintended by-products of the industrial revolution and power generation that we have only started to understand in the last few decades (Oberdörster et al., 2005). Airborne carbonaceous Ultra-Fine Particles (UFPs) typically

found in vehicle fumes are associated with adverse respiratory and cardiovascular effects. The health risks of many engineered nanoparticles including those heavily researched in tribology are relatively unknown. Moore et al. (2017) attempted to mimic the uptake of MoS_2 via ingestion and inhalation. At $1\,\mu g\,mL^{-1}$ the nanoparticles were not toxic to any of the cell lines but did cause inflammation and penetrated the membranes of the cells. Similar research has been done with graphene oxide (Chang et al., 2011), the cell viability was not significantly affected until the concentration of graphene oxide was over $50\,\mu g\,mL^{-1}$.

The potential benefits in nano-tribology research are too great to ignore; however, while the health risks of these nanoparticles are still relatively unknown, great care should be taken when working with them in a lab setting to transport and dispose of them safely. The risk of inhalation or ingestion must be minimised.

2.3 Lubricating nanogreases

A common issue with nanoparticles in lubricating oils is the agglomeration and settling of nanoparticles after dispersion. This can be compensated for by using dispersants; however, as discussed in section 2.2, these can harm the effectiveness of some nanoparticles. Lubricating greases, which are oils mixed with a thickener agent such as lithium 12-hydroxystearate (M. A. Delgado et al., 2006), do not have the same issue as oils as their high viscosity means greases can hold the particles in suspension and retain their effectiveness (Fu et al., 2019). This section will look at various greases containing nano-additives, operated as an lubricants between metal contacts.

Preparation

One of the first challenges with nanogreases is how to effectively and thoroughly mix the nanoparticles with the viscous grease. There are two methods that are mainly used by researchers, both of which require reducing the viscosity sufficiently to effectively stir nanoparticle into them. The first is by heating the grease to above 100 °C and magnetically

stirring the additives into the heated grease (Singh et al., 2018; Zhao et al., 2014). This is usually followed by returning the mixture to room temperature then running multiple times through a triple roll mill for good homogenization. The second method uses a mixing machine that at very high revs, the shear rate dramatically reduces the viscosity of the grease through "shear-thinning", enabling additives to be mixed effectively (Fu et al., 2019).

Singh et al. (2018) mixed reduced reduced Graphene Oxide (rGO), $CaCO_3$, and α-Al_2O_3 particles separately with a Lithium 12-hydroxystearate thickened mineral oil grease. The nanoparticles were first dispersed in toluene using an ultrasonic probe before the solution was added "drop-wise" into the 110 °C base grease. The mixture was stirred for 90 min before going through the triple roll mill. Zhao et al. (2014) used a similar method with self manufactured spherical Nano-Calcium Borate (NCB) particles of 70 nm⌀. These were added to the lithium grease and mechanically stirred for 10 min before grinding five times through a triple roller mill.

Fu et al. (2019) added graphene particles of approximately 3.46 µm laterally and only 6.5 nm thick to an unspecified base grease. These were added to the grease at 1 wt%, 2 wt%, 3 wt% and 4 wt%. The mixing machine, run at 3500 rpm, was able to reduce the grease's viscosity enough for good dispersion.

Tribology of nanogreases

When looked at under High-Resolution Transmission Electron Microscopy (HRTEM) (see Figure 2.14g), Al_2O_3 nanoparticles (mean diameter 40 nm) were shown to have destroyed the thickener structure in the grease (Singh et al., 2018). This led to greatly reduced tribologcal performance compared to the rGO (500 nm) and $CaCO_3$ (50 nm) particles which adhered to the structure (Figure 2.14e). Al_2O_3 grease did have a similar tribological performance to the base grease, suggesting that the damaged microstructure did not greatly affect the lubricant's viscosity. Analysing the viscosity of the different nanogreases would have been helpful to understand what effect the damaged structure had on the

grease.

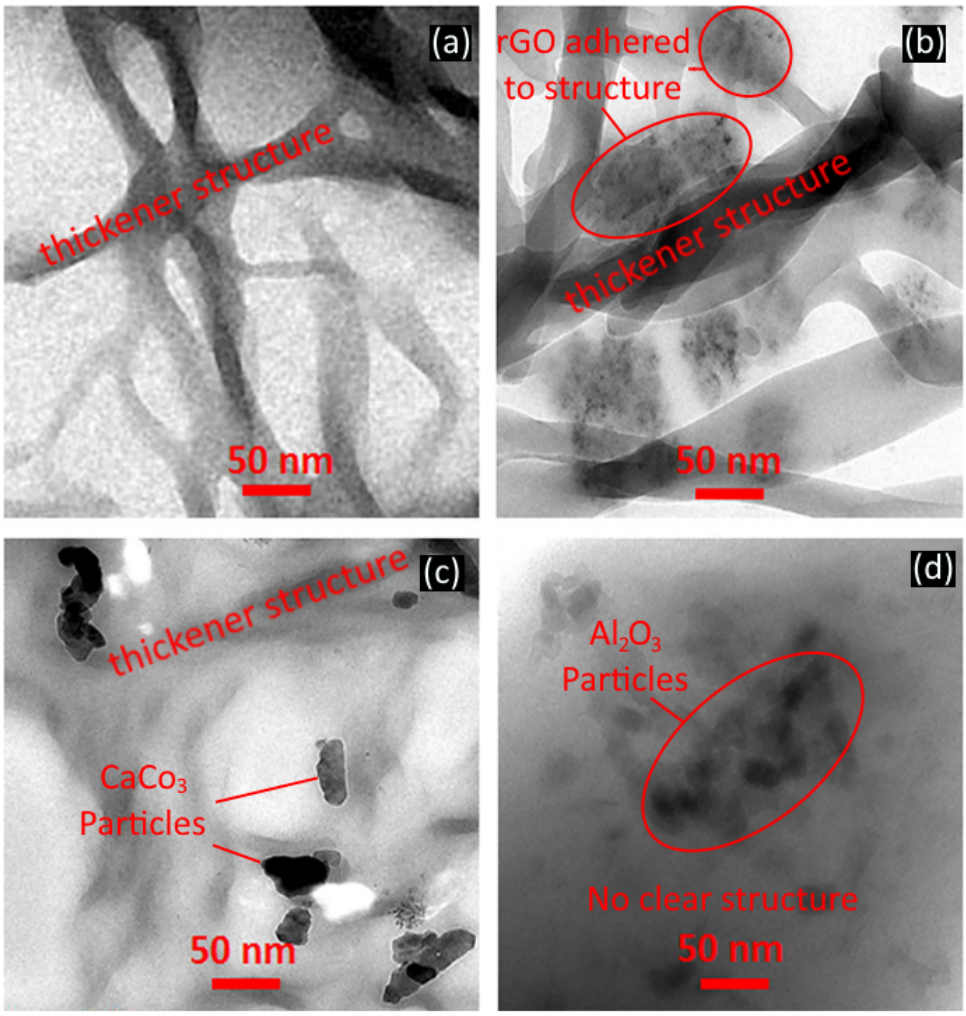

Figure 2.14: HRTEM images of mineral oil grease with lithium 12-hydroxystearate thickening structure (Adapted from Singh et al. (2018)). (a) without nanoparticles, (b) with rGO nanoparticles adhered to the structure, (c) with $CaCo_3$ nanoparticles and (d) with Al_2O_3 nanoparticles and no visible lithium structure.

The rGO grease had the greatest reduction in friction and wear in the four ball tribotester (392 N at 1200 rpm for 1 h at 75 °C). The described mechanism was that low shear strength between layers in the rGO reduced friction and the adherence of particles to the grease structure helped them be drawn into the contact. $CaCo_3$ also reduced both the COF and WSD when compared to the base grease. Raman spectroscopy found some other products such as CaO in the wear scars so the authors believed that some surface modification had occurred as well as possible third body interactions which were identified as the mechanisms by which friction was reduced.

The nanogreases, containing 1.5 wt%, 3 wt%, 6 wt% and 10 wt% NCB, were tested against the base grease in a SRV tester with a 10 mm AISI 52100 ball on a disc of the same material at 25 Hz and 200 N load (2.715 GPa p_o) with a 1 mm stroke for 10 min (Zhao et al., 2014). The COF for the base grease increased to around 0.135 over the first 250 s before gradually decreasing and settling at approximately 0.125. With 6 wt% NCB-grease, friction stayed consistently at 0.120. The Wear Scar Width (WSW) of the lower specimens showed a 15 % decrease compared to the control and further testing showed that the load carrying capacity doubled from 300 N to 600 N with the introduction of NCBs.

The authors hypothesised that at high loads, a rise in temperature in the contact area affected the lithium grease's film forming ability leading to scuffing and seizure between the friction pairs; the introduced NCBs formed a deposit layer and separated the rubbing surfaces. SEM images of the two lower wear scars from the initial 200 N load test showed the control to be severely worn with obvious grooves and deposits on the surface, by contrast, the NCB wear scar was very faint with manufacturer's finishing marks still visible. XPS spectra showed peaks in the Ca 2p region relating to calcium oxides. The B 1s region was very noisy but the authors suggested small peaks pointing to B_2O_3 combined with the calcium oxide peaks meant that tribochemical reactions had occurred and a protective tribofilm had been formed. Without comparison to the control peaks or to known spectra for calcium borate, it is difficult to prove that any reactions have occurred.

In Fu et al. (2019)'s paper, the four concentrations of graphene particles were compared with the base grease in a four-ball-tribotester at 1200 rpm and 400 N load for 1 h. Given that the initial Hertzian contact diameter was 0.3 mm and the smallest wear scar was 31 % greater than that, the authors surmised that boundary lubrication conditions had been met. The 2 wt% mixture produced the smallest wear scars and the lowest COF in the above stated test. When the load was reduced below 300 N, the base grease had the smallest wear scar. Changing the rpm of the test had little effect on the COF across the greases though the wear scars did increase with speed. The authors did not state if

the length of the test was kept constant, or the number of revolutions. If time was kept constant, then the increased travel over the contact area would be expected to lead to the increased wear scar diameter. Thermal conductivity and diffusivity increased with Graphene concentration. Although extensive testing was done to show which concentrations of graphene in the unspecified grease performed best in a variety of tribological regimes, very little analysis was done to understand the mechanisms of improvement.

These papers show that good dispersion of nanoparticles can be achieved and under high pressure conditions, the additives can have a beneficial effect. Using greases could be one method for keeping additives in the contact of a mechanical finishing process. Further study is needed to understand if some additives can damage the grease structure to the point that they are no longer able to provide good dispersion.

2.4 Mechanochemical surface modification

As discussed in section 2.2, when using sulphide TMDCs, new metal sulphides can be formed on the surface with the substrate metal during the wear process. This is caused by a mechanochemical reaction occurring due to the nanoparticles wearing against the metal (Tannous et al., 2011). Sintering sulphides into metals has also been shown to improve tribological properties even in dry friction (Sato et al., 2016). This section looks at taking these mechanisms out of the wear process and applying them to methods of mechanical finishing before the materials are worn. The idea is to take the beneficial effects of the tribofilms formed by TMDCs without the commercial and environmental difficulties of using nanoparticles in fully formed lubricants (Oberdörster et al., 2005; Rabaso et al., 2014a).

Varenberg et al. (2016) shot-peened cast iron with hard Al_2O_3 microparticles and much softer Cu_2S microparticles, first separately then combined, and ran a friction and wear test on each of them in base oil (SN 90). The results were then compared to an unpeened surface. Al_2O_3 smoothed and hardened the cast iron surface through plastic deformation, while the Cu_2S was there to reduce on the surface of the iron and create iron

sulphates and sulphides. A schematic of the shot-peening system and the hypothesised surface interactions are shown in Figure 2.15.

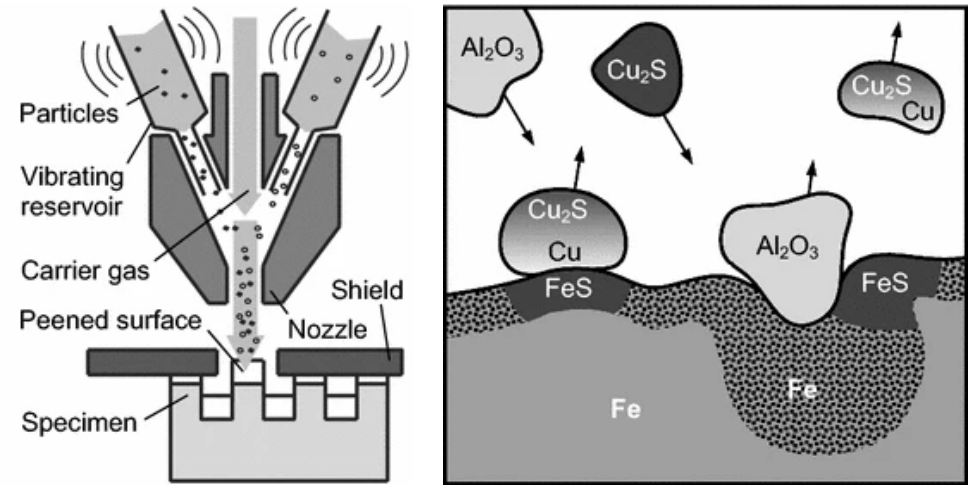

(a) Shot peening system (b) Surface–Microparticle interactions

Figure 2.15: The shot-peening system for delivering Cu_2S and Al_2O_3 microparticles to the cast iron surface and a graphic of the proposed interactios (Varenberg et al., 2016).

The reduction potential of a chemical species is defined as its tendency to be "reduced" by gaining an electron (Gupta et al., 2016). The opposite of reduction is Oxidation. If a substance is highly likely to oxidise (like iron) it is more difficult for it to lose that oxygen bond once formed. In other words, it is harder to cause a reduction reaction, therefore it has a low reduction potential. More stable metals, that are harder to oxidise (like gold), have a much higher reduction potential, so they have a greater tendency to lose that oxygen bond. Due to the positions of oxygen and sulphur on the periodic table, it can be assumed that elements with high reduction potential have a similar tendency to lose a sulphur bond. Varenberg et al. (2016) chose Cu_2S over WS_2 or MoS_2 as copper has a higher standard reduction potential (Vanýsek, 2010) than either molybdenum or tungsten, so it should be more likely to lose sulphur to the iron. Copper sulphide has also been shown to rapidly reduce mechanochemically with iron and magnesium by Calka et al. (2009).

Separately, the Al_2O_3 and Cu_2S peened surfaces reduced the COF from ≈ 0.1 to ≈ 0.08 and ≈ 0.06 at their lowest, respectively (Varenberg et al., 2016). When used together, the COF reached just a little more than 0.01. The presence of iron sulphide and sulphate

when using Cu_2S was confirmed through XPS. The surface analysis was performed after the wear test so it is not known if the Fe-S bonds were formed by the shot peeing or during wear. The initial maximum Hertzian contact pressure for these experiments were 3.8 or 6.3 MPa in base oil with a sliding speed between $0.1\,\mathrm{m\,s^{-1}}$ and $0.9\,\mathrm{m\,s^{-1}}$. The highest speed was when the very low friction occurred. At the lower speeds, the surface only shot-peened with Cu_2S had the lowest friction ≈ 0.115. This suggested that although the Cu_2S peened iron produced a softer surface, a protective sulphide film was more beneficial in the more severe regime. The higher friction in the hybrid surface may have been due to the presence of loose alumina particles ploughing through the surface when at higher speeds the lubricant film was thick enough for this not to occur.

Stav et al. (2019) performed a similar shot-peening process with the same microparticles on cast iron. Though they were able to show a reduction in friction across the Stribeck curve, they believed that the XPS peaks they observed were indicative of Cu_2S and Cu_2SO_4. Though the formation of iron sulphides and sulphates were possible, these would have to be much smaller concentrations than those measured for the copper compounds.

A development on Varenberg et al. (2016)'s paper uses a similar shot-peening technique to improve the surface of a cutting tool (Qi et al., 2019). Though the cutting forces were not significantly improved by the hybrid system, the cutting tool surface was less worn after the operation. The EDS maps of the tool after the cutting process suggested that they had successfully created a sulphide surface on the tool though chemical bond analysis was not used to confirm this. The pre-cutting EDS maps showed high concentrations of copper and sulphur and low iron, so it is still unclear if the iron sulphide was formed by the shot peening or during the cutting process.

Though some of the mechanisms for improvement are still unclear, the research into mechanical finishing processes that combine hard and soft particles interacting with a metal surface show that they can produce a mechanochemical interaction that improves its tribological properties. Alternative finishing processes could benefit from research using similar particular additives.

Triboconditioning

Triboconditioning® by Applied Nano surfaces (ANS, Uppsala, Sweden) is a surface finishing process that combines burnishing with deposition of a tribochemical compound. The extreme pressure from the mechanical treatment on the component surface with the deposited compound forms a low-friction antiwear film based on tungsten disulphide in a single finish operation (Zhmud, 2012). This process has been shown to significantly reduce the surface roughness of commercial engine cylinder bores even compared to ones that have been run-in for 200 h (Zhmud et al., 2020). Unfortunately, there is little information on the tribochemical compound or the exact process of triboconditioning as it is a commercial secret. Similarly it is unclear how the compound is bonded to the surface, whether or not is similar to a WS_2 tribofilm or if it is a compacted film that has adhered to the original surface instead.

Though Triboconditioning® appears to be a commercially viable mechanical finishing process with a chemical aspect to it, there is very little technical information about the process itself. Where it stands in relation to the research discussed in this review is unclear and very little in the way of inspiration for possible developments in a mechanochemical finishing process can be gained.

2.5 Understanding to innovation – aims and objectives

2D nanoparticles such has TMDCs and graphene have been shown to be beneficial in lubricated regimes at reducing friction and wear though there have been issues with introducing them to fully formulated oils ready for commercial use. Their known mechanism for reducing friction and wear is easy sliding between layers and protective tribofilm formation. Hard spherical nanoparticles such as SiO_2 and Al_2O_3 are known to reduce friction and wear by separating contacts, surface polishing and acting as nanobearings, turning sliding into rolling friction. Some research has been done to combine these two different types of nanoparticles but the mechanisms for their interaction are still not properly

understood.

The successful sulphide tribofilms that MoS_2 has been shown to form during wear has led to research into using a mechanical finishing process, shot peening, with hard Al_2O_3 and soft Cu_2S particles in an attempt to mechanochemically create a sulphide layer on the surface of cast iron with beneficial tribological properties. Further research into other mechanical finishing processes to generate a mechanochemical reaction could lead to exciting possibilities for real word applications.

These discoveries through the study of the reviewed literature have led to the following aims and objectives:

Aim: To begin the development of a new mechanochemical finishing process that reduces friction and wear in metal components.

Objectives:

1. Prove the concept of using a simple mechanical finishing process with sulphide additives to induce a tribofilm-like surface.

   Measures of success:

   (a) Observe new metal sulphides that were not produced without additives through use surface analysis equipment such as EDS and XPS.

   (b) Determine the mechanisms by which these reactions occurred supported by experimental analysis.

   (c) Outline avenues for improving and optimising the process.

2. Understand the synergistic properties and mechanisms of nanoparticles that offer mechanical improvements working with nanoparticles that are more chemically reactive in hybrid nanofluids.

   Measures of success:

   (a) Show statistically significant improvements in friction and/or wear with hybrid nanofluids when compared to separated equivalents.

   (b) Develop a provable hypothesis for at least one synergistic mechanism that is supported by observations through a range of surface analysis techniques, including XPS, EDS and profilometry.

3. Discover if the mechanochemically generated surfaces in objective 1 offer tribological benefits over purely mechanical processes.

   Measures of success:

   (a) Observe statistically significant reductions in friction and/or wear when compared to purely mechanically finished samples.

   (b) Develop provable hypotheses for tribological mechanisms leading to any improvement or otherwise, supported by friction data and surface analysis techniques.

4. Develop a method of surface finishing that keeps additives in the contact patch.

   Measures of success:

   (a) Visual inspection of interacting surfaces during and after the finishing process shows additives in the contact area.

   (b) A consistent coverage of chemically bonded additive material with low variance in concentrations within and between specimens.

Novelty The expected novelty of the work undertaken in this thesis will be in two key areas. Firstly, the research undertaken will improve the understanding of synergistic mechanisms between hard ceramic nanospheres and chemically reactive TMDCs when acting together as additives in a lubricant. Secondly, this work will aim to show that a new method of mechanochemical finishing that uses less specialist equipment than previously researched can be used to change both the physical and chemical properties of a surface for improved tribological performance.

Chapter 3

Methods and Materials

3.1 Introduction

This chapter presents all the necessary methods and materials used to understand the mechanisms of tribofilm formation and attempt to mechanochemically generate a tribologically superior surface through a mechanical finishing process.

3.2 Friction and wear

Throughout the thesis, the focus of the tribological testing is on specimen tests. These are cheaper and have potential for more widely applicable results than component, system or full machinery tests with finer control over individual variables (Institution of Mechanical Engineers, 2014). Any positive results found in these simpler tests, however, would need further experimentation in the more complex test environments in order to show applicability to real world applications.

Contact mechanics

A variety of geometries for the contact area between contacts are employed in tribological research. Fuel lubricity tests such as ASTM D6079 uses point contact or ball-on-flat geometry (Jääskeläinen, 2006) which typically has the highest contact pressure along with the four-ball tribotester which is one bearing pressed into and spun against three stationary bearings (Peña-Parás et al., 2015). The lowest contact pressure occurs with area contact, when pin-on-disc/flat-on-flat geometries are used (Galda et al., 2016). A final geometry used in this thesis is line contact, which is a cylinder with its curved surface sliding on a flat plate (Gelinck and Schipper, 2000). The size of the contact area and the pressure acting on that area is calculated using Hertzian contact mechanics (Hutchings and Shipway, 2017). Point, line, and low pressure contacts are used in the research presented in this thesis.

Point contacts: Relevant when two balls are in contact or a ball with a flat surface. The contact radius r under normal load P is given by:

$$r = \sqrt[3]{\frac{3PR^*}{4E^*}} \tag{3.1}$$

Where R^* is the relative radius between the contacting bodies (when one body is flat, R^* is simply the radius of the ball) and E^* is the reduced modulus which is calculated from the Young's moduli (E_1 and E_2) and Poisson's ratios (υ_1 and υ_2) of the respective surfaces with:

$$\frac{1}{E^*} = \frac{1-{\upsilon_1}^2}{E_1} + \frac{1-{\upsilon_2}^2}{E_2} \tag{3.2}$$

The maximum and mean Hertzian contact pressure (p_o and p_m respectively) are given by:

$$p_o = \frac{3}{2}p_m = \frac{3P}{2\pi r^2} = \sqrt[3]{\frac{6PE^{*2}}{\pi^3 R^{*2}}} \tag{3.3}$$

For anything other than full hydrodynamic lubrication, the contact area will increase during wear, so these calculations will only give the initial values for r, p_o and p_m.

Line contacts: Applies when a cylinder is in contact with a flat surface. The contact area is a rectangle of length L by width $2b$, where the value of b is given by:

$$b = \sqrt{\frac{P}{L}\frac{4R^*}{\pi E^*}} \tag{3.4}$$

Because the lower body is flat, R^* is the radius of curvature for the cylinder. The contact pressure equation for line contacts is:

$$p_o = \frac{4}{\pi}p_m = \frac{P}{L}\frac{2}{\pi b} = \sqrt{\frac{P}{L}\frac{E^*}{\pi R^*}} \tag{3.5}$$

Similarly to point contact, the area of contact will increase with wear.

Area contact: Occurs when both bodies are flat. The contact pressure is simply the normal load over the area of the smaller body. This would not be expected to change with wear.

Reciprocating motion: All the wear testing in this thesis will using reciprocating sliding. The aim is to generate a surface that is tribologically superior in a variety of applications. As reciprocating motion has a range in velocity, it operates along much of the Stribeck curve. Positive results in terms of reduction in friction and/or wear in the research undertaken will have more widely applicable results as the methods used will have to be effective in the full range of lubrication.

High Frequency Reciprocating Righ (HFRR)

The High Frequency Reciprocating Rig (HFRR) by PCS instruments (London,UK) is widely used for testing fuel lubricity specified by test method standards such as ISO 12156, ASTM D6079 and ASTM D7688.

The rig's frequency range is 10 Hz to 200 Hz, the stroke length can range from 20 µm to 2.0 mm and the maximum operating temperature is 450 °C. The standard upper specimen is a 6 mm⌀ ball and the lower specimen, a 10 mm⌀ disc. Its simplicity to set up and run make it popular for benchmark comparison tests between lubricants or the effectiveness of additives (Alves et al., 2016; Rabaso et al., 2014a). Friction, specimen temperature and contact potential are all taken in real-time through a host PC and software made by PCS instruments specifically for the HFRR. A Meiji metallurgical microscope (Meiji Techno UK, Axbridge, UK) fitted with a camera connected to the host PC allows for the upper specimen wear scar to be measured immediately after testing using the same software.

For the experimentation in chapter 5, HFRR tests were performed using PCS AISI 52100 bearing steel specimens analysing the effect of SiO_2 and MoS_2 nanoparticles in a variety of concentrations in SN 100 oil. Tests were performed at ambient temperature as a base level in line with literature (Xie et al., 2016a), and at 50 °C to increase the regime severity by reducing the viscosity of the lubricant and increasing the likelihood

of chemical reactions. Frequency was always 20 Hz, this value also taken from other nanoparticle literature (Alves et al., 2016).

Limitations: As the upper specimen is limited to a 6 mm⌀ ball only, contact pressure will always be very high. The normal load is applied via hanging free weights up to 1 kg below the contact point forming a maximum 9.81 N load. With the commonly used bearing steel AISI 52100 specimens, the initial maximum contact pressure ranges from 0.74 GPa to 1.60 GPa. This limited range reduces the applicability of the results to real world applications compared to machines capable of using a variety of specimens. Additionally, the HFRR uses an electro-magnetic oscillator on a pivot to generate the reciprocating motion. This oscillator and the specimen are on one side of the pivot and a counterweight is on the other which is set to exactly counterbalance an unloaded specimen arm containing the upper specimen. This is to ensure that the load applied to the contact for testing is the only normal force. However, when oscillation is in progress, the centre of mass for the unloaded system is constantly moving which means it is not always over the pivot so the normal force on the specimen is also changing (Plint, 2010). Assuming the counter balance is correct when the stroke is at the midpoint, the force is greater than the desired testing load when the specimen is furthest from the pivot and smaller when the specimen is closest.

TE 77 high frequency friction machine

The TE 77 High Frequency Friction Machine (TE 77) made by Phoenix Tribology Ltd (Kingsclere, UK) is a highly versatile reciprocating friction rig. Unlike the HFRR, the upper specimen holder is replaceable so can be fitted to hold balls for ball-on-flat, cylinders for line-on-flat, or discs as low pressure specimens. All of these upper specimens will be used in this thesis.

The stroke is provided by motor and cam box where the cam can be rotated on the motor shaft to change the stroke length between 0.4 mm and 25 mm. A load of up to 1000 N is applied separately by a load bridge acting directly over the contact area

and is unaffected by the position in the stroke. The TE 77's adaptability enables good reproduction of reciprocating contacts found in real-world applications (Kamps et al., 2015).

Test sequences and data acquisition is achieved through host PC software COMPEND 2000 also made by Phoenix Tribology. For this thesis, low speed data files were made with the modulus mean friction over each second recorded throughout each test giving an overview of general changes over time in the contact. High speed data can also be collected which can take measurements at 20 kHz allowing the change in friction over single stroke to be measured.

The geometries used throughout this thesis are shown in Figure 3.1.

TE 77 - low load adapter

Performing tests with the HFRR are an easy way to generate quick comparative friction data and is used for multiple standard fuel lubricity tests. However, Plint (2010) showed with moments that the way in which the load and stroke are provided causes the normal load to be inconsistent through the stroke. This is evidenced by wear scar profiles from the HFRR taken in chapter 5. The Low Load Adapter (LLA) for the TE 77 by Phoenix Tribology allows for the same tests to be performed as the HFRR but without the inconsistent load due to the mechanical drive system combined with the load bridge which are unaffected by stoke position or resistance force. Figure 3.2 shows the adapted TE 77 loaded for a test.

The load arm provides a 4:1 conversion between the weight applied to the arm and the normal load acting in the contact, so a 200 g (1.96 N) load applies a 7.85 N force to the contact. Wear scars from tests in the HFRR are not directly comparable to those taken with the LLA as due to differences in the methods for loading and actuation, the LLA consistently produces large wear scars according to Plint (ibid.).

In chapter 5, a variety nanofluid mixtures are tested using the LLA as a continuation of work performed using the HFRR.

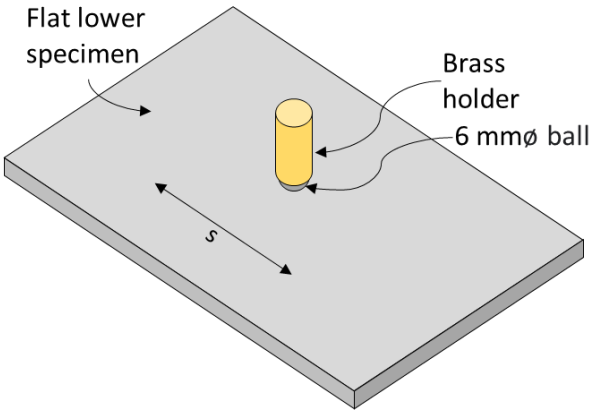

(a) Point contact: used in chapter 6 and with the Low Load Adapter in chapter 5

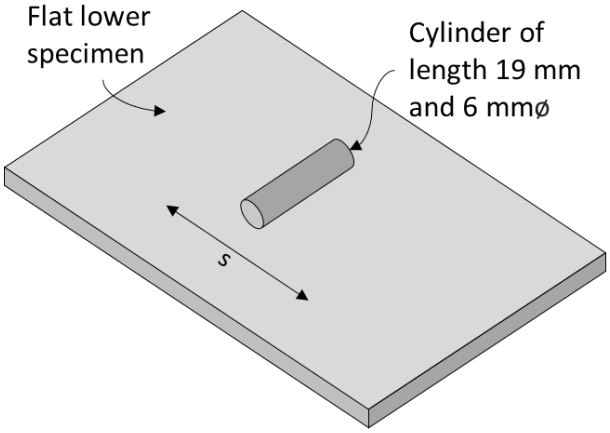

(b) Line contact: used in chapter 4 and chapter 6

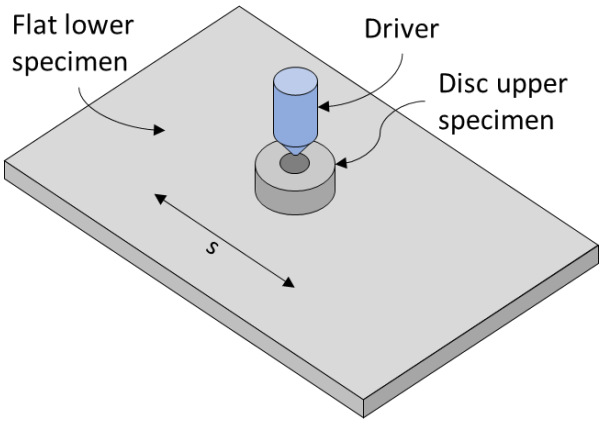

(c) Area contact: used in chapter 4

Figure 3.1: Schematics of TE 77 contact geometries used during thesis.

Figure 3.2: Image of TE77 low load adapter

3.3 Morphology and characterisation

In tribology, it is key to understand the mechanisms that cause changes in friction and wear. Visualisation of physical damage such as scratches, pits or scuffs as well as an overall surface roughness need apparatus capable of sensitivity down to at least individual microns. If nanoparticles are being used in a lubricant then their morphology must also be understood. Chemical changes can also occur in the top few nanometres of a worn surface, particularly if different materials are being worn together or additives are used in the lubricant, therefore methods for characterising the atomic make up of a surface are also needed. This section details the methods and apparatus employed throughout this thesis to analyse wear scars and the morphology of nano-additives.

Alicona InfiniteFocus microscope

The Alicona InfiniteFocus (Bruker Alicona, Graz, Austria) is an optical microscope that uses focus variation to build a true colour 3D image of the measured surface. This is achieved by moving the camera vertically through the optical axis, continuously receiving image data from the surface and then converting all the received data into 3D information

by analysing the variation in focus along the vertical axis. Software in the host PC allows for cross-section profiles to be taken of the measured surface so that surface roughness values for a specific area such as a wear scar can be obtained. A mounting stage with x, y & z-control enables scanning of multiple areas on a single specimen to build a larger 3D image.

The Alicona InfiniteFocus was utilised in chapter 5 for scanning the HFRR wear scars. The data taken was employed to analyse cross-sectional wears scar depth profiles and calculate wear scar volume. In chapter 6, 3D false-colour images were taken to show wear scar depth along the stroke. There is not a global origin on the Alicona, so for each scar, 0 in the *z-axis* was estimated to be the unworn specimen surface. It was preferred to other profilometry techniques such as a stylus profilometer as it enables the taking multiple measurements quickly from a single scan and the 3D images it produces offer a more human readable comparison between wear scars.

Hitachi TM3030 - SEM and EDS

Scanning Electron Microscopy (SEM) A focused high-energy electron beam is scanned across a surface in a vacuum to produce an image at much greater magnification than is possible with an optical microscope (in some cases, down to 1 nm). When the high-energy electrons interact with the surface the energy is dissipated through a variety of signals. This signals include Back Scatter Electrons (BSE), secondary electrons, and photons (characteristic X-rays). Detectors read the BSEs and secondary electrons to form the SEM image. Secondary electrons originate from the sample surface and are a result of an interaction between the electron beam and the sample. They have a lower energy than the backscattered electrons and help to show morphology and topography. BSEs are electrons from the original beam that have been deflected by the nuclei of atoms in the sample. Heavier nuclei deflect electrons more strongly so appear brighter in the image than those of smaller nuclei where less electrons are deflected enough to leave the material, so impurities and contrasts in surface composition can be indicated through

these BSEs (Egerton, 2016a).

The electron beam penetrates the sample to the depth of a few microns. Penetration depth depends on the accelerating voltage and density of the material. Figure 3.3 shows how the signals change with sample depth. Backscattered electrons originate from deeper in the surface than secondary electrons, which explains why BSEs are not useful for observing surface topography.

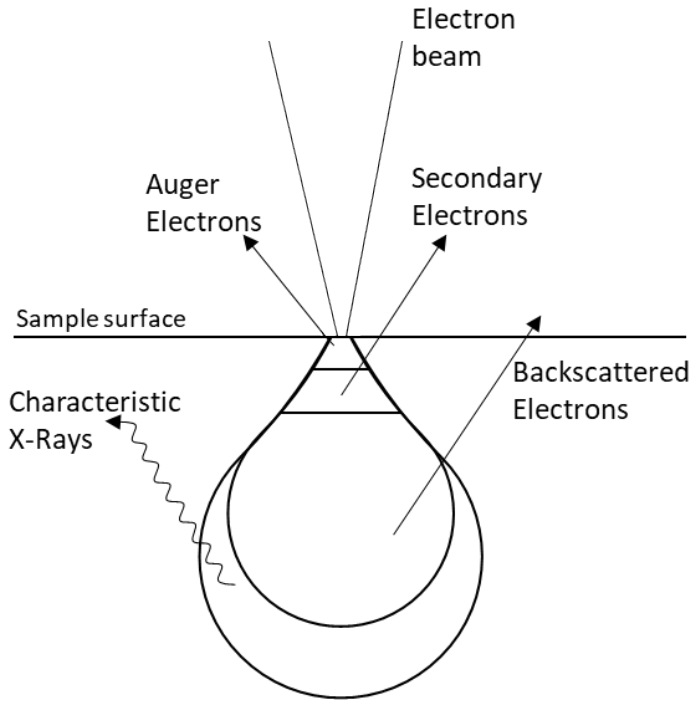

Figure 3.3: Dissipated signals from electron beam in SEM

Energy Dispersive X-Ray Spectroscopy (EDS) Sometimes denoted "EDX", Energy Dispersive Spectroscopy (EDS) is usually attached to an electron microscopy instrument as one of the signals generated as a result of dissipating energy from the electron beam are X-rays that can be used to characterise the atoms from which they were emitted. These X-rays are generated when a high energy electron from the beam excites an electron in the inner shell of an atom which is ejected from the shell causing an electron from a higher energy outer shell to fill the hole left behind. The difference in energy between the two cells is released in the form of an X-ray, the wavelength of which is unique to each element (Telegdi et al., 2018). An energy-dispersive spectrometer measures the emitted

x-rays and indicates the corresponding elements present in the sample. Coupled with a SEM, it enables an accurate map of the elements present in the sample to be generated. As indicated in Figure 3.3, characteristic X-rays are typically emitted from a few microns deep in the sample. In the case of analysing tribofilms, if the film is only nanometres deep, then they may not be observed by EDS.

Hitachi TM3030 tabletop SEM This easy to use SEM machine is utilised in every experimental chapter. It is fitted with BSE and Bruker Quantax EDS detectors. The Hitachi TM3030 (Hitcahi High-Tech, Krefeld, Germany) is capable of up to 60 000× zoom enabling quick and easy surface imaging of wear scars down to individual microns. The EDS detector enables observation of the elements present in the surface which in combination with the SEM images give evidence to the wear mechanisms present in the lubrication regime and some of the friction and wear reductive mechanisms that any additives may have introduced. The lack of secondary electron detection mean that sample topography is not obvious from the images and other analytic methods are needed such as the Alicona InifiniteFocus.

Jeol 1400 - TEM

Transmission Electron Microscopy (TEM) An electron beam is aimed at a specimen stage in a vacuum. The kinetic energy of the beam is strong enough to pass through thin areas of a TEM specimen to the detector (Egerton, 2016b). Electrons that come into contact with specimen can be scattered and do not reach the detector so these areas appear dark on the generated image and where the direct beam hits the detector, these areas come up bright giving a 2D image of the specimen. In the case of highly crystalline structures the electron beam can be scattered onto the detector in a diffraction pattern which can indicate the orientation of the crystals (Williams and Carter, 2009), though this will not be utilised in this thesis. Some TEMs have resolutions capable of observing the position of individual atoms. In tribology TEM is regularly utilised for analysing the morphology of nanoparticles.

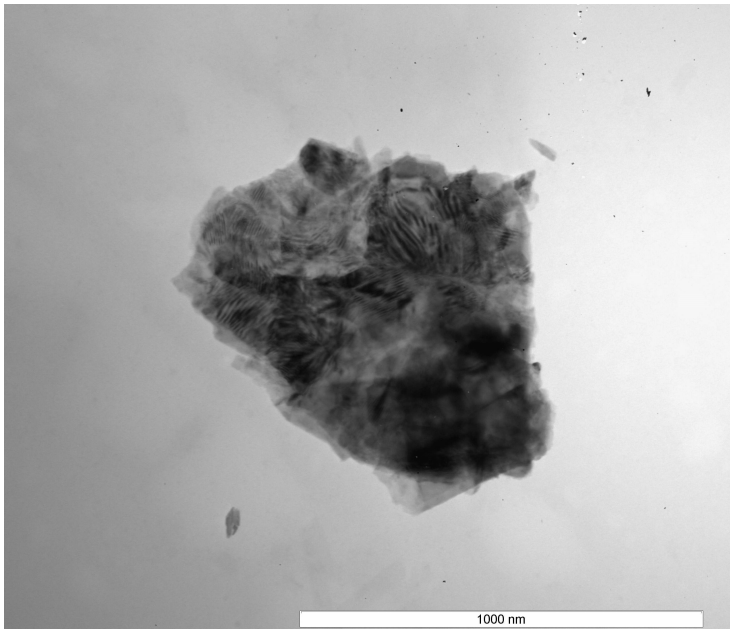

Figure 3.4: An agglomeration of MoS_2 nanoparticles observed using the Jeol JEM-1400 at 80 000× magnification.

Jeol JEM-1400 This TEM was operated in chapter 5 for examining the size and morphology of MoS_2 and SiO_2 nanoparticles. The JEM-1400 (JEOL Ltd, Tokyo, Japan) was run at 80 kV accelerating voltage. Nanoparticles were dispersed in water or ethanol. One drop of the solution was deposited on carbon microgrid paper then left to dry before being observed in the TEM. Images were taken with between 80 000× and 400 000× magnification. Figure 3.4 is an example image taken using the Jeol JEM-1400.

XPS

X-ray Photoelectron Spectroscopy (XPS) is a chemical analysis technique that provides information about the material composition based on the electronic state of the species present in the material (Asefa and Dubovoy, 2017). An X-ray beam, is emitted from an anode material, usually Al Kα or Mg Kα. These anodes have photon energies of 1486.6 eV and 1253.6 eV respectively. The X-ray beam interacts with the molecules on the specimen surface in high vacuum. The absorption of X-ray photons by the sample ionises surface atoms and inner-shell electrons are emitted. The energy of these emitted electrons is equal to their binding energy in the atom so analysing the electron gives details of the atom from

which it was ejected. The binding energy is affected by the chemical environment so if an atom is chemically bonded, there is a shift in the energy of the emitted electron. This shift can be detected, giving information on the chemical bonds in the sample surface (Tougaard, 2013). XPS is highly surface sensitive, detecting with a probing depth of ≈1 nm to 10 nm.

In chapter 4, samples were analysed using an AXIS Supra XPS (Kratos Analytical Ltd, Manchester, UK) at Aston University (Birmingham, UK) to discover if iron – sulphur bonds hand been formed on cast iron specimen surfaces. The Al anode Kα source gave a photon energy of 1486.6 eV. The Kratos Axis Ultra Hybrid was also utilised in chapter 5 at the University of Manchester using the same source anode to understand the composition of chemical species in steel specimen wear scars.

HAXPES

Hard X-Ray Photoelectron Spectroscopy (HAXPES) is generally defined as XPS which uses X-ray energies above 2 keV. The advantage of higher energy photons is that the beam is able to penetrate deeper into the sample, giving chemical analysis of the bulk material rather than just the top few nanometres in the surface. Until recently the vast majority of HAXPES had to be performed using a synchrotron (a type of cyclic particle accelerator)(Hendel et al., 2016; Ueda et al., 2010). Only in the last ten years have laboratory-based HAXPES systems started to have a competitive energy resolution and speed of acquisition using Chromium (Kα= 5.42 keV) or Gallium (Kα= 9.25 keV) based X-ray sources (Kalha et al., 2021).

In chapter 5, specimens were analysed using the HAXPES Lab (Scienta Omicron, Uppsala, Sweden) at the University of Manchester for further species identification in the wear track of steel specimens. This machine was the first laboratory based HAXPES in the world that uses a monochromated liquid metal Ga Kα source, giving a photon energy of 9.25 keV. It produces sampling depths in excess of 30 nm (Regoutz et al., 2018). All data obtained using the HAXPES was analysed using CasaXPS (Casa Software Ltd,

Teignmouth, UK).

Thesis map of analytical apparatus

Table 3.1 is a simple table showing which chapters each of the discussed morphology and characterisation methods were used for easy reference.

Table 3.1: A map of the morphology and characterisation apparatus used in each experimental chapter.

Analysis apparatus	**Chapter**		
	4	**5**	**6**
Alicona	–	✓	✓
SEM/EDS	✓	✓	✓
TEM	–	✓	–
XPS	✓	✓	–
HAXPES	–	✓	–

3.4 Materials

Table 3.2 lists all the particles used as additives in mechanical processes throughout the thesis based on the work of Varenberg et al. (2016) and Xie et al. (2016a).

Table 3.2: Particles used as additives in mechanical processes throughout the thesis listed alphabetically. Diameter is the maximum of any individual particle without agglomeration. Data taken from manufacturers' data sheets or obtained through observation(Honeywell Specialty, 2017; Sigma-Aldrich, 2017a,b, 2020). The chapters where these particles are studied are also shown

Particle	**Form**	**diameter**	**molecular weight**	**Chapters**
		μm	g/mol^{-1}	
Cu_2S	micro-powder	45	159.16	4, 6
MoS_2	2D nanoparticles	0.09	160.07	5
SiO_2	nanopsheres in ethanol	0.05	–	5
Al_2O_3	micro-powder	45	101.96	4, 6

Cu_2S microparticles and SiO_2 nanoparticles were obtained directly from Sigma Aldrich (Merck KGaA, Darmstadt, Germany) and Al_2O_3 from FischerScientific (Loughborough, UK)

SN100, an unadditised base oil was used as the base oil throughout most of the thesis. Its properties are shown in Table 3.3.

Table 3.3: Material properties for SN100.

density (km^{-3})	0.875
kinematic viscosity at 40 °C ($mm^2\,s^{-1}$)	20
kinematic viscosity at 100 °C ($mm^2\,s^{-1}$)	4
viscosity index	95
flash point (°C)	190

The specimens that were operated as contacts in tribological tests throughout the thesis are specified in Table 3.4.

Table 3.4: Specifications for the specimens used in wear tests throughout the thesis. The chapters in which each were used are also shown. Grey cast iron specimen finish and hardness was affected by processes performed in chapter 4, so initial values are not relevant.

Geometry	Material	Finish	Hardness	Chapters
Upper Specimens				
12 mm⌀ disc	mild steel	9 µm *Ra*	65-77 HRB	4
6 ⌀×19 mm cylinder	AISI 52100	0.1 µm	60-67 HRC	4, 6
6 mm⌀ ball	AISI 52100	0.05 µm *Ra*	58-66 HRC	5, 6
Lower Specimens				
60 × 20 × 4 mm plate	grey cast iron	–	–	4
10 mm⌀ disc	AISI 52100	0.02 µm *Ra*	190-210 Hv30	5
58 × 38 × 4 plate	BO1 tool steel	0.4 µm	62-64 HRC	6

3.5 Summary

This chapter sets out all the materials and methods applied throughout the experimental chapters in this thesis. The following items were included:

- A brief introduction to contact mechanics and a description of the three reciprocating motion experimental apparatus.
- A description of the variety of surface analysis equipment and techniques necessary for understanding the mechanisms in effect during the wear process.

- An outline of the micro and nano-additives utilised to improve the tribological performance of lubricants and surfaces.

All of these are utilised in order to achieve the aims and objectives outlined in chapter 2, to find a simple mechanical method for improving the tribological properties of metal components in reciprocating contact.

Chapter 4

Mechanical finishing with Cu_2S microparticles

4.1 Introduction

There has been a great deal of research conducted to assess the tribological properties of Transition Metal Dichalcogenides (TMDC) such as MoS_2 (Rabaso et al., 2014b; Tannous et al., 2011) and WS_2 (Ratoi et al., 2013; Wu et al., 2018) used as nano-additves for lubricants to reduce both friction and wear in recent years. This research is discussed in depth in section 2.2. When studying the tribological mechanisms by which these nanoparticles reduce friction, researchers have found tribofilms containing new metal-sulphur bonds between the sulphur from the nanoparticles and the substrate metal for both magnesium (Xie et al., 2016b) and steel (Ratoi et al., 2013; Tannous et al., 2011). These tribofilms are formed during the wear process.

The tribological properties of metal sulphides have been extensively explored, through both sintering (Sato et al., 2016) and self-lubricating sulphide coatings (Lee and Park, 2006) and have been shown to greatly reduce friction and wear.

As the mechanical process of wear has been shown to cause chemical reactions between metal sulphide particles and metal substrates to produce tribologically superior surfaces, some experimentation has been done using shot-peening, a mechanical finishing process, and copper sulphide to mechanochemically create a tribofilm-like layer on a cast iron surface before subjecting it to wear (Stav et al., 2019; Varenberg et al., 2016). Cu_2S microparticles when shot-peened alongside hard Al_2O_3 ceramic particles produced a sulphide/sulphate layer that could reduce friction in low pressure wear. Without the Al_2O_3, Varenberg et al. (2016) found that the chemical interaction between the Cu_2S and the cast iron was greatly reduced and tribological advantage diminished. This indicates a need for harsher mechanical conditions, in this case generated by the Al_2O_3, to enable the necessary environment for chemical reactions to occur.

Hypothetically, if a mechanical process such as shot-peening is capable of causing a mechanochemical reaction with the right additives, then other mechanical processes could also be capable of the same. Honing uses hard abrasive material, often made with silicon carbide or alumina abrasives, to remove asperities from a surface and improve the finish.

The abrasive could perform a similar role to Al_2O_3 particles in the mechanochemical shot-peening process as it causes high stress in localised positions on the surface. With the introduction of a sulphide with a high reduction potential in the contact between the abrasive material and the surface to be honed, a mechanochemical reaction may be encouraged and a tribologically superior surface generated.

The work presented in this chapter uses honing with added Cu_2S microparticles in an attempt to generate a mechanochemical reaction with a cast iron surface forming a protective sulphide layer with superior tribological properties to the original surface. As a simple initial way to introduce Cu_2S to the honing process, the microparticles are spread on grit paper and honed against a cast iron substrate. This method will need refinement for future development but is effective as a proof of concept technique. Cu_2S is chosen because copper has a higher standard reduction potential than either molybdenum or tungsten (Vanýsek, 2010) and copper sulphide has been shown to rapidly reduce mechanochemically with iron (Calka et al., 2009).

4.2 Materials and methods

Materials

Cu_2S microparticles of $<45\,\mu m\varnothing$ in powder form were acquired from Sigma-Aldrich. Lower specimens suitable for the TE 77 High Frequency Friction Machine (TE 77) were manufactured from a grey cast iron rod and two sets of upper specimens were used: 19 mm long AISI 52100 steel cylinders of $6\,mm\varnothing$ for a line contact (Figure 3.1b) and $12\,mm\varnothing$ mild steel discs which were ground to 1200 grit ($\approx 9\,\mu m$ abrasives) to be used as low pressure specimens (Figure 3.1c). SN100, a simple hydrocarbon base oil, was the lubricant for all the wear tests.

Honing process

Honing was performed using 600 grit (600 µm abrasives) silicon carbide paper. Initially, 100 mg of Cu_2S was spread on the paper then the cast iron specimens were honed by hand using a simple rig that ensured honing at 60 deg to the wear direction. The quantity of Cu_2S spread onto the paper was later increased to 1 g to increase the sulphide uptake to the iron surface. Control samples were also honed using the same paper but without the addition of Cu_2S particles. Specimens were cleaned with acetone in an ultrasonic shaker to remove any loose material from the surface.

In every iteration of the process, at least three specimens including Cu_2S and the same without were honed.

Surface analysis

Surface analysis was performed on all the honed lower specimens using the Hitachi TM3030 desktop Scanning Electron Microscopy (SEM) machine with Energy Dispersive Spectroscopy (EDS) capabilities to assess the honed surfaces and identify any increase of sulphur in the cast iron surface. Some specimens were then analysed using AXIS supra X-ray Photoelectron Spectroscopy (XPS) at Aston University's Energy and Bioproducts Research Institute to understand if iron sulphides or sulphates had been formed by the honing process.

Wear tests

Wear tests were performed on the TE 77. The upper specimen was initially a 19 mm long AISI 52100 steel cylinder with a 6 mm⌀. Experiments were conducted at 2.5 Hz with a 12.5 mm stroke, this lead to a maximum sliding velocity of $\approx 0.1\,\mathrm{m\,s^{-1}}$. In order to understand how a variety of loads would effect friction in the modified surface, a load ramp test was used. The load increased by 50 N every 15 min from 50 N to 200 N (p_o 142 MPa to 283 MPa) leading to a total runtime of 1 h.

Further wear tests were performed after changing the upper specimen to a 12 mm⌀ disc. The load was set to a constant 286 N leading to a maximum initial Hertzian contact pressure of 3.8 MPa. The reciprocating speed was set to 23 Hz while the stroke was kept at 12.5 mm to give a maximum sliding speed of 0.9 m s^{-1}. These parameters were selected to create a similar environment in the centre of the stroke to that seen in Varenberg et al. (2016)'s paper where greatest friction reduction was seen.

4.3 Results and discussion

Surface analysis

After the first attempt at honing with 100 mg of Cu_2S, the cast iron plates were compared to controls that were honed without the microparticles under SEM. Figure 4.1 shows an example of both.

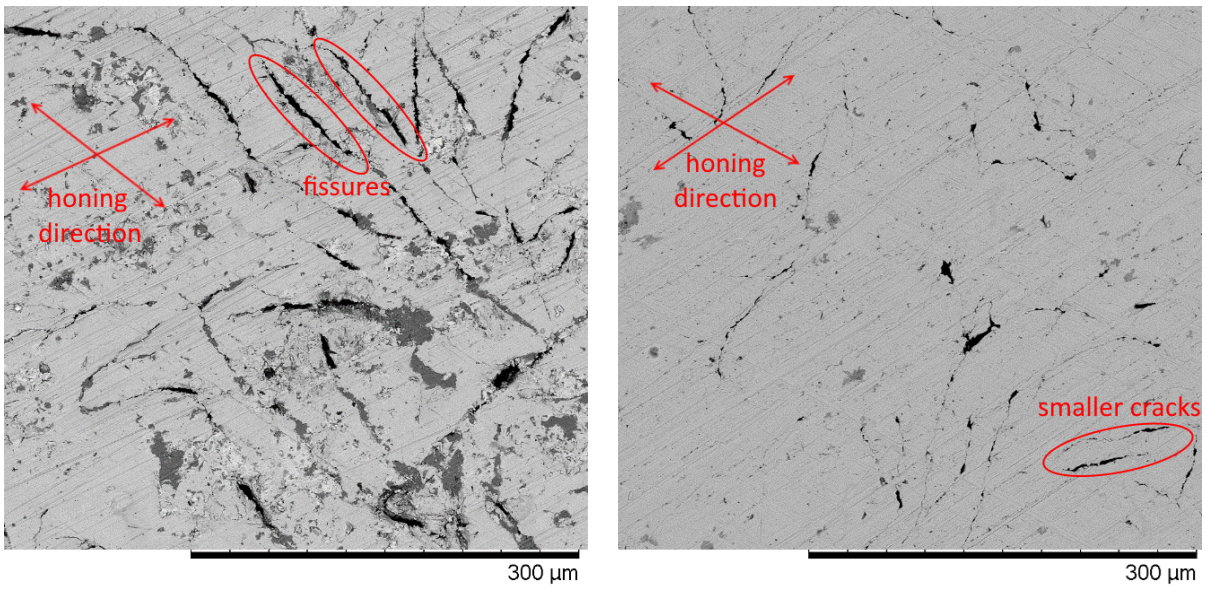

(a) Control honed sample (b) Sample honed with 0.1 g Cu_2S

Figure 4.1: SEM images of cast iron samples honed a) without Cu_2S and b) with 0.1 g of Cu_2S microparticles

In Figure 4.1a, the direction of honing can clearly be seen as well as a multitude of large fissures. These cracks are also present in the specimen honed with Cu_2S but significantly smaller (Figure 4.1b). The cracks were likely pre-existing defects in the material and not

a result of the honing process. One hypothesis is the less damaged appearance of the Cu_2S honed sample could be a result of the soft Cu_2S microparticles being smeared into the defects having a "surface healing" effect similar to how nanoparticle lubricants can fill asperity valleys forming a smoother surface (Seyedzavvar et al., 2020). Varenberg et al. (2016) found that the surfaces shot-peened with only Cu_2S produced a smoother surface but with lower hardness than any of the other surfaces. A similar process may have been observed here. EDS spectra for the samples actually showed a reduced quantity of copper in the additised samples compared to the controls (from 3.25 % to 1.56 %, Figure 4.2), however the average sulphur content increased to 0.34 atomic% when grey cast iron has <0.1 % ordinarily. This suggests that the cracks have not been filled by the microparticles, but that some mechanochemical reaction has occurred as a higher quantity of sulphur is present than can be accounted for by pure Cu_2S and what was already in the iron.

In an attempt to further increase the sulphur uptake of the cast iron, the honing process was repeated with an increased quantity of Cu_2S microparticles (1 g) spread on the silicon carbide paper. The mean atomic percentage of copper and sulphur in the different samples is shown in Figure 4.2. SEM images were taken of the new samples and EDS was performed on the surface. An SEM image of a honed sample, along with EDS maps showing copper and sulphur in the same region can be seen in Figure 4.3.

There is a greatly increased quantity of sulphur (1.7 %) in this specimen compared to the control or the samples honed with only a tenth of the Cu_2S. The EDS maps in Figure 4.3 show that the sulphur appears in regions where copper is also present. This suggests that most of the sulphur has not reduced from the Cu_2S and formed Fe-S bonds, rather Cu_2S has become smeared and embedded in the surface of the substrate material. Figure 4.2 shows that the increase in copper was significantly greater in quantity than that of sulphur. If all the additional copper present was still in the form of Cu_2S then there would be no more than double the atomic percentage of copper than sulphur. In fact, the quantity of additional copper is eight times greater than that of sulphur. This indicates that the honing process generated an environment that was sufficient to cause reduction reactions to occur in the microparticles but instead of iron sulphide forming,

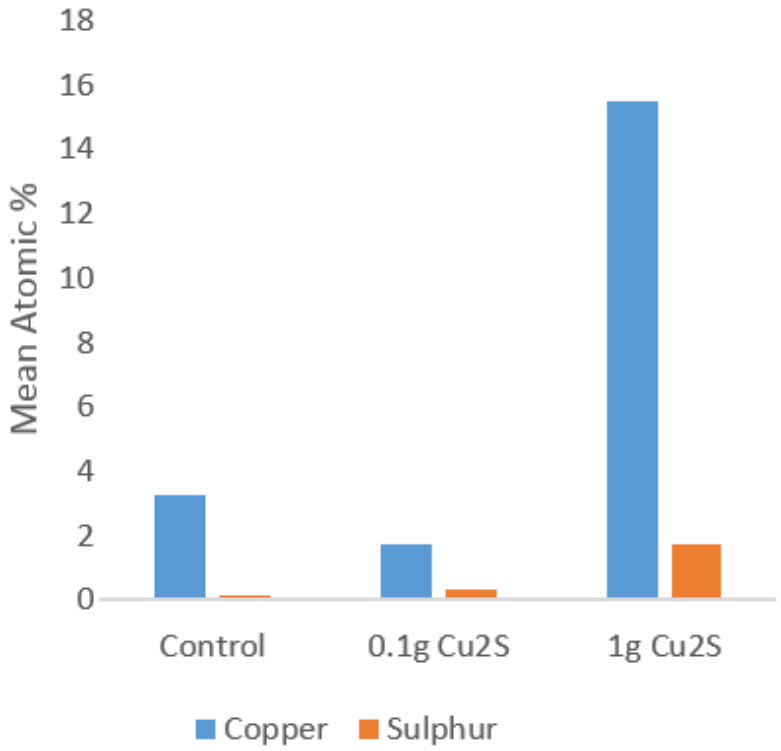

Figure 4.2: Atomic % of honed surfaces made up of copper and sulphur as shown by EDS

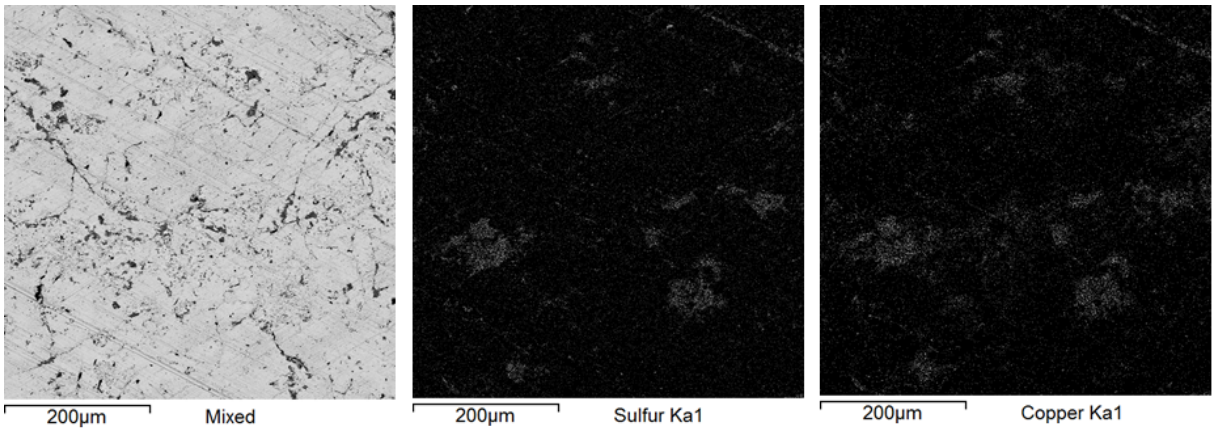

Figure 4.3: SEM image of 1 g Cu_2S honed sample and EDS maps showing sulphur and copper

the copper has combined with the iron, perhaps in a tribosintering process (Tao et al., 2018), and most of the sulphur has been lost.

XPS

XPS analysis was performed on three of the samples honed with 1 g of Cu_2S. An example of the S 2P spectra can be seen in Figure 4.4. There is a double peak at ≈161.5 eV and

≈162.7 eV which is typical of metal sulphides and another much smaller peak ≈168.7 eV which is representative of metal sulphides. In combination with the the EDS results the XPS spectra suggest that the majority of the sulphur present in the analysed sample is in the form of Cu_2S embedded in the surface, however there could be a small quantity of iron sulphides and sulphates present represented in the smaller sulphide peak (162.7 eV) and the sulphate peak at 168.7 eV.

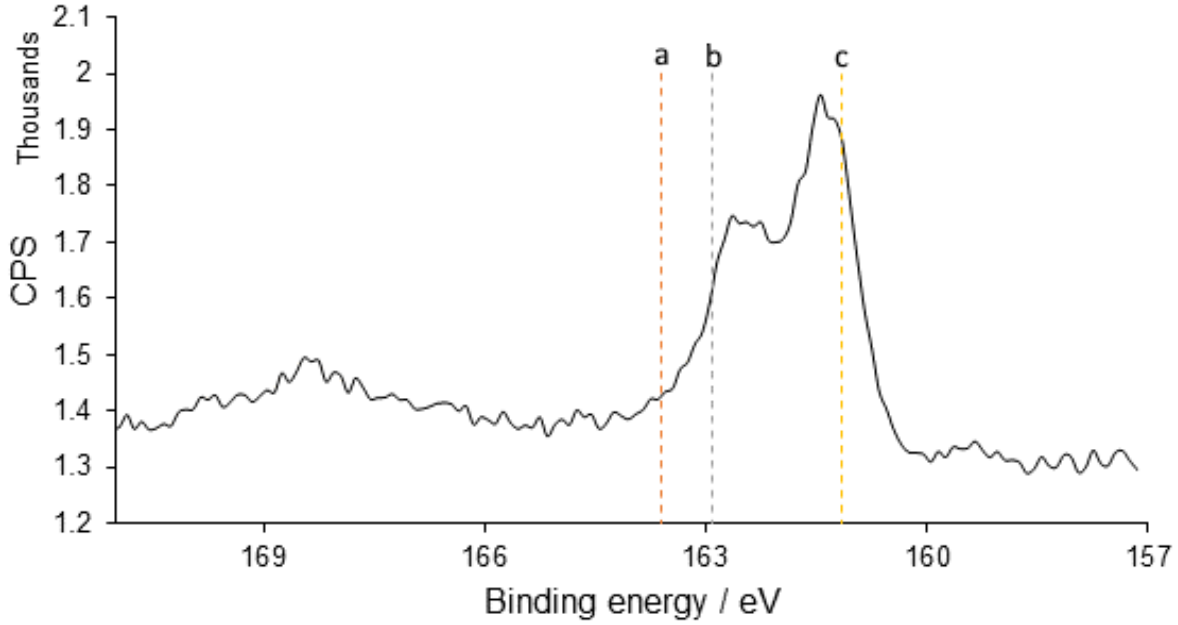

Figure 4.4: XPS S 2p spectra of Cu_2S honed specimen. a) typical S 2p peak, b) typical FeS_2 sulphide peak c) typical Cu_2S sulphide peak

The great increase in copper content has already indicated that the honing process was able to generate reduction reactions in the microparticles. The copper atoms split from the sulphur and the pressure and heat induced by the finishing processes was sufficient to force the loose copper particles into iron to form an iron composite surface similar to sintering (Lu and Ishiyama, 2015). While the majority of loosed sulphur atoms have been lost, the small sulphide and sulphate peaks suggest that some have successfully reacted with the iron.

Wear tests

The mean Coefficient Of Friction (COF) from the line contact 1 h load ramp tests are shown in Figure 4.5. There is a very slight reduction in friction in the samples honed with additives. A standard t-test was performed on the friction data. With the three tests that were performed each for the controls and Cu_2S honed samples, there is ≈95 % statistical confidence that honing with Cu_2S reduces friction once the load is ≥100 N which could be considered statistically significant.

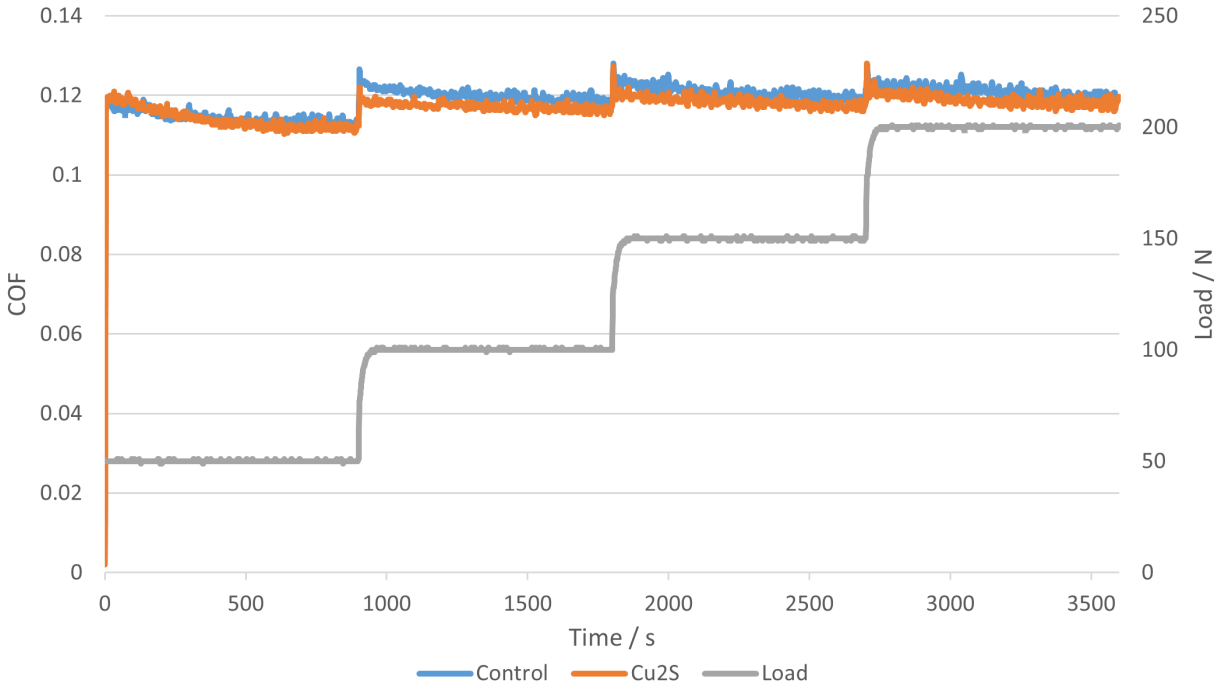

Figure 4.5: Mean COF of control and Cu_2S honed sample in a 1 h test at 2.5 Hz with 12.5 mm stroke with a line on flat contact

Varenberg et al. (2016) describes the difference in COF between the cast iron shot peened by Cu_2S and Al_2O_3 and the other samples as greatest when the pressure was very low (3.8 MPa p_o) and the sliding velocity was at its highest (0.9 m s^{-1}). In order to run a test in a similar envelope, low pressure specimens were used with a 286 N load and a reciprocating speed of 23 Hz to give a maximum sliding speed of 0.9 m s^{-1}. Figure 4.6 shows the mean COF over time results of these tests.

As Figure 4.6 shows, the COF for both the control and the Cu_2S honed specimens was very low (below 0.01). In the paper discussed (ibid.), the authors thought it was re-

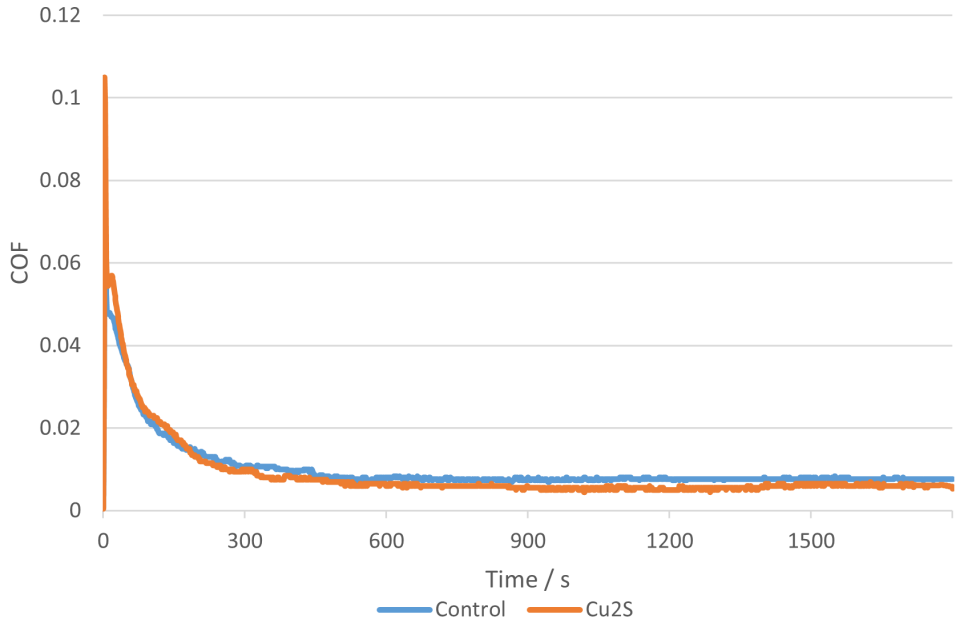

Figure 4.6: Mean COF of control and Cu_2S hone samples in a 30 min test at 23 Hz with 12.5 mm stroke and 286 N load

markable that the friction was so low for their shot peened specimens, however the results presented here show that given the low pressure and high speed, a mechanochemically improved surface is not the cause for such low friction in this case.

Figure 4.6 does once again show that the Cu_2S honed specimens performed slightly better than the controls but a similar statistical test to that performed on the previous set of results only showed 70 % confidence in the improvement made by the addition of Cu_2S. Many more than the three tests already undertaken would have to be performed in order to attribute this to more than statistical error.

4.4 Summary

Honing, a mechanical finishing process, was performed on cast iron plates with Cu_2S microparticles introduced to the honing region in an attempt to force a mechanochemical reaction which caused the sulphur to reduce from the copper and bond with the iron in the surface of the plate to form a tribologically superior iron sulphide/sulphate surface. The key results are summarised below:

- Initial honing with 100 mg Cu_2S smeared on the grit paper failed to significantly increase the sulphur content of the surface of cast iron plates compared to the control sample but did reduce the size of defects in the material suggesting a possible surface healing effect.

- The quantity of Cu_2S involved in each honing process was increased to 1 g. The atomic percentage of sulphur observed in the surface through EDS increased from 0.15 % to 1.7 % compared to the control and 8 times as much copper was present. This suggested that conditions in the contact area were suitable for a reduction reaction to occur in the Cu_2S particles but it was the copper that sintered into the iron and much of the sulphur had been lost in the process.

- XPS showed that most of the sulphur present was still in sulphide form, likely still in the form of Cu_2S with perhaps a small quantity forming iron sulphides and sulphates.

- Wear tests using both a line contact and a low pressure flat-on-flat contact on the second set of samples produced only a very small reduction in friction compared to the control samples. T-test analysis showed 95% confidence that the improvement in friction reduction with the line contact tests was significant when the load was greater than 50 N, but the low pressure results could be considered statistically insignificant.

Overall, analysis showed that the Cu_2S honing process was able to generate a mechanochemical reaction in the surface of the cast iron plates, however, a protective layer that improved the tribological properties of the plate was not achieved with the processes described in this chapter and further testing is needed before this can be seen as a viable method of improving the performance of a material in a wear environment.

Chapter 5

SiO_2 and MoS_2 as nano-additives in lubricants

5.1 Introduction

Extensive research has been conducted to assess the tribological proprties of Transition Metal Dichalcogenides (TMDC)s such as MoS_2 nanoparticles in recent years, particularly as lubricant additives to reduce both friction and wear (Rabaso et al., 2014b; Tannous et al., 2011). They are well known for their strong covalently bonded thin layers with weak Van der Waals forces between layers and good adherence to many materials leading to easy sliding so reducing friction and protective tribofilm formation reducing wear (Krishnan et al., 2019). The mechanisms of a variety of forms of MoS_2 nanoparticles have been studied. Inorganic Fullerene-like (IF)-like nanoparticles and nanotubes are thought to gradually exfoliate on the asperities of the surfaces during the friction process leading to the afore mentioned effects (Tannous et al., 2011).

The mechanisms of nanospheres such as silica and alumina have also been examined (Peng et al., 2010). These are hard and brittle nanoparticles known for their high hardness and nanobearing effect, rolling between the two sliding surfaces (Liu et al., 2017) as well as surface polishing effects leading to reduced surface roughness after wear (Kotia et al., 2019). MoS_2 has been observed to have the greatest reduction in friction in boundary lubrication regimes between metal contacts (Rosentsveig et al., 2009). In the referenced examples, with steel contacts lubricated with Polyalphaolefin (PAO), reduction was highest when the pressure exceeded 1 GPa. The performance of SiO_2 depends heavily on particle size and concentration (Peng et al., 2010), Xie et al. (2016b) believed that as the lubricant film thickness became close to or smaller than the diameter of nano-SiO_2, the friction and wear would increase as the high hardness of the particle means it is unlikely to deform but instead plough furrows in the contact surfaces.

Though MoS_2 has been shown to reduce friction dramatically in boundary lubrication, the regime is much more complicated in reciprocating motion. Twice every cycle, the range in sliding speed means that the lubrication regime can move from boundary through to Elastohydrodynamic Lubrication (EHL) and back. This means that additives that perform well in one regime may not be as beneficial between reciprocating contacts.

Fan et al. (2017) compared a range of nanoparticles including different forms of MoS_2 in a reciprocating regime in multialkylated cyclopentanes (MACs). The reduction in Coefficient Of Friction (COF) was minimal, however, the reduction in wear was far greater.

The idea of combining the effects of both nanoparticles in lubricants is quite new. Xie et al. (2016a) combined SiO_2 with MoS_2 in magnesium-steel contacts with EOT5# engine oil at ambient temperature and found that there were some synergistic effects, between 312 MPa and 446 MPa p_o using a point contact and mean sliding speed of $0.8\,\mathrm{m\,s^{-1}}$, where the COF was lower than using either of the nanoparticles individually. The concentration pf nanoparticles, both used individually and in combination were 0.1 wt% SiO_2 and 1.0 wt% MoS_2. The same authors also experimented with using a consistent overall 1 wt% concetration for the nanoparticles but changed the ratio of SiO_2 to MoS_2 (Xie et al., 2017). 0.25:0.75 SiO_2 to MoS_2 ratio showed the greatest reduction in friction with 1 wt% MoS_2 showing less wear but slightly higher COF than 1 wt% SiO_2 with 312 MPa p_o and $0.08\,\mathrm{m\,s^{-1}}$ sliding speed.

As discussed in previous chapters, using a combination of hard and soft nanoparticles has been explored by Varenberg et al. (2016) using CuS_2 and Al_2O_3. A similar mechanism could occur with nanoadditves in lubricated wear as the SiO_2 surface polishing attributes could help to grind the MoS_2 into the contact areas. The increased severity of very localised conditions may encourage a chemical reaction to occur, thereby improving the MoS_2 tribofilm formation.

In chapter 4, Cu_2S microparticles were used along with mechanical finished processes in an attempt to mechanochemically create, outside of the wear process, a protective layer similar to the tribofilms created by TMDCs as lubricant additives in wear. The work presented in this chapter aims to combine the 2D nature and tribofilm formation of MoS_2 with the nanobearing and surface polishing effect of SiO_2 in order to create a superior nanofluid for reducing friction and wear in reciprocating steel contacts. The hypothesis is that mechanically increasing the severity of the contact between sliding pairs where MoS_2 is present through the use of hard, spherical nanoparticles in boundary lubrication will increase the likelihood of a tribofilm being formed. If true, it can be used

as a proof of concept for mechanical finishing processes like that seen in chapter 4 and evidence that further experimentation in the area is needed. An extensive range of surface analysis techniques were used in order to best understand the mechanisms that affected the resulting wear scars.

5.2 Materials and methods

MoS_2 nanoparticles of <90 nm⌀ were acquired from Sigma Aldrich (Sigma-Aldrich, 2017b). These nanoparticles were used as they were the size that were available at the time of the experiments, though literature has shown that the size of MoS_2 particles are less important than its ability to break up in to 2D flakes once it has entered the contact (Rabaso et al., 2014b; Wang et al., 2022; Xie et al., 2016a). <50 nm⌀ SiO_2 nanopspheres dispersed in ethanol were also acquired from Sigma Aldrich (Sigma-Aldrich, 2020). The SiO_2 particles were the smallest available, as Peng et al. (2010) had shown these to be best at reducing friction when compared to larger sizes. These nanoparticles were observed using a JEOL 1400 Transmission Electron Microscopy (TEM) prior to testing. The particles, dispersed in ethanol, were dropped onto a standard copper microgrid for observation and further understanding of their morphology.

Formulation of lubricants

Various mixtures were prepared for tribological testing. The base oil, and control was SN100, the properties of which are shown in Table 3.3. For the High Frequency Reciprocating Rig (HFRR) tests, an MoS_2 mixture of 1 wt% concentration was made, this was based on concentrations commonly used effectively in literature for these particles (Rabaso et al., 2014a; Xie et al., 2016a). Initially, a mixture with a concentration of 1 wt% SiO_2 was also used for comparison, with the intention of comparing the two directly, however later HFRR tests were also performed with 0.5 wt%, again inline with similar concentrations seen in literature (Xie et al., 2016a). Two Hybrid nanofluids were also made, the first was a 1:1 mixture of SiO_2 and MoS_2 with both at 0.5 wt% of the

base oil and the second was 1:2 ratio mixture with the MoS_2 at 1 wt%. With the smaller total concentration of nanoparticles expected to be less likely to cause chemical reactions with the surfaces while the larger concentration perhaps more likely to have detrimental agglomerations.

For the later TE 77 High Frequency Friction Machine (TE 77) tests, a variety of concentrations of the nanoparticles were used in an attempt to find the optimum value for each nanoparticle separately and together in a hybrid nanofluid. These mixtures are detailed in Table 5.1.

Table 5.1: Concentrations of SN100 base oil and nanoparticles for TE 77 Low load adapter tests. Hybrid ratios are MoS_2:SiO_2.

Mixture	**Concentration** (wt%)			
SN100 (base oil)				
MoS_2	0.5	0.75	1.0	2.0
SiO_2	0.1	0.25	0.5	
Hybrid	1 at 1:1	1.5 at 2:1	2.5 at 4:1	

MoS_2 was combined with the oil in a glove box. For the SiO_2 nanofluids, the SiO_2-ethanol solution was combined with the base oil and then heated to 80 °C until the ethanol evaporated leaving SiO_2 in the base oil. Prior to each tribological test, the nanoparticles were dispersed and agglomerations broken up by using an ultrasonic shaker for 1 h.

Tribology tests

Initially, reciprocating tests were performed using an HFRR from PCS instruments. A schematic of the set up is shown in Figure 5.1 and the "HFRR" sections of Table 5.2 show the test parameters. The HFRR was chosen as it had similar contact geometry to tests performed by Xie et al. (2016b) and required significantly less lubricant per test (1 mL to 2 mL) than using the standard TE 77 tests of the previous chapter (10 mL to 13 mL) allowing for many more tests to be performed with the same quantity of nanoparticles.

The initial set of benchmark tests with 1 wt% concentration in each of the nanofluids and with a 1:1 ratio in the hybrid were run at four loads, 1.96 N, 3.92 N, 5.89 N and 7.85 N.

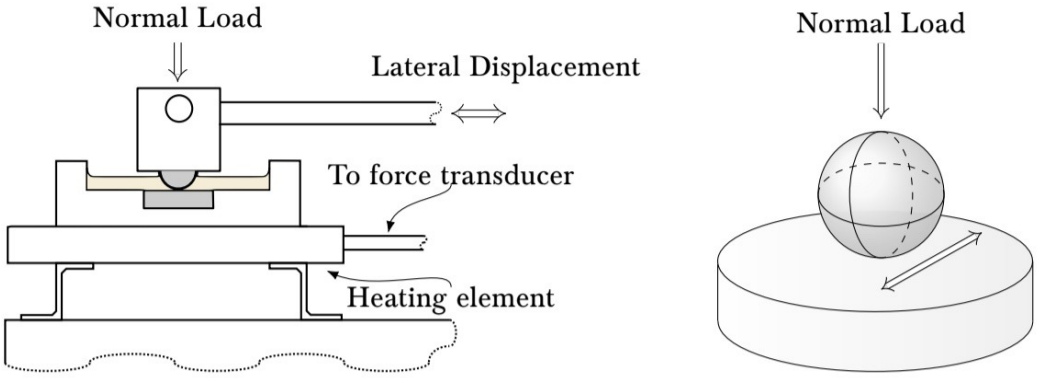

Figure 5.1: Schematic of HFRR(Eckold, 2016)

The corresponding initial contact pressures are shown in Table 5.2. These tests were run for 30 min at 23 °C.

In order to reduce the lubricant film thickness in the regime and to make any variantion in wear rate more noticeable, further tests were run for 90 min at 50 °C. The load was kept at 8 N and the concentration of the SiO_2 nanofluid was reduced to 0.5 wt%, advised by optimal concentrations found in literature (Peng et al., 2010; Xie et al., 2016b). The initial 1:1 hybrid was used and a 2:1 MoS_2 to SiO_2 mix at 1.5 wt% was introduced.

Further reciprocating tests were performed using the Low Load Adapter (LLA) for the TE 77 from Phoenix Tribology. An image showing the set up is shown in Figure 3.2 and the "LLA" section of Table 5.2 shows the test parameters. The load arm multiplies the load by 4 with moments, so a 200 g load produces a vertical force of 7.85 N on the specimens. All tests were performed at least in triplicate.

Table 5.2: Design of Experiments - A complete list of the different friction tests performed in this chapter. Each line of parameters was tested at least in triplicate

	Concentration		**Tribo-tester parameters**			
Machine	MoS2 (wt%)	SiO2 (wt%)	Load (N)	p_o (GPa)	Time (h)	Temp. (^{o}C)
HFRR	0	0	1.96	0.79	0.5	23
	0	0	3.92	1.00	0.5	23
	0	0	5.89	1.14	0.5	23
	0	0	7.85	1.26	0.5	23
	1.0	0	1.96	0.79	0.5	23
	1.0	0	3.92	1.00	0.5	23
	1.0	0	5.89	1.14	0.5	23
	1.0	0	7.85	1.26	0.5	23
	0	1.0	1.96	0.79	0.5	23
	0	1.0	3.92	1.00	0.5	23
	0	1.0	5.89	1.14	0.5	23
	0	1.0	7.85	1.26	0.5	23
	0.5	0.5	1.96	0.79	0.5	23
	0.5	0.5	3.92	1.00	0.5	23
	0.5	0.5	5.89	1.14	0.5	23
	0.5	0.5	7.85	1.26	0.5	23
HFRR	0	0	7.85	1.26	1.5	50
	1.0	0	7.85	1.26	1.5	50
	0	0.5	7.85	1.26	1.5	50
	0.5	0.5	7.85	1.26	1.5	50
	1.0	0.5	7.85	1.26	1.5	50
LLA	0	0	7.85	1.26	1.0	50
	0.5	0	7.85	1.26	1.0	50
	0.75	0	7.85	1.26	1.0	50
	1.0	0	7.85	1.26	1.0	50
	2.0	0	7.85	1.26	1.0	50
	0	0.1	7.85	1.26	1.0	50
	0	0.25	7.85	1.26	1.0	50
	0	0.5	7.85	1.26	1.0	50
	0.5	0.5	7.85	1.26	1.0	50
	1.0	0.5	7.85	1.26	1.0	50
	1.96	0.5	7.85	1.26	1.0	50

Surface analysis methods

Immediately after each test, the upper specimen balls from the HFRR tests were wiped clean with ethanol, all other specimens were immersed in ethanol and placed in the Ultrasonic Shaker for 10 min then wiped clean to remove any debris from the surfaces. The balls' average Wear Scar Diameter (WSD) were measured using an optical microscope. Wear depth and wear scar topography analysis for the flat specimens was performed using an Alicona InfiniteFocus microscope providing the width, depth and volume of the scar. The Hitachi TM3030 tabletop Scanning Electron Microscopy (SEM) with Energy Dispersive Spectroscopy (EDS) capabilities was used to analyse, visually and chemically, the lower specimen wear track. Chemical bond analysis on specimens was performed using X-ray Photoelectron Spectroscopy (XPS) and Hard X-Ray Photoelectron Spectroscopy (HAXPES).

5.3 Results and discussion

Nanoparticle morphology

Before any tribological tests, the nanoparticles were placed under the JEOL 1400 TEM to understand the morphology of the nanoparticles. The captured images are shown in Figure 5.2. In Figure 5.2a, the nanospherical form of the individual SiO_2 particles can clearly be seen. The particles are relatively uniform in size with all of them less than 50 nm⌀. There is some evidence of agglomeration but these should be broken up by the ultrasonic shaker prior to testing. Figure 5.2bi shows a large agglomeration of MoS_2 nanoparticles of around 1 µm across with clearly visible layers of nanoparticles which would be expected to separate under excitation or wear due to their weak van der Waals force. This highlights the need for using an ultrasonic shaker in order to break up the agglomerates and disperse the MoS_2 in the base oil before a tribological test. Figure 5.2bii shows a single flake not part of an agglomeration which matches the <90 nm description.

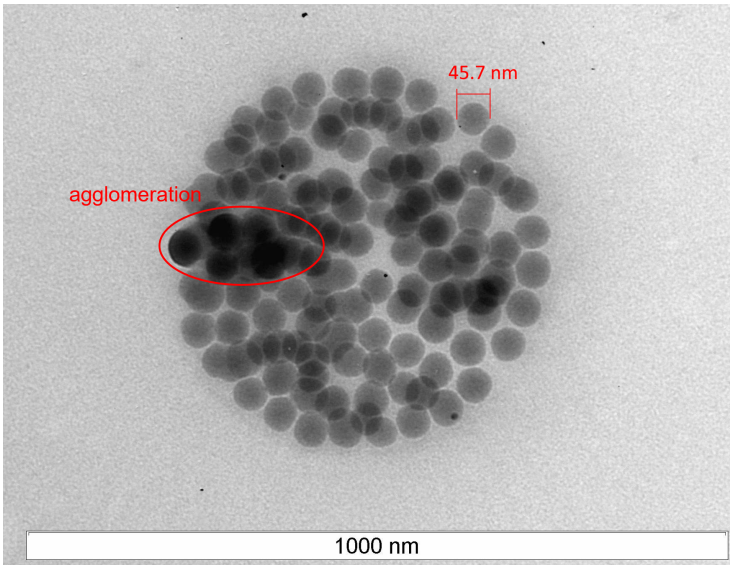

(a) TEM image of SiO_2 nanospheres

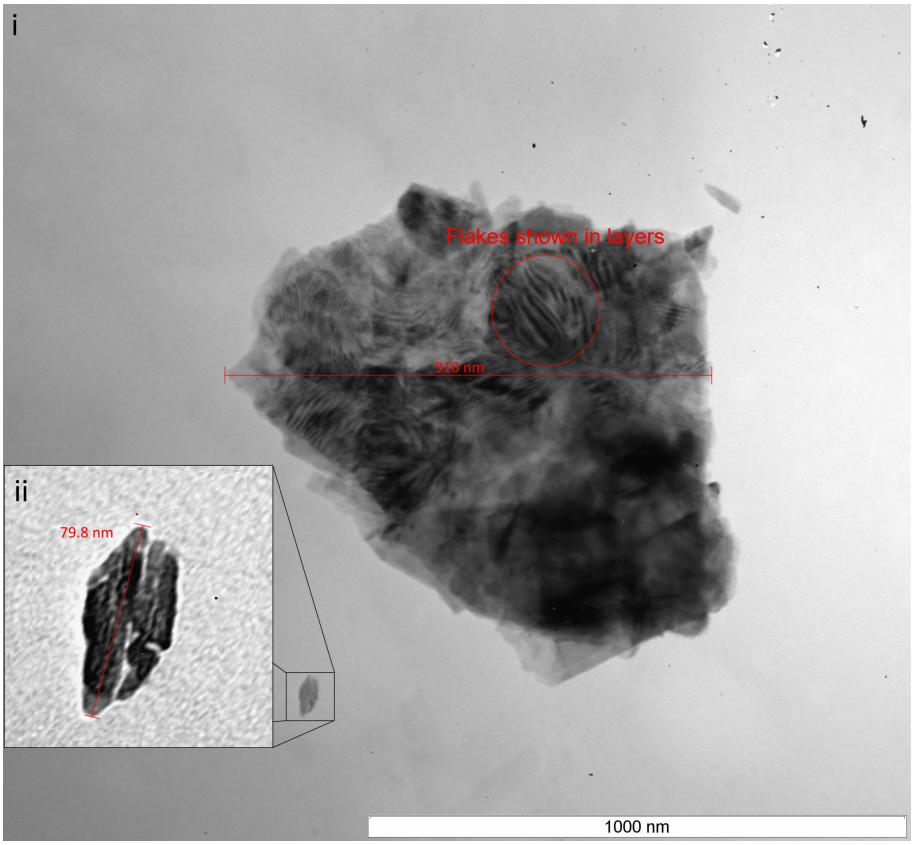

(b) TEM image of MoS_2 nanoparticles. i) large agglomeration ii) individual particle

Figure 5.2: TEM images of the nanoparticles used in this chapter.

HFRR tribological tests

The initial ambient temperature benchmark tests in the HFRR proved to be highly inconsistent. The COF results are represented in Figure 5.3. Though at every load, at least one of the nanofluids had a lower mean COF than the base oil, only for the SiO_2 mixture at 0.6 N was this true for every test. In the majority of test sets, the results were highly variable and there was not a significant reduction compared to the base fluid. This is likely due to the nature of reciprocating motion, neither of the nanoparticles perform optimally across the range of the stroke and it is likely that particles were being pushed out of the wear area in many cases therefore limited in their effectiveness.

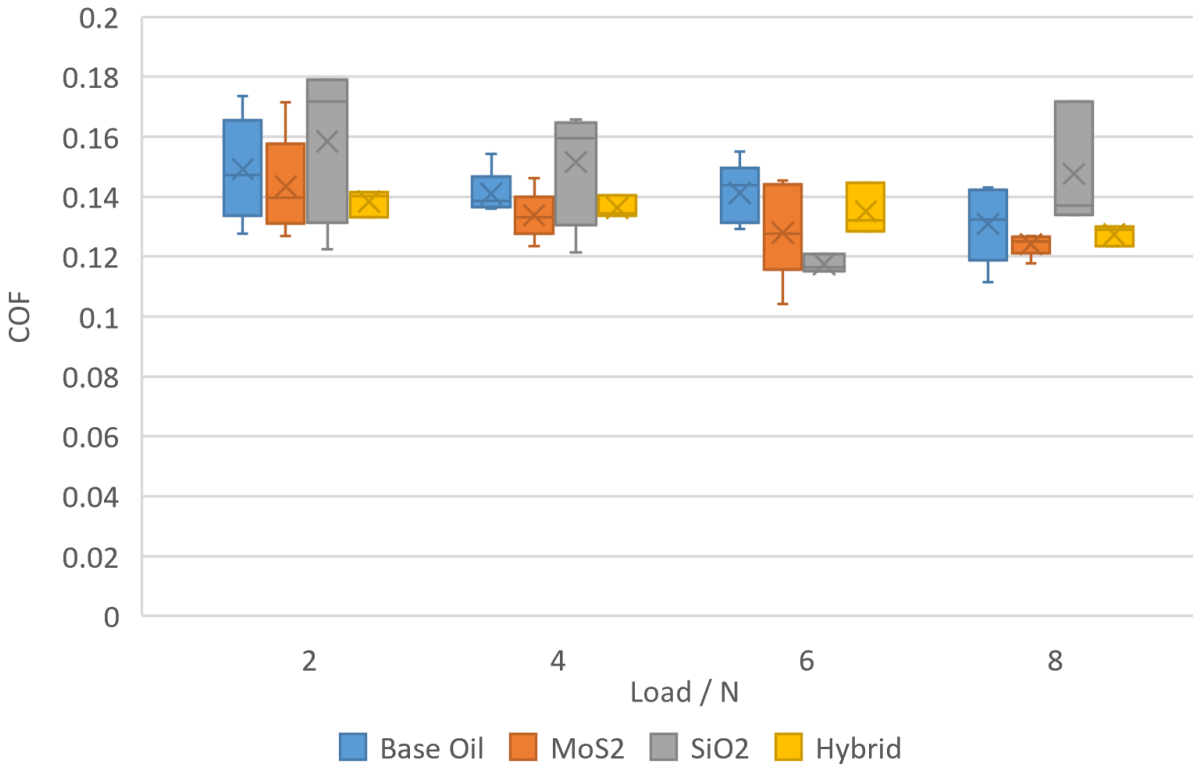

Figure 5.3: Mean COF of initial 23 °C tests shown as boxplots. All nanofluids are at 1 wt% concentration and the hybrid ratio is 1:1

As discussed in section 5.1, Fan et al. (2017) found that though there was little reduction in COF, MoS_2 could greatly reduce wear in reciprocating regimes. After each test, the wear scar on the ball was measured. The results for average WSD are shown in Figure 5.4.

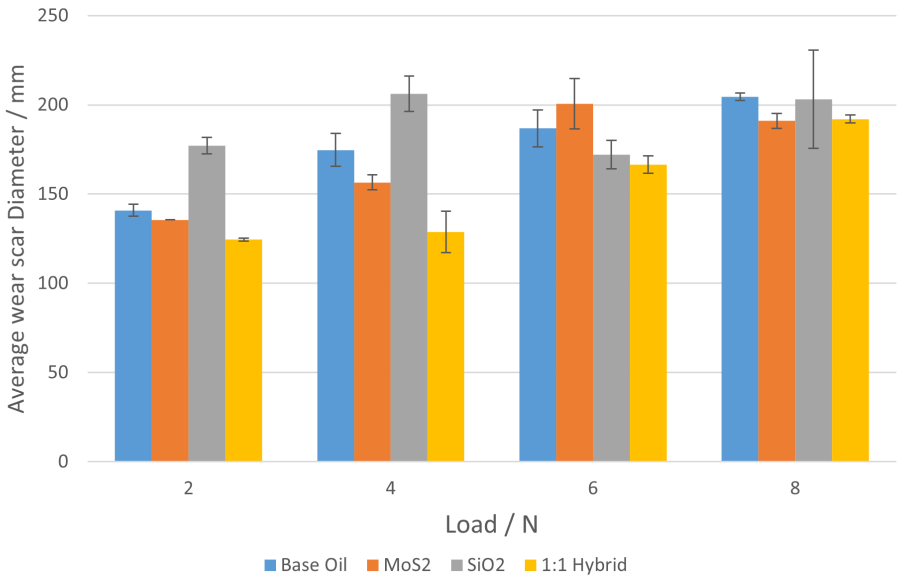

Figure 5.4: Mean WSD of upper ball specimens in initial 23 °C tests. Error bars represent one standard deviation from the mean.

The results here show that although the hybrid nanofluid never had the lowest average COF at any load, there could have been some synergistic effect when it came to wear reduction as the WSD was lowest in all cases except at 8 N where it was almost identical to that of the MoS_2 mixture.

As well as the WSD of the upper specimen, the wear profile and the wear volume of the lower specimen wear scars were analysed using the Alicona InfiniteFocus microscope. Figure 5.5 shows as estimate of the average wear volume of the scars when using the 6 N load. The estimate was calculated from multiple scans of the cross-sectional wear profile. Though in this regime the MoS_2 nanofluid had the widest average WSD for the upper specimens, the lower specimens had signficantly lower average wear volume than the base oil. In fact, all of the nanofluids reduced the wear volume of the discs significantly in comparison with the base oil, with SiO_2 producing the least wear in line with its lowest friction seen in Figure 5.3.

Following the tests at 23 °C, the temperature was increased to 50 °C at the load of 8 N in order to maximise the severity of the regime. This is because MoS_2 has been shown to be more effective in boundary lubrication regimes and for SiO_2 to grind the surface, the lubricant film must be thinner than the nanospheres. The test length was

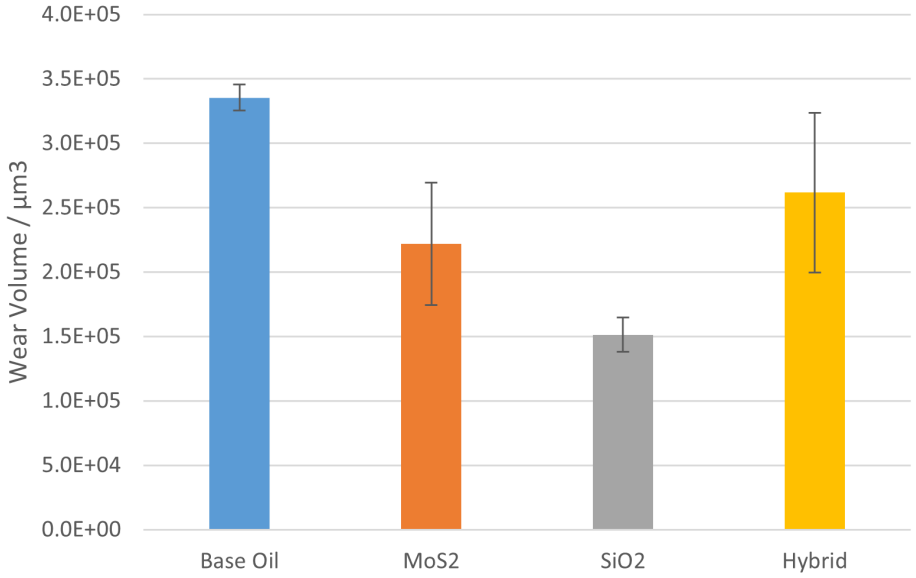

Figure 5.5: Average wear volume of lower specimen scars with 6 N load

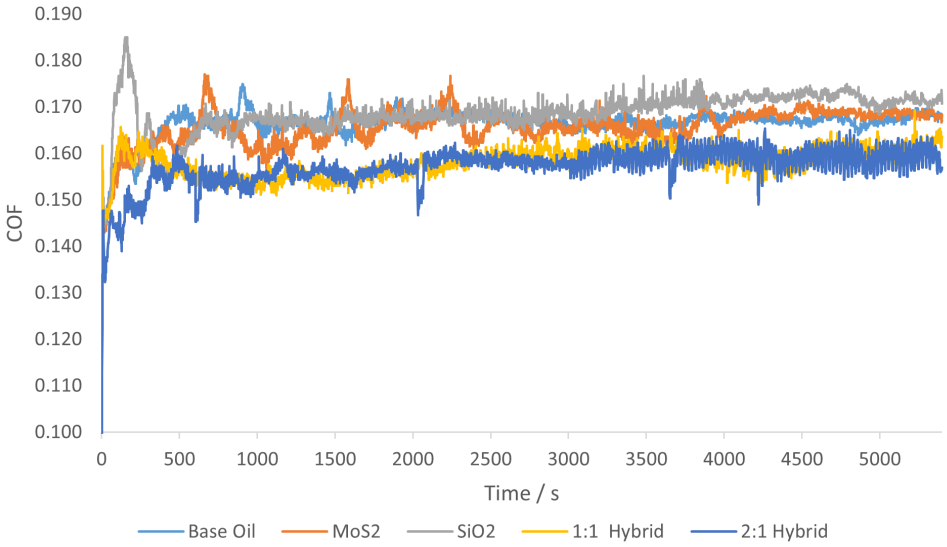

Figure 5.6: COF over time for nanofluids at 50 °C with 8 N load

also tripled in an attempt to generate significant differences in wear volume between the nanofluids. The concentration of SiO_2 was reduced to 0.5 wt% as informed by literature (Bao et al., 2017; Xie et al., 2016b). An additional hybrid mixture with a 2:1 ratio of MoS_2 to SiO_2 at 1.5 total wt% was also tested to keep the MoS_2 concentration consistent with the non-hybrid mixture.

Figure 5.6 shows the mean COF over time for the different nanofluids with an 8 N load with the more severe regime. The graph is cut off at COF 0.1 for clarity. The COF

for all the lubricants was between 0.150 and 0.170 after the initial running in period, which is higher than all the results at the same load but lower temperature. This is unsurprising as the higher temperature leads to a thinner film thickness meaning that boundary lubrication is the most prevalent regime. The hybrid lubricants consistently had the lowest COF between 0.150 and 0.165 with the other three fluids fluctuating around 0.17. This suggests there could be a synergistic effect though the improvement is only small.

The initial running-in period is very different for each of the lubricants. The results shown in Figure 5.6 are an average over three tests but similar run-in profiles to the mean were seen in each individual test. The nanofluid containing 0.5 wt% SiO_2 showed a rise in COF to 0.185 before falling below its final stable friction of approximate 0.168. A similar profile was also seen in the 1:1 Hybrid results but with a less pronounced rise. This indicates that the SiO_2 nanoparticles were causing an initial increase in friction before the regime settled. This could have been because some agglomerates still remained after the ultrasonification process and greatly increased the friction before being broken down over the first 10 min of wear. The MoS_2 nano-lubricant and the base-oil had a comparatively smooth increase in COF over the same period. MoS_2 is a much softer material and in combination with the weak van der Waals forces, agglomerations and layers of the nanoparticles were likely broken down easily without causing significant increases in friction.

ANOVA single-factor analysis was performed in order to understand whether or not the improvement in COF from the two hybrid lubricants was statistically significant. Setting an α value at 0.05 and comparing the tests from all five lubricants, the p-value came out as 1.36×10^{-5} which showed that at least one of the groups was significant. Both Bonferroni correction and Tukey's Honestly Significant Difference (Tukey's HSD) post hock tests showed that the two hybrid lubricants were significantly lower than all the other lubricants but not each other. This suggested that some synergistic effect had occurred with the two nanoparticles but further analysis of the wear scars would be needed to understand the mechanisms of improvement.

Surface analysis (HFRR)

Following the wear tests the surfaces were analysed using an Hitachi TM3030 tabletop SEM with EDS capabilities. Figure 5.7 shows SEM images from the lower specimen wear tracks for four of the lubricants in the high temperature HFRR tests. The images show the centre of the wear scar which is where the fluid film is strongest but also where any effect additives have made throughout the track should be most obvious as the ends may show debris and material pushed out of the track rather than just that firmly bonded to the surface.

The SEM image for the scar lubricated by base oil, Figure 5.7a, shows a rough looking surface with large dark patches in the direction of wear. EDS showed these patches to have high concentrations of oxygen, likely iron oxide. Figure 5.7b shows a slightly less oxidised wear track with many flakes that EDS confirmed to be MoS_2 left on the surface. The thorough cleaning of the specimens make it unlikely that loose particles would remain meaning that the MoS_2 flakes must be embedded into the surface, though the conditions in the wear process were not inducive to the formation of a tribofilm and this small amount of material transfer to the wear scar was not enough to reduce the friction compared to the control. The SiO_2 scar, Figure 5.7c, shows a clear direction of motion with a couple of furrows and a large black spot that EDS showed to be carbon. There is no evidence of the silica nanoparticles being embedded in the wear track.

Figure 5.7d shows the wear scar lubricated by the hybrid nanofluid. There is a clear dark stripe through the middle of the wear scar. In order to understand whether or not this could be a tribofilm, EDS was performed to make maps of oxygen, silicon, sulphur and molybdenum from the SEM image. These maps are shown in Figure 5.8. Iron is not shown in this image as it was prevalent throughout the map by virtue of being the base material.

There is a clear increase in oxygen throughout the wear scar when compared to the unworn areas above and below the scar in the image. The highest concentration of oxygen appears to be throughout the suspected tribofilm area, this result is repeated in the other

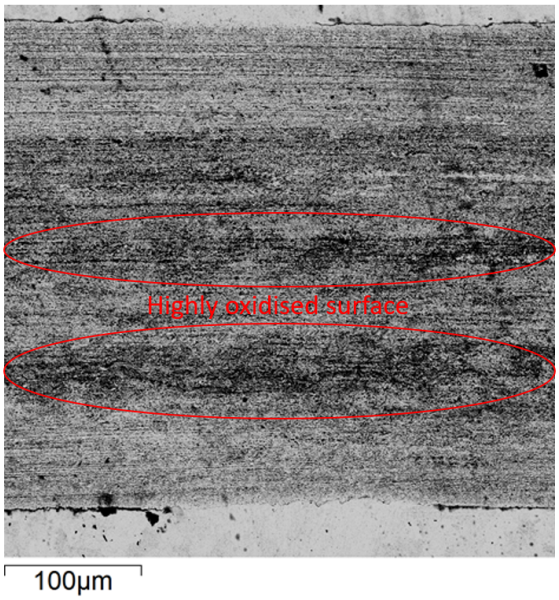

(a) Base Oil

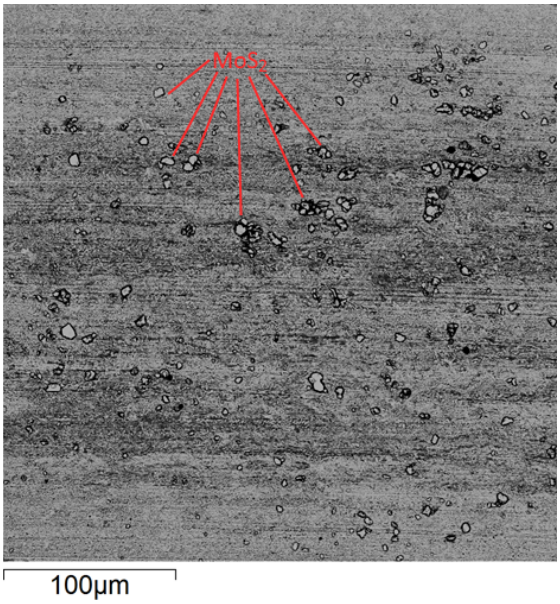

(b) MoS_2

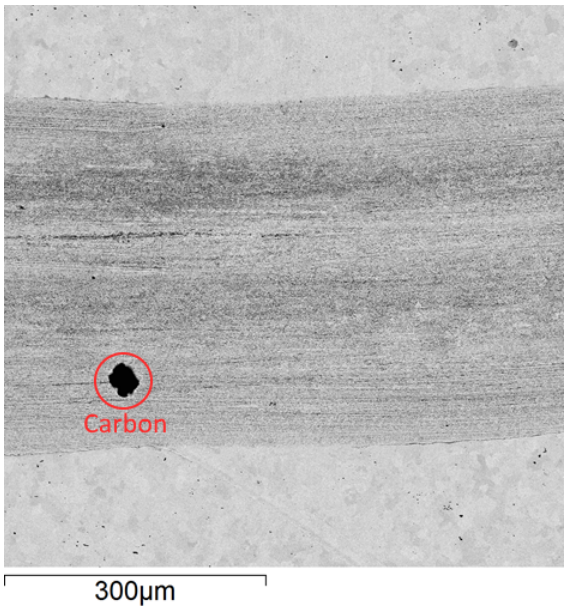

(c) SiO_2

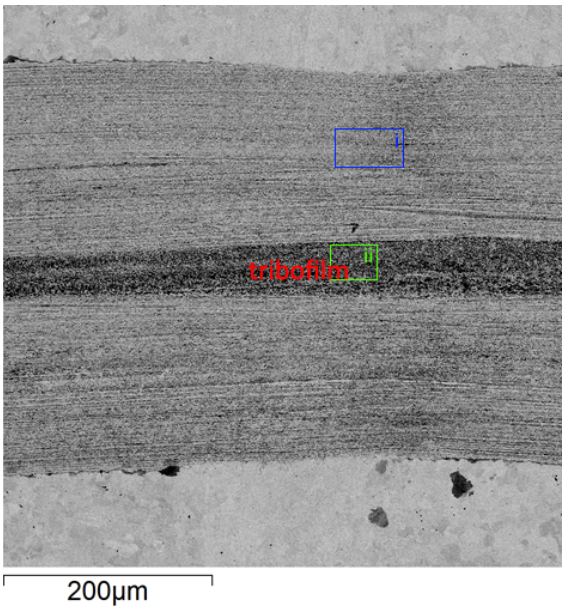

(d) Hybrid

Figure 5.7: SEM images of the centre of each lower specimen wear scar from 90 min, 50 °C, 0.8 N load tests. a) base oil, b) MoS_2, c) SiO_2, d) 1:1 Hybrid

three elements though there is a lot of noise in the other images and for silicon the difference is only faint which suggests only minimal SiO_2 remains in this area. This is evidence that a tribofilm has been formed only in the very centre of the wear scars. The elemental composition clearly includes oxidised iron and probably some embedded MoS_2. Analysis of the chemical bonds in this area is needed to see if the iron sulphides and sulphates seen in other literature ((Ratoi et al., 2013; Tannous et al., 2011)) are present.

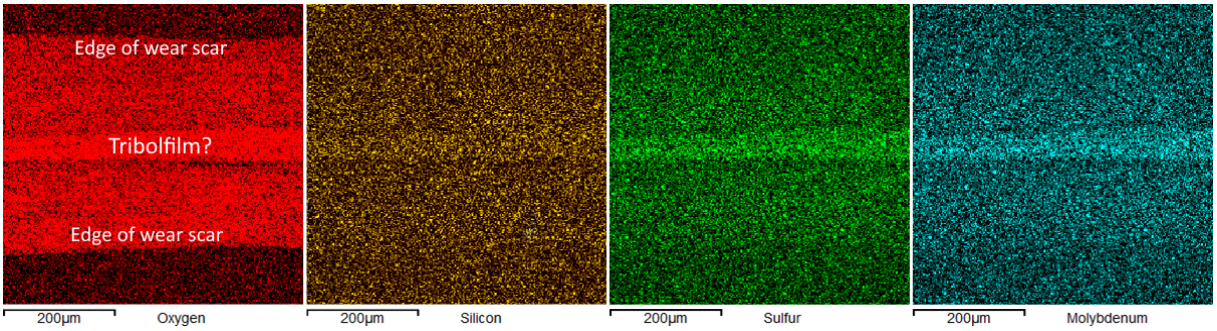

Figure 5.8: EDS maps of oxygen, silicon, sulphur and molybdenum from the hybrid lubricant wear scar SEM image

The wear scars from the 50 °C tests were analysed using the ALICONA infinite focus microscope and profile measurements of the cross section of the wear scars were taken. Figure 5.9 shows an example of these cross sections from each of the lubricants. The maximum depth of all of the wear scars are between 3 µm and 4 µm with both the SiO_2 and MoS_2 lubricated wear scars appearing to have similar profiles to the base lubricant.

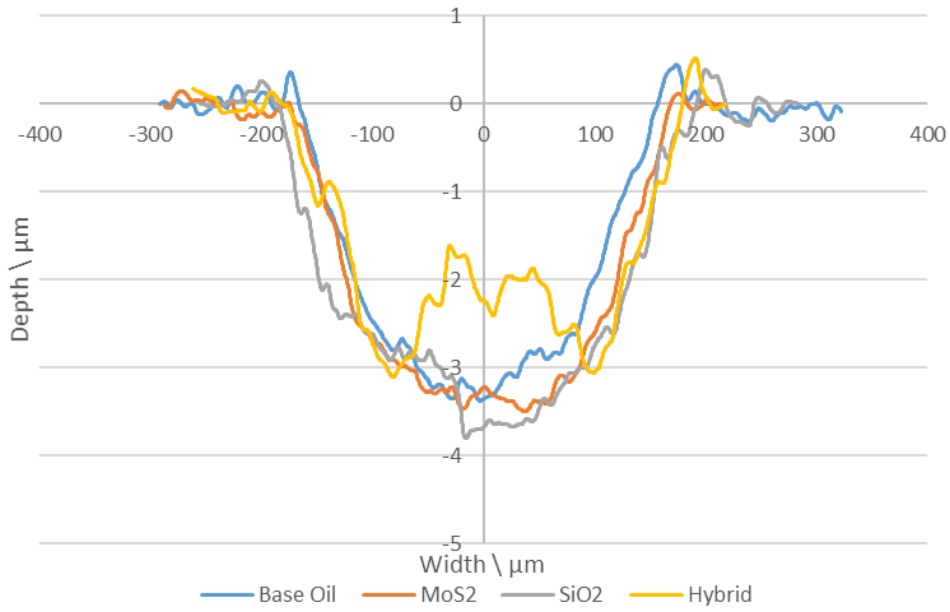

Figure 5.9: Representative cross-sectional profile of wear scars from each of the lubricants from 50 °C tests

For the base oil and MoS_2 and SiO_2 nanofluids, the cross-section wear scar profile is as expected, given that the upper specimen was a ball, with a relatively smooth curve down to the deepest point at the centre of the track. For the hybrid scar however, there is a raised section in the centre. This raised section is, in places, over 1 µm shallower than the

deepest parts running either side of it. Combining this result with the image shown in Figure 5.7d, this raised section coincides with the suspected tribolfilm seen in the centre of the wear scar. The formed tribofilm appears to have protected the middle of the wear scar to the point that there are two trenches either side of it that are almost twice as deep in places. Referencing Equation 3.1, if the contact patch is circular, the initial contact area is ≈109 µm in diameter. The contact patch is expected to grow over time as the material is worn but this is similar to the width of the raised section of the profile seen in Figure 5.9. Measuring the wear profile of the scar on the ball was not possible as it is only in a fixed position when in the upper specimen holder for the HFRR so it is not known whether the wear profile is mirrored in the ball. Alternatively a wear profile similar to that seen in the other wear scars may have first been formed before the tribofilm started to build up in the centre and gradually thickened to 1 µm as the wear continued. However it was formed, it is clear that the tribofilm is highly resistant to wear.

Hypothesis

Figure 5.7 and Figure 5.9 clearly show that the hybrid nanofluid performed differently to either the SiO_2 or MoS_2 nanofluid. A tribofilm containing molybdenum and sulphur was only formed when the silica nanospheres were also present in the oil. This suggests a mechanochemical effect similar to that discussed in the Varenberg et al. (2016) paper could be active. The current hypothesis for the formation of this wear scar is that the hard silica nanospheres grind the MoS_2 into the surface performing in a similar way to the surface polishing effect studied by Kotia et al. (2019). This grinding along with the pressure between the upper and lower specimen caused highly localised temperature increases allowing chemical reactions between the MoS_2 and the iron in the steel specimens creating a protective tribofilm formed of partly MoS_2 and iron sulphide along with other oxides similar to the diagram shown in Figure 2.2.

XPS and HAXPES

To confirm the hypothesised tribofilm composition, the three hybrid scars were analysed at the University of Manchester using XPS and HAXPES.

Standard XPS was not able to focus on the wear scars without also taking in results from the surrounding unworn disc. Sulphur and molybdenum were barely distinguishable from the signal noise as most of the received X-rays originated from outside the scar. Because of this the specimens were moved to the HAXPES which performs the analysis with higher precision and a tighter focus on the wear scars within the specimens.

Analysis of the hybrid wear scars under the HAXPES showed strong S 1s peaks and smaller Mo 2p peaks in the 2450 eV to 2650 eV binding energy range (Figure 5.10). In all three hybrid wear scars, the ratio of counts per second of sulphur to molybdenum, according to those peaks, was greater than double. The average atomic% for the elements present in the hybrid wear scars can be seen in Table 5.3.

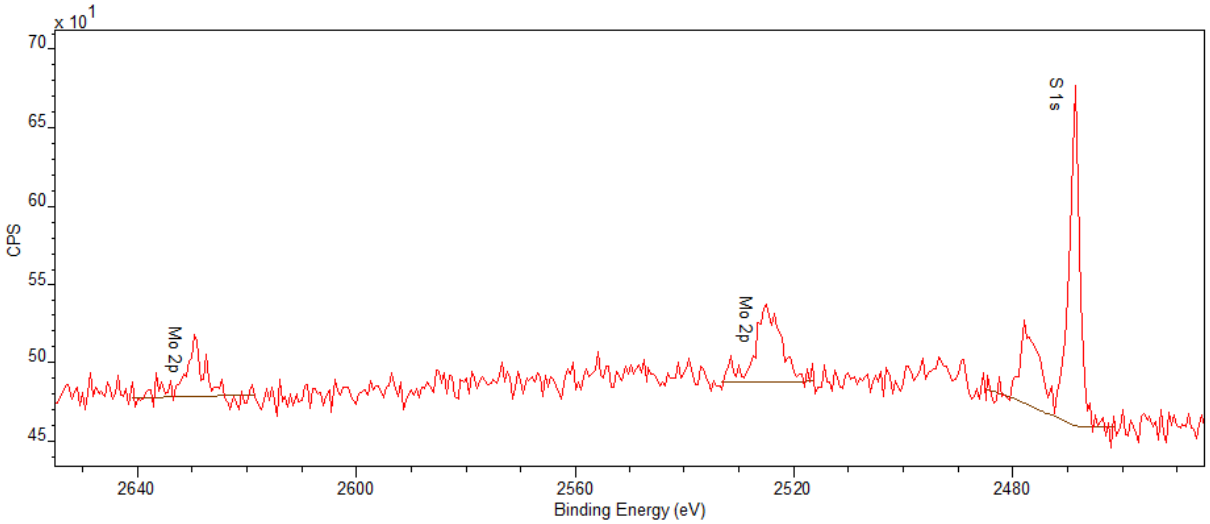

Figure 5.10: Mo 2p and S 1s peaks in 2450 eV to 2650 eV range in HAXPES, red: Hybrid wear scar spectra, green: control wear scar spectra

The tribofilms within the wear scars were still too small for the HAXPES to focus on specifically so the percentages shown in Table 5.3 would be general for the whole wear scar and some of the area around, reducing the quantity of molybdenum and sulphur found in proportion to elements found abundantly in the substrate material and the rest of the scar like carbon, iron and oxygen. A maximum of 0.5 atomic% of the 0.65% attributed to

Table 5.3: Table showing the average atomic % of elements in the wear scars according to HAXPES, using C 1s, O 1s, Fe 2p 3/2, Mo 2p and S 1s spectra as well as the metallic/sulphide components of iron and sulphur.

element	atomic%
Carbon	29.44
Oxygen	34.30
Iron	36.12
(metallic)	9.05
Molybdenum	0.25
Sulphur	0.89
(sulphides)	0.65

sulphides could still be MoS_2, which means, even including the trace amounts of sulphur present in AISI 53100 (<0.025 %) the additives and wear have introduced a further 0.36 % sulphur to the material. This suggests that iron sulphides and sulphates have formed in the tribofilm and that mechanochemical reactions have occurred.

The overall peaks in the spectra looking at sulphur, iron and molybdenum were, split into component peaks to understand the likely chemical bonds present. These components for another of the hybrid wear scars are shown in Figure 5.11.

Figure 5.11a shows a primary peak at ≈2468.9 eV that is attributed to metal sulphides. The majority of this is likely MoS_2 embedded within the tribofilm, though Table 5.3 showed that not all the sulphides can be purely bonded with MoS_2 and likely some of it will have also bonded with the iron, likely as FeS_2 or $FeMo_2S_4$ (Tannous et al., 2011). The secondary peak centred between 2475 eV and 2478 eV is attributed to sulphates, these are likely to be iron sulphates such as $FeSO_4$ (Mantovan et al., 2018).

The Fe 2p region, shown in Figure 5.11b, has a distinct peak at ≈706.5 eV representing metallic iron as well as iron that is bonded to sulphur. The larger peak is made of at least three component peaks depicting various iron oxides and sulphates (Biesinger et al., 2011). As previously discussed, the spectra shown is taken from the entirety of the wear scar, not only the tribofilm. Figure 5.8 showed that oxygen was prevalent throughout the worn area which explains the very large oxide peaks.

Finally, Figure 5.11c depicts the Mo 3d region which overlaps with S 2s, the same region shown in Figure 2.5. The largest peak at ≈225.4 eV shows sulphur in the form of

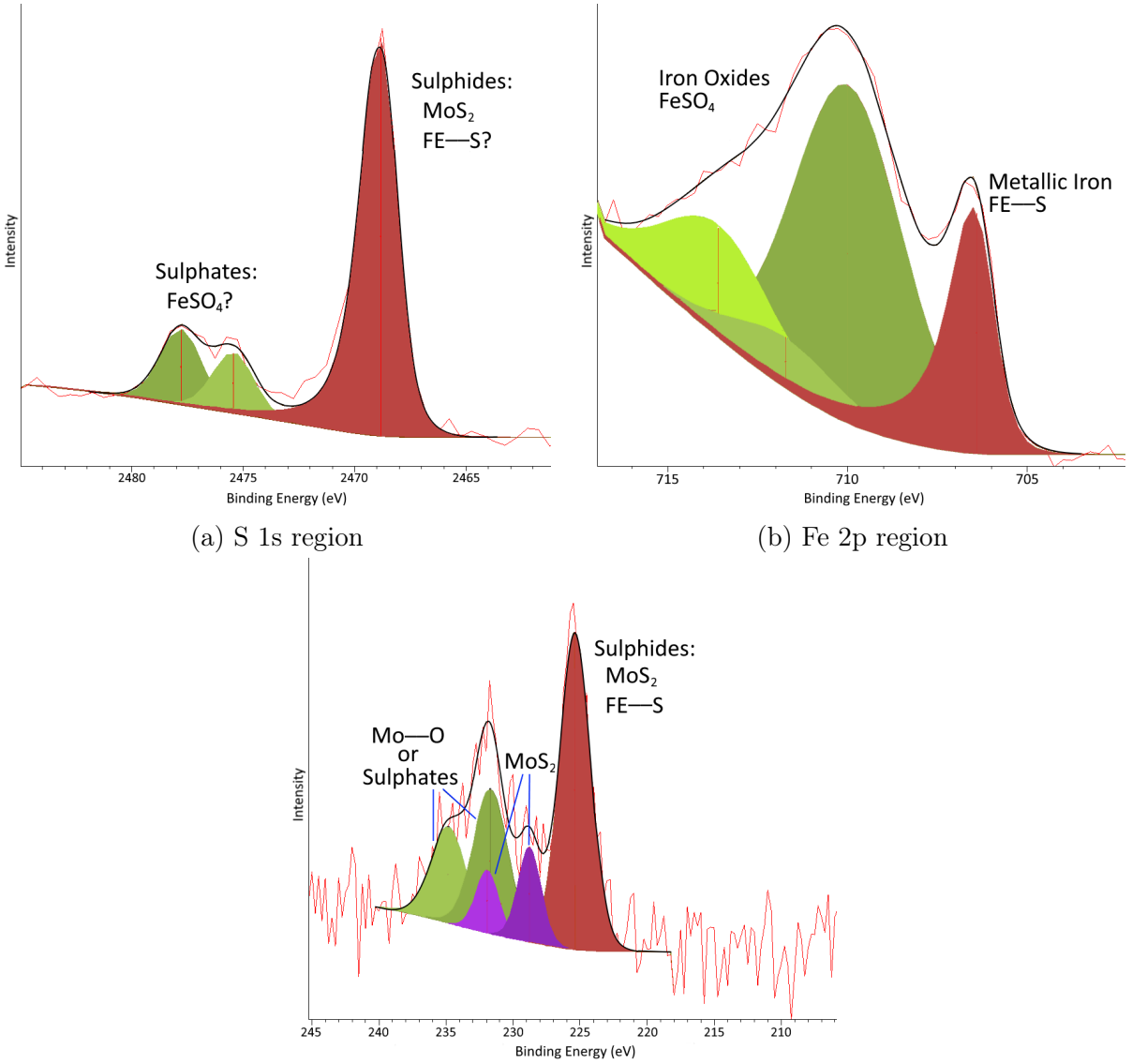

(a) S 1s region

(b) Fe 2p region

(c) Mo 3d/S 2s region

Figure 5.11: HAXPES spectra of the S 1s, Fe 2p and Mo 3d/S 2s ranges from one of the hybrid wear scars. (a) shows the S 1s region, (b) the Fe 2p region and (c) the combined Mo 3d/S 2s region.

MoS_2 and perhaps some iron sulphides. A small doublet at ≈228.8 eV and ≈232.0 eV is molybdenum in the form of MoS_2. The pure metallic Mo^0 doublet seen in Figure 2.5 is not present but a large doublet at ≈231.7 eV and ≈234.9 eV could represents molybdenum oxides (Tannous et al., 2011) or sulphates in the form of $FeSO_4$ (Mantovan et al., 2018).

The three regions shown in Figure 5.11 combined give strong evidence that the composition of the tribofilm may be somewhat similar to that described by Ratoi et al. (2013) and depicted in Figure 2.2. Embedded MoS_2 particles are certainly present but chemical

reactions caused by the severe nature of the wear and the additional impacts that the SiO_2 introduced led to iron sulphates and sulphides being formed. This lead to a tribofilm with superior wear resistance compared to specimens lubricated by any of the other mixtures.

TE 77 low load adapter tests

Figure 5.3 showed that the mean COF could be very inconsistent when all variables were kept constant. One of the reasons for this could be the HFRR and the mechanisms by which it transfers load to the contact point and achieves reciprocating motion which are detailed in section 3.2. This is also evidenced by Figure 5.12 which shows a cross section profile along the length of a hybrid wear scar acquired using the Alicona InfiniteFocus microscope.

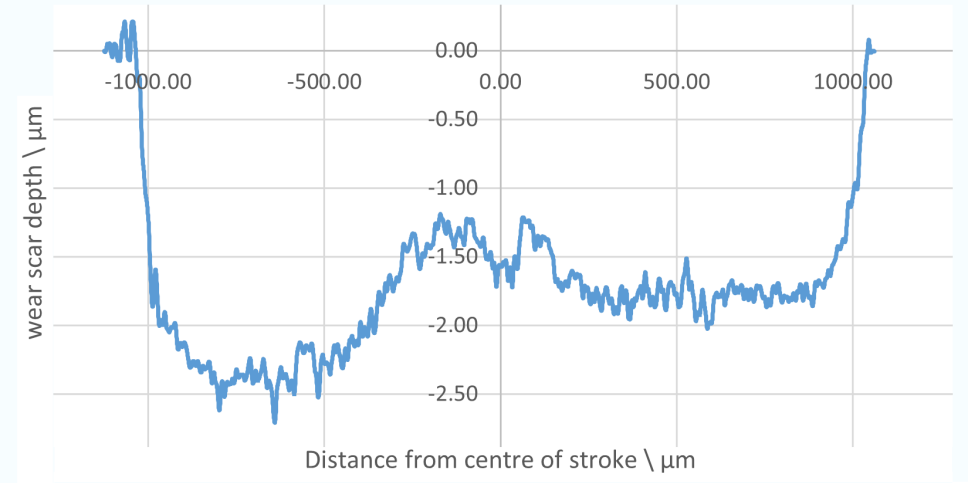

Figure 5.12: Graph showing cross section of wear profile along the length of stroke, x-axis = position on stroke (µm), y-axis = wear scar depth (µm).

A section in the middle of the stroke is less worn than either end. This is expected given that sliding speed is highest mid stroke so the friction regime is less severe. However, the right end of the scar is less deep than the left. The sliding speed should be the same for both which suggests that the load at either end is not consistent, as Plint (2010) suggests. The inconsistent profile was repeated throughout all the wear scars. For this reason, further testing was performed on the TE 77 LLA which applies the load independently of the stroke. Reciprocation is generated by a cam and motor, so is very reliable.

With the test parameters kept as similar as possible to the 50 °C tests from the HFRR but for only 1 hr, a variety of nanofluids were tested. The median COF for all the single nanoparticle fluids is shown in Figure 5.13.

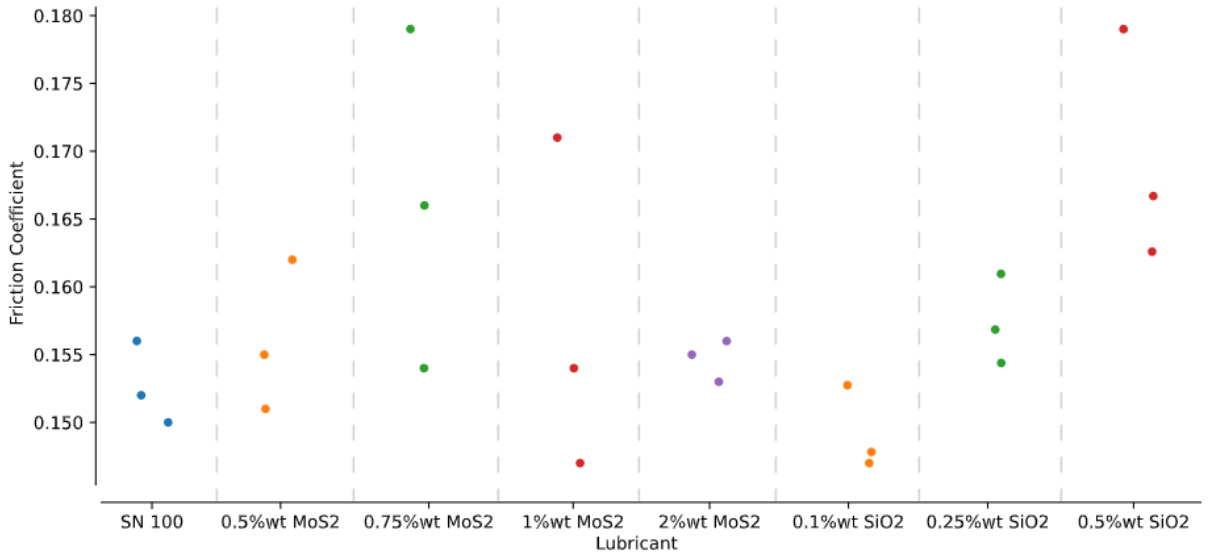

Figure 5.13: Median friction for MoS_2 and SiO_2 mixtures

There is huge variance in many of the results, particularly for the MoS_2 mixtures. MoS_2 deposits in the bath away from the contact area were observed after testing suggesting that the nanoparticles are pushed out of the contact and settle during testing with the agitation generated by the reciprocating motion insufficient to keep the particles dispersed.

At 2 wt%, the medians are close together but at a similar COF to the base oil so it is unclear if the MoS_2 had any impact in the contact area. Large agglomerates either unsuccessfully broken down by the Ultrasonic Shaker or formed during the test may be responsible for the increases in friction in the lower concentrations as the inability of the MoS_2 to remain dispersed has already been demonstrated.

For the SiO_2 nanofluids, results appear more reliable. At 0.25 wt% and 0.5 wt% the median COF increases in comparison to the base oil but there is a small decrease at 0.1 wt%. The increase from the higher concentrations is likely due to abrasion caused by the excessive quantities of hard particles in boundary or mixed lubrication (Xie et al., 2016b). At 0.1 wt%, the quantities of nanoparticles may have been low enough to avoid causing too much abrasion and a combination of surface polishing and/or third body

lubrication through acting as nanobearings could be responsible for the small decrease in friction (Peng et al., 2010). SEM images of the wear scars could confirm the hypothesised mechanisms. All the SiO_2 results suggest that these particles were more consistently dispersed throughout the tests and affected the contact area whether it be positively or negatively.

The Hybrid mixtures all used 0.5 wt% SiO_2 in an attempt to encourage a mechanochemical reaction with the nanospheres' abrasive properties. A variety of MoS_2 concentrations were used. Figure 5.14 shows that only the mixture containing 1 wt% MoS_2 had similar friction to the base oil. Due to the SiO_2 results before, this is as expected because the hard particles are believed to increase abrasion if there are too many of them.

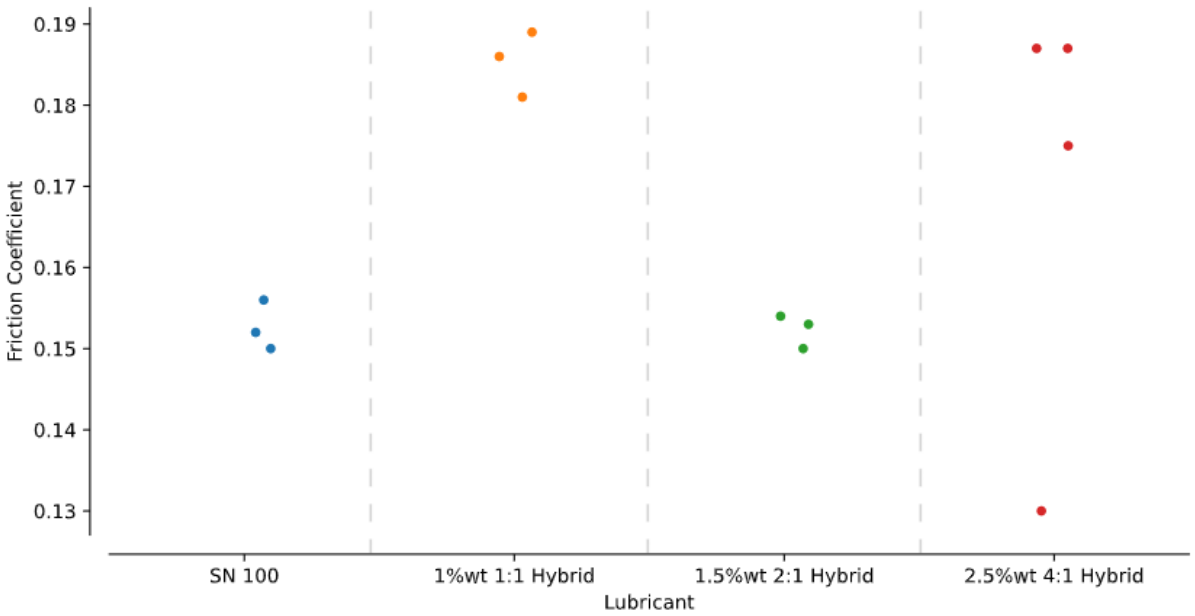

Figure 5.14: Median friction for Hybrid mixtures

One test in the 4:1 hybrid performed significantly better and may have had good synergystic tribofilm formation but using the same variables, a further three tests all performed at a similar level to 0.5%wt MoS_2 mixture. The topography of the wear scars was scanned using the Alicona InifiniteFocus. Cross-sectional wear profiles were taken from the scans and are shown in Figure 5.15.

The MoS_2 and control wear scars are close to 6 µm in depth. The anomalous hybrid

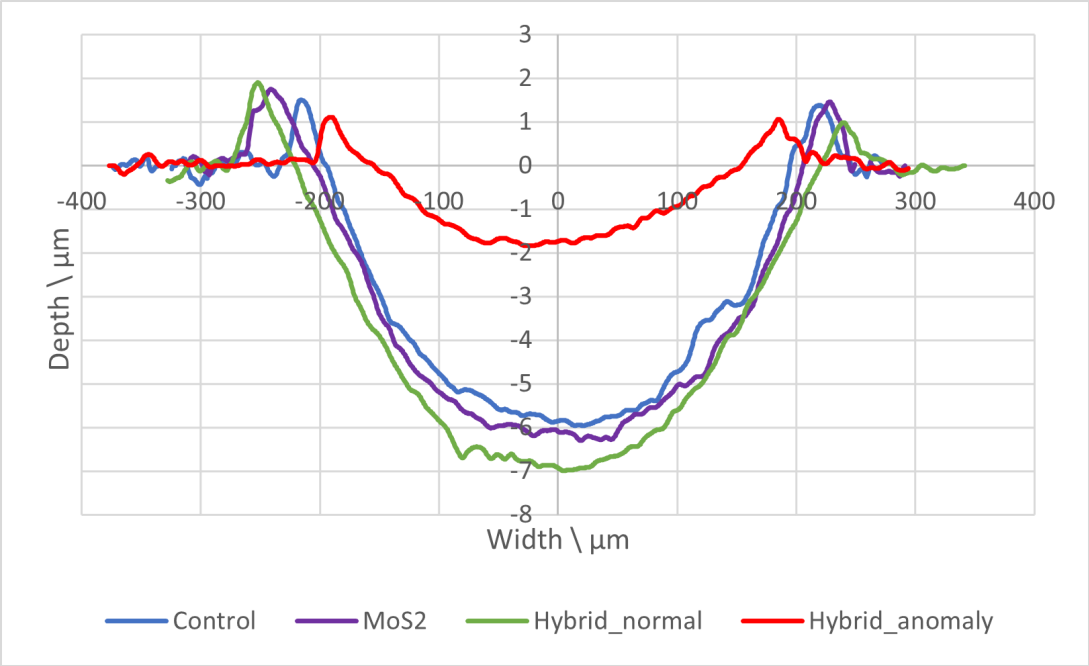

Figure 5.15: Representative cross-sectional wear profiles of scars made in the Low Load Adapter taken from Alicona scans. All measurements are in microns.

wear scar has a depth less than a third of that, whereas the other hybrid scars are closer to 7 µm at maximum depth.

Table 5.4 presents the variances of median friction coefficient with constant variables in the HFRR and the LLA when the load and temperature were similar (≈8 N and 50 °C). While the normal load in the HFRR has been shown to not be consistent throughout the stroke, it produced highly repeatable results under these conditions.

Table 5.4: Sample variance of median coefficient of friction in equivalent tests from the HFFR and TE 77 LLA

	Sample Variance $\times 10^6$	
	HFRR	LLA
Base Oil	1.33	9.33
1 % MoS_2	4.00	106.67
0.5 % SiO_2	9.33	108.33
1:1 Hybrid	6.33	16.33
2:1 Hybrid	4.33	4.33

There are some key differences between the HFRR and the LLA adapter that could contribute to contrast in repeatability, one is the shape of the lubricant baths which can be seen in Figure 5.16. The HFRR has a rectangular bath where the wear direction is normal

to two walls 21.85 mm apart. The LLA bath is circular with a diameter of 27.7 mm. The surface area of 1 ml of liquid in each bath is 654.4 mm^2 and 602.6 mm^2 respectively.

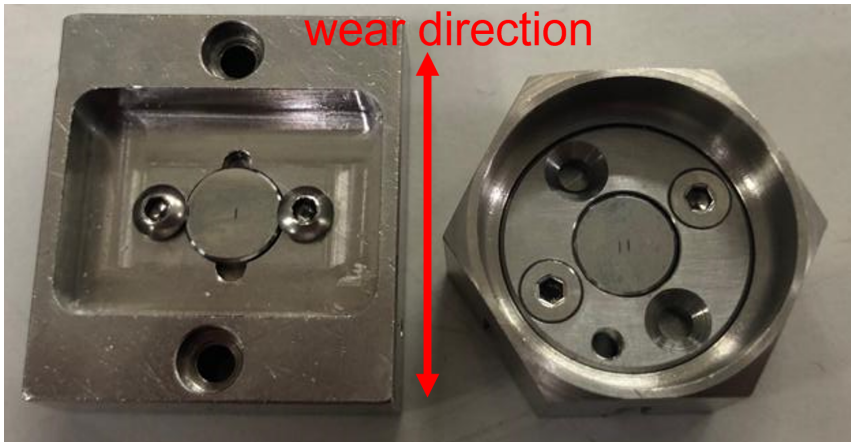

Figure 5.16: Lubricant baths for the HFRR (left) and TE 77 Low load adapter (right)

These differences in geometry will effect how physical waves caused by the reciprocating motion will travel and reflect. A square tank is 18 % more effective at damping waves than a circular tank of the same surface area (Ibrahim, 2001). However, a wave generated by the oscillation during a wear test must travel further in the LLA bath in order to reflect off the bath wall and return to the contact area than it does in the HFRR. This increased distance may reduce energy in the wave sufficiently to decrease its ability to break up agglomerations and agitate nanoparticles to keep them dispersed in the mixture compared to the HFRR.

An alternative reason for the LLA's inconsistency is the way in which the applied load is transferred to the upper specimen. Figure 5.17 depicts how the normal load is applied through a threaded screw that attaches the load link to the upper specimen holder. A polymer stepped spacer on the screw prevents rotation in the specimen holder and helps prevent damage to the components.

If the screw is wound too tight, the spacer clamps to the reciprocating head preventing the specimen holder from having free vertical movement, which in turn stops the desired normal load from being applied to the contact. If the screw is wound too loosely, the alignment of the load link will be slightly off-centre causing vibration in the load arm with the reciprocation and providing and inconsistent load. In order to mitigate these

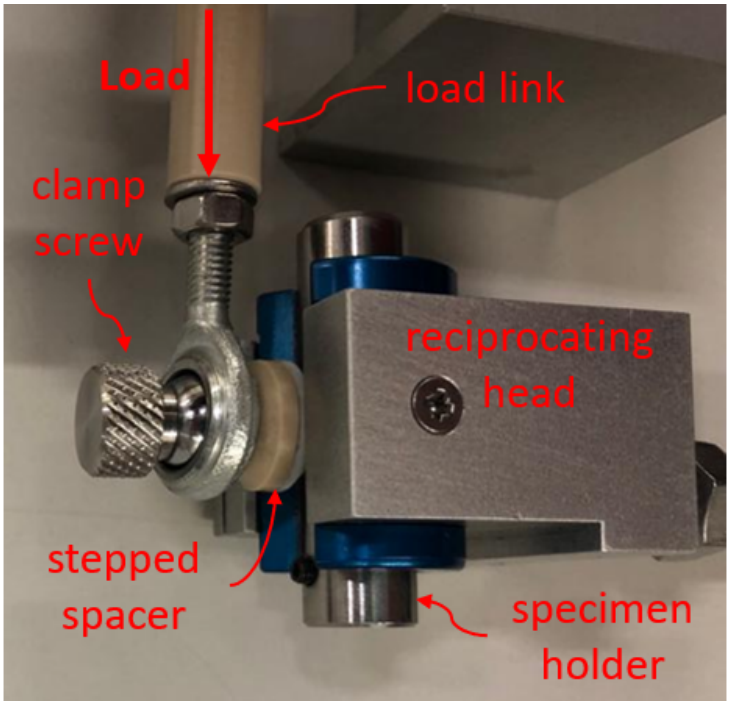

Figure 5.17: Image of the load link through to the reciprocating head of the low load adapter

potential problems as much as possible, the screw was wound until the spacer provided resistance against the reciprocating head and then unwound half a turn. Whilst this should be consistent, and no vibration was humanly visible when using this method, the winding was done entirely by hand and so there would be slight variations from test to test.

SEM and EDS was performed on the 4:1 Hybrid scars to see if any tribofilm similar to that seen in Figure 5.7d was formed in the low load adapter and to understand if there were significant chemical differences between the anomalous wear scar and the others. In the wear scar SEM images (Figure 5.18), an area running through the middle of them all was highly oxidised similarly to that observed in the base oil scar in Figure 5.7a. This area was ≈128 µm and ≈175 µm in width for the standard wear scars and the anomaly respectively.

The average sulphur content within the unique wear scar was lower than the other 4:1 hybrid scars (0.205 Atomic% and 0.483 Atomic% respectively), however, EDS mapping showed that in the areas highlighted in Figure 5.18b there were high concentrations of

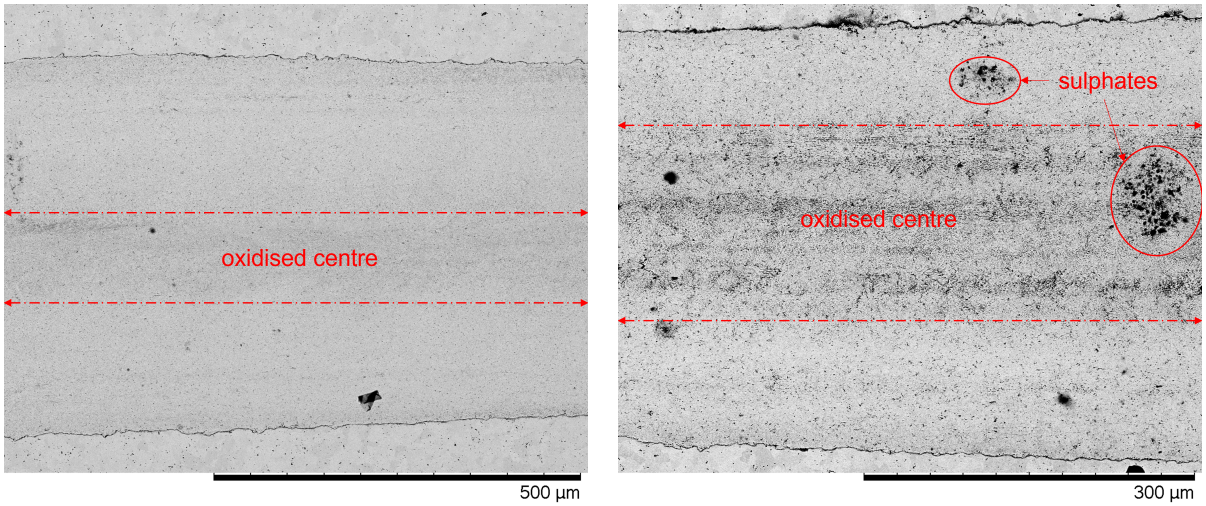

(a) Standard 4:1 Hybrid wear scar (b) Anomolous 4:1 Hybrid wear scar

Figure 5.18: SEM images of wear scars generated in the TE 77 Low Load Adapter using 4:1 Hybrid lubricant. (a) Is a representative example of the standard wear scars and (b) is the anomalous scar.

sulphur and oxygen suggesting that metal sulphates had been formed. Table 5.5 shows the differences in chemical content between the unique scar and the standard hybrid scars. The carbon content is significantly higher than the quantity typically found in AISI 52100 steel (≈1 %). This is common in scars that have been lubricated with oil (Seyedzavvar et al., 2020; Wan et al., 2014) and is likely adsorption of the oil to the surface or small quantities of ethanol that was used to clean the surface could remain and influence the carbon quantities. Other than sulphur content key differences in the quantities are reduced oxygen and increased silicon in the anomaly.

Table 5.5: Average atomic % within the wear scars of the anomalous 4:1 Hybrid scar compared to the average of the other scars. The elements represented in the last row are typical additives in AISI 52100 steel such as manganese and chromium.

	Atomic %	
	Unique Hybrid	Other Hybrid
Carbon	21.593	20.834
Iron	56.403	53.382
Molybdenum	0.082	0.042
Oxygen	18.488	23.191
Silicon	0.777	0.404
Sulphur	0.206	0.473
Other	2.454	1.676

Table 5.5 and Figure 5.18 show some minor differences in the composition of the wears scars generated using all the same variables but it is clear that a tribolfilm similar to that formed in the HFRR with the 2:1 Hybrid mixture has not been formed and the proposed synergistic effect has not been repeated using the LLA. The small quantity of extra sulphur and molybdenum found in the standard wear track was clearly not able to beneficially effect either the friction or wear. The hypothesised inconsistency in dispersion and agglomeration could be the reason for more silicon in the anomaly as SiO_2 nanospheres may have been able to separate the surfaces and act as bearings rolling between them. However, due to this one anomalous result of four, it is perhaps more likely that the difference is due to the desired normal load not being properly applied through the LLA clamp screw. The change in friction was far greater than any of those seen between solely MoS_2 mixtures using constant variables.

5.4 Summary

MoS_2 and SiO_2 nanoparticles were analysed with a TEM and subsequently tribologically tested in both the HFRR and TE 77 low load adapter as additives in SN 100 base oil. Multiple concentrations of each nanoparticle were used both separately and together in hybrid mixtures. A variety of surface analysis techniques were employed on the generated wear scars to understand the mechanisms by which the nanoparticles operated within the contact area.

The key results are summarised below:

- TEM analysis confirmed the spherical nature of the SiO_2 nanoparticles with little evidence of agglomeration. MoS_2 was shown to be 2D with large agglomerates which needed to be broken up with an Ultrasonic shaker prior to testing.

- Initial ambient temperature tribological tests in the HFRR proved to generate highly inconsistent COF results with no lubricant performing better at multiple loads than any other and there was large variance within multiple tests with the same variables.

The hybrid mixture produced the smallest wear scar diameter on the upper specimen.

- When the temperature of the HFRR tests was increased to 50 °C, the Hybrid mixtures had slightly lower COF than the control lubricant and the two containing either only MoS_2 or SiO_2. This slight improvement was shown to be statistically significant with ANOVA single factor analysis.

- SEM images of the wear scars from the high temperature tests showed that when MoS_2 was added on its own, small flakes of MoS_2 were left embedded in the surface of the wear track. These did not have a significant impact on either the COF or the volume of wear. In the hybrid wear tracks, a thin tribofilm was generated in the centre of the wear track. This tribofilm protected that section of the track and EDS and HAXPES confirmed that it contained iron sulphides and sulphates as well as MoS_2 and other oxides. This proved that a synergistic interaction had occurred between the SiO_2 and MoS_2. The hypothesised mechanism for this interaction was that the SiO_2 "helped" the MoS_2 mechanochemically react with the iron in the lower specimen surface due to the surface polishing aspect of the hard nanospheres. Without the SiO_2, no chemical reaction occurred.

- The theory that some of the inconsistency in results was a result of the loading and reciprocating mechanisms in the HFRR was explored and further testing of the nanofluids was performed using the TE 77 Low Load Adapter.

- Low load adapter tests at the same temperature and load as the HFRR had a very large variance even when all variables were constant. This was put down to a combination of two factors. The first was that the different shape of the lubricant bath reduced the consistency with which the reciprocating motion agitated the lubricant enough to keep MoS_2 dispersed and prevent agglomeration. The second factor was a clamping screw that transferred the normal load to the upper specimen

and held the specimen holder in the reciprocating head. The screw could prevent the normal load from being properly applied if wound too far.

- The tribofilm formed in the HFRR was not reproduced in the low load adapter.

This chapter provided some evidence that the combination of hard and soft particles can be used beneficially to mechanochemically generate a protective tribofilm on a metal surface in certain conditions but good, consistent dispersion is essential for reliable results.

Acknowledgements

I wish to acknowledge the support of the Henry Royce Institute for me through the Royce PhD Equipment Access Scheme enabling access to XPS and HAXPES facilities at Royce@Manchester; EPSRC Grant Number EP/R00661X/1

Chapter 6

Grease micro-additives inducing superior surfaces

6.1 Introduction

A major problem encountered in previous chapters with regards to attempting to generate a tribofilm has been keeping the nanoparticles in the contact area and well dispersed throughout the oil. At the end of a test, MoS_2 would have visibly settled on the substrate material, outside the contact area. One method to avoid this, not previously attempted in this thesis, would be to use grease. The high viscosity of grease keeps nanoparticles well dispersed once thoroughly mixed (Fu et al., 2019).

One of the challenges with using grease, however, is effectively mixing the nanoparticles. The high viscosity must be overcome to ensure good homogeneous dispersion. This can be done by temporarily reducing the viscosity through increasing the temperature (Singh et al., 2018) and mechanically stirring the particles or through mixing the grease at very high speeds causing shear-thinning (Fu et al., 2019) to have the desired effect for good dispersion of the nanoparticles. If the temperature method is used then a further process is used to break up any agglomerations such as a triple roller mill (Singh et al., 2018; Zhao et al., 2014).

MoS_2 has been shown to successfully reduce friction and wear when used between metal contacts in grease, with tribofilm formation believed to be one of the key mechanisms for improving the tribological properties of the material (Rawat et al., 2019; Sifuentes et al., 2021). Al_2O_3 has been shown to damage the thickening structure of lithium grease leading to a slightly worse but comparable tribological performance when compared to the base grease due to high abrasion from the particles in the contact (Singh et al., 2018).

As discussed in previous chapters, copper has a higher standard reduction potential than molybdenum (Vanýsek, 2010), meaning that sulphur may more easily reduce from Cu_2S and attach itself to iron in a steel substrate than from MoS_2. This hypothesis has been tested with some success using shot-peening previously (Qi et al., 2019; Varenberg et al., 2016) and while honing using Cu_2S did not produce the desired mechanochemical effect in chapter 4, it will be used again in the present study.

In this chapter, a line contact will be used with a variety of greases in an attempt to

mechanochemically create a large area of sulphide film with superior tribological properties. This acts like a lubricated burnishing process. to then be further tested in boundary lubrication conditions with ball-on-flat tests in a simple base oil. A multipurpose lithium mineral oil grease will be used as the base. Cu_2S microparticles will be added as the sulphide source for the tribofilm and Al_2O_3 micropartilces will be added to some of the greases to increase the severity of the contact to increase the likelyhood of a tribochemical reaction. A fully formulated commercial grease already containing MoS_2 will also be tested.

If successful, an adaption of the initial grease procedure could be used as a mechanical finishing process to improve the wear resistance of metal components.

6.2 Materials and methods

Formulation of greases

The base grease used in this chapter was COMMA's multipurpose lithium grease (Moove Lubricants Limited, Gravesend, UK). A second fully formulated commercial grease was used as a comparison with greases formulated in this chapter. This grease was COMMA's CV Lith-Moly grease containing MoS_2 (Moove Lubricants Limited, Gravesend, UK).

The additives used with the base grease were Cu_2S microparticles of less than 45 µm acquired from Merck and Al_2O_3 of the same size from Fischer Scientific. The concentrations of the microparticles in the grease are shown in Table 6.1.

Table 6.1: Greases tested to create tribolayer. wt % indicates quantity added to base grease.

Grease	**Cu_2S** *wt%*	**Al_2O_3** *wt%*
Multipurpose Base Grease	0	0
Lith-Moly commercial grease	0	0
2% Cu_2S	2	0
5% Cu_2S	5	0
Hybrid	5	0.5

As the additives being used are microparticles rather than the nanoparticles utilised in chapter 5, the surface area per volume is significantly lower, therefore, higher concentrations of sulphide particles are needed to increase the likelihood of reactions occurring. For Al_2O_3, the larger particles still have high hardness so the concentration was set at 0.5 wt%, as higher concentrations could be overly abrasive to the surface. As Cu_2S is easily deformed, the larger particles can still be smeared across the surface.

The greases were mixed by first bringing the base grease to 110 °C then slowly adding the microparticles to the greases while mixing with a magnetic stirrer. The stirring continued for 1 h at the same temperature. Newly mixed micro-greases were then placed in an ultrasonic shaker and kept at 80 °C for a further 30 mins to break up any agglomerations.

TE 77 grease tribofilm process

In an attempt to make the potential tribofilm area as large as possible, an AISI 53100 steel line contact of length 19 mm and 6 mm⌀ was used on a BO1 steel flat plate that was purchased directly from Phoenix Tribology Ltd (Kingsclere, UK). Specimens were worn against each other in Phoenix Tribology's TE 77 High Frequency Friction Machine (TE 77). The stroke was 20 mm and the frequency, 2 Hz. The grease was spread over the contact area. After heating the plates and greases to 50 °C, the load started at 400 N and ramped up by 40 N every 5 minutes up to 920 N. The test finished with 20 min at a constant load of 920 N. The maximum load was selected as the lubricant film failed above that load (Coefficient Of Friction (COF) would rapidly increase to >0.5). After the test, the specimens were cleaned by ultrasonic shaker while immersed in ethanol then wiped dry. This was to ensure any additives still present were adhered to the surface.

Wear testing

A series of point contact tests were performed on the surfaces generated by the greases with SN 100 base oil as a lubricant. An untreated plate was also tested as a control. The upper specimen was always a 6 mm AISI 52100 steel ball.

Two sets of tests were run at 23 °C at 2.5 Hz and 10 mm stroke length for 30 min which is 4500 cycles with a maximum sliding speed of $0.16\,\mathrm{m\,s^{-1}}$. The first set of tests had, a normal load of 5 N which generated a maximum initial Hertzian contact pressure of 1.1 GPa, the second set increased the load to 50 N for a p_o of 2.3 GPa.

A final set of tests was performed to generate increased wear with the aim of more contrast in scar depth between the different surfaces. The temperature was 50 °C, the load was kept at 50 N, the stroke length reduced to 5 mm and frequency risen to 5 Hz. This kept the maximum sliding speed at $0.16\,\mathrm{m\,s^{-1}}$ but with an increased test time of 1 h, the number of cycles was now 18 000.

The grease-worn plates were all compared to a control plate that had no additional processes applied to it after purchasing from Phoenix Tribology. Each set of tests was performed in triplicate. A complete list of all wear the wear test and their parameters is shown in Table 6.2.

Table 6.2: Design of Experiments - A complete list of the different friction tests performed in this chapter. Each line of parameters was tested at least in triplicate

Burnish Grease	**Additives (wt%)**		**TE77 Parameters**					
	Cu_2S	Al_2O_3	Load (N)	p_o (GPa)	Time (h)	Temp. (^{o}C)	Frequency (Hz)	Stroke (mm)
None	N/A	N/A	5	1.1	0.5	23	2.5	10
Base	0	0	5	1.1	0.5	23	2.5	10
Base	5	0	5	1.1	0.5	23	2.5	10
Base	5	0.5	5	1.1	0.5	23	2.5	10
Lith-Moly	0	0	5	1.1	0.5	23	2.5	10
None	N/A	N/A	50	2.3	0.5	23	2.5	10
Base	0	0	50	2.3	0.5	23	2.5	10
Base	5	0	50	2.3	0.5	23	2.5	10
Base	5	0.5	50	2.3	0.5	23	2.5	10
Lith-Moly	0	0	50	2.3	0.5	23	2.5	10
None	N/A	N/A	50	2.3	1	50	5	5
Base	0	0	50	2.3	1	50	5	5
Base	5	0	50	2.3	1	50	5	5
Base	5	0.5	50	2.3	1	50	5	5
Lith-Moly	0	0	50	2.3	1	50	5	5

Surface morphology and characterisation

The lower specimen plate surfaces were observed using the Hitachi TM3030 Scanning Electron Microscopy (SEM) machine both after the tribofilm formation process and the wear tests. Analysis of the elemental composition of the surface was also performed through the TM3030's Energy Dispersive Spectroscopy (EDS) capabilities.

Surface roughness calculations on the grease-worn surfaces were made using multiple profiles measured in the Alicona InfiniteFocus microscope. These profiles were ≈1.5 mm in length and normal to the direction of wear. The Roughness Average (Ra) was calculated by summing the absolute distance of ≈1500 points (Z_i) away from the mean ($\bar{Z}$) and dividing by the number of points (N), or:

$$Ra = \frac{1}{N}\sum_{i=1}^{N}|Z_i - \bar{Z}| \tag{6.1}$$

Lower specimen wear scars generated in the point contact tests were also analysed using the Alicona InfiniteFocus microscope. Upper specimen balls used in the point contact wear tests were observed using a Meiji metallurgical microscope which could then measure the Wear Scar Diameter (WSD) through the program, HFRRPC (PCS Instruments).

6.3 Results and discussion

Grease-worn surface analysis

The specimens were analysed with the Hitachi TM3030 after the initial rubbing with the grease and additives in the TE 77. EDS found that chemical composition of the surfaces were not consistent throughout each surface. Only with the Lith-Moly grease did the analysed area consistently contain >0.2 atomic% sulphur throughout. The mean element quantities found by EDS in each surface is shown in Table 6.3.

Table 6.3: Mean atomic % of elements present in the surfaces generated with greases containing different additives. The elements represented in the last row are typical additives in BO1 tool steel, i.e. manganese, silicon and chromium.

	Mean Atomic %				
	Base Grease	2% Cu_2S	5% Cu_2S	Hybrid	Lith-Moly
Carbon	50.007	19.574	15.768	44.554	43.382
Copper	0	0.012	0.331	1.149	0
Iron	45.803	68.077	44.491	45.834	45.230
Molybdenum	0	0	0	0	0.069
Oxygen	3.121	9.633	38.217	7.134	9.679
Sulphur	0	0.048	0.063	0.183	0.530
Other	1.069	2.656	1.129	1.146	1.110

When 2 wt% Cu_2S was added to the grease, only an average of 0.048 % sulphur was found on the surface and only a quarter of that for copper. In many of the positions analysed, no sulphur was detected at all. The Cu_2S content was deemed to be too low to be effectively transferred or reacted with the surface. Similarly to when EDS was performed on the honed surfaces in chapter 4, the other mixtures where Cu_2S was used as an additive, the quantity of copper found in the surface is greater than double that of sulphur, suggesting that some of the latter had been lost during the process. Qi et al. (2019) and Varenberg et al. (2016) did not specify the element quantities so it is unknown whether they had the same results when shot-peening Cu_2S microparticles. The addition of Al_2O_3 appeared to increase the uptake of copper and sulphur to the surface without any aluminium remaining, though the maximum found in one place was 4× greater than the average so there was a far less consistent coverage than the Lith-Moly grease was able to produce. For the surface generated using the Lith-Moly grease, the EDS spectra showed the sulphur content present in the scans between 0.277 % and 1.015 % depending on where the scan was taken from. Figure 6.1 shows an SEM image of the rubbed surface. Points 1 and 2 were selected as they were in areas that were of high contrast to each other in the SEM image suggesting differing chemical composition. Point 3 was selected as a transition area between dark and light areas.

Point 2 in Figure 6.1 indicates where 1.015 % sulphur was found. The same spectrum indicated that only 0.068 % of the atoms present were molybdenum. This is strong evi-

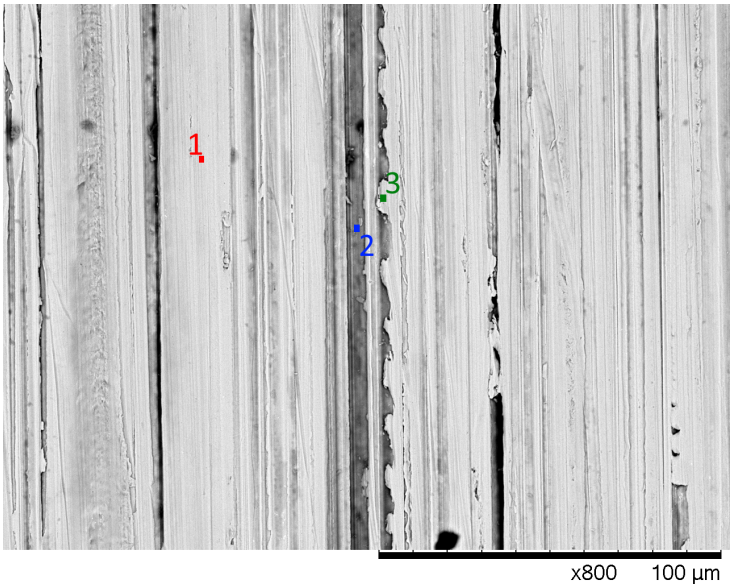

Figure 6.1: SEM image of the steel plate rubbed with commercial lith-moly grease. The three points indicate where EDS spectra were taken.

dence that a reaction has occurred and a sulphide/sulphate film has formed that contains insufficient molybdenum to be purely MoS_2. In all three points where the spectra were taken, more than twice as much sulphur was present than molybdenum.

The original plate had been pre-ground using 0.4 µm abrasives, according to Phoenix Tribology. This grinding was done parallel to the direction of wear in the TE 77. This means that the pre-purchased grinding, the grease-wear process and later point contact friction tests all operate in the same direction. This could cause several problems, one being that the point contacts will follow lines of single asperities made by either process so could lead to inconsistencies between tests on the same surface. The average roughness on each of the surfaces was measured in the Alicona. The surface roughness, normal to the direction of wear is shown in Table 6.4.

Table 6.4: Surface Roughness, *Ra*, of grease-worn surfaces

	Ra (µm)
Untreated	0.933
Base grease	0.867
5% Cu_2S	0.837
10:1 Hybrid	0.787
Lith-Moly	0.705

The grease-wear process appears to have reduced the surface roughness compared to

the untreated plate. All the greases that contained additives produced a smoother surface than the base grease which could be attributed to Cu_2S and MoS_2 being smeared into some of the asperities. Al_2O_3 also improved *Ra* compared to the grease only containing Cu_2S. This suggests, as shown in Figure 6.2, that the film thickness of the grease was large enough that the hard alumina particles did not plough into the surface leaving deep furrows (Figure 6.2c) but also thin enough that some surface polishing could be achieved by those same particles (Figure 6.2b). The commercial Lith-Moly grease produced the lowest surface roughness in the steel plate. This is unsurprising as it is likely to have been commercially tested to contain the ideal MoS_2 particle size and concentration to operate in harsh contact conditions.

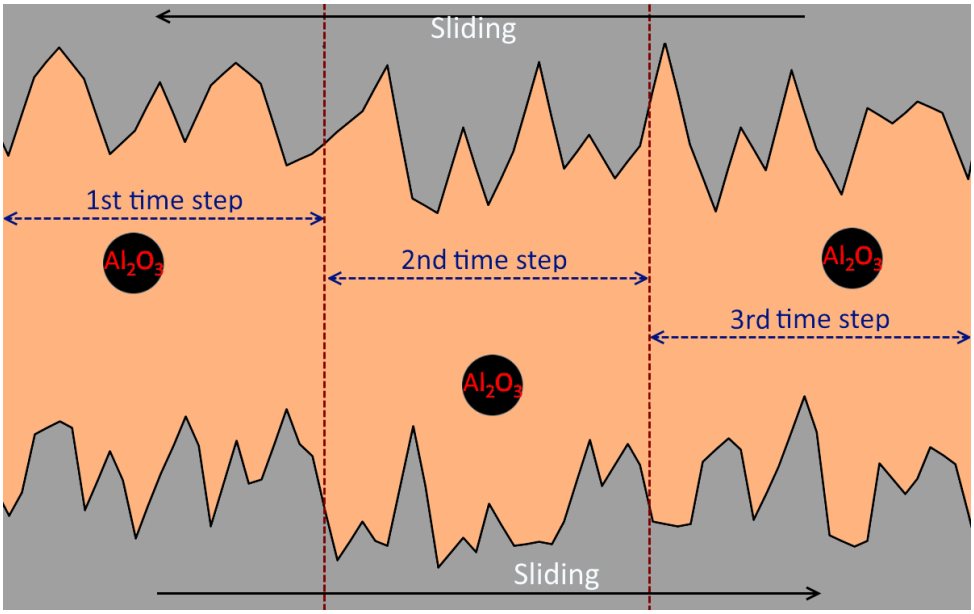

(a) Film too thick for Al_2O_3 to be effective

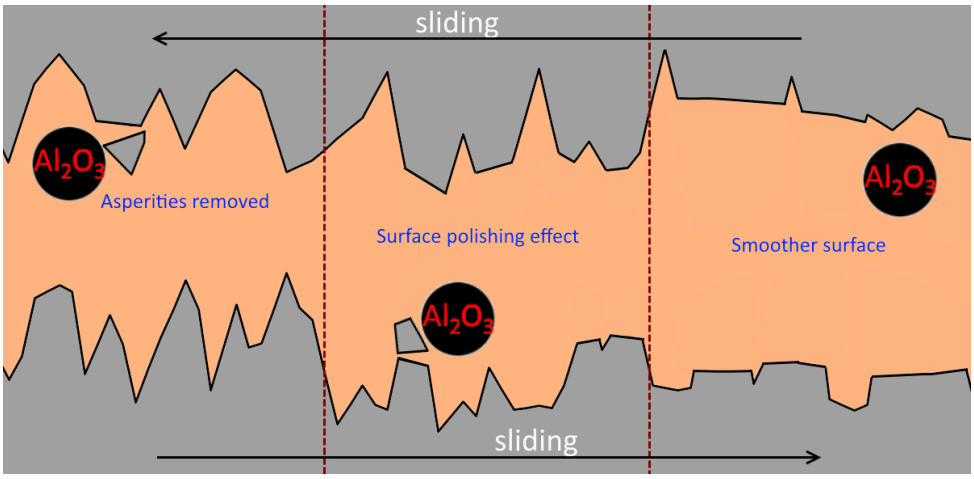

(b) Film right thickness for surface polishing to occur

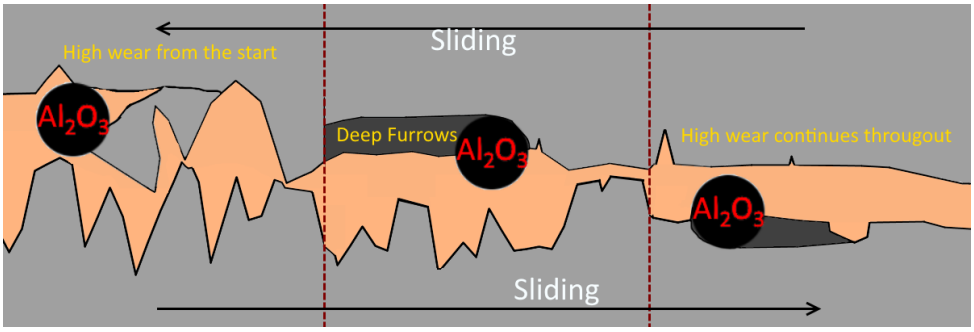

(c) Film thickness smaller than diameter of particle, Al_2O_3 causes massive wear.

Figure 6.2: How Al_2O_3 nanospheres interact with sliding metal surfaces in different lubricating film thickness.

Wear tests

The first set of wear tests in the TE 77 using SN 100 as the lubricant were with the 5 N load and 10 mm stroke. The median friction for all the tests done are shown in Figure 6.3.

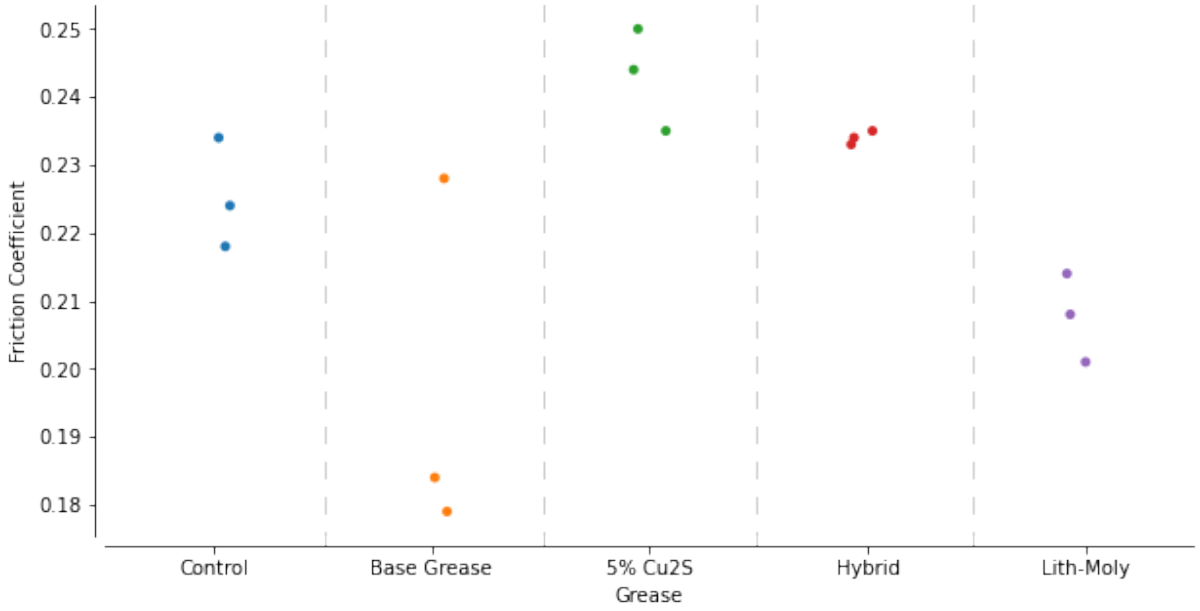

Figure 6.3: Median Friction coefficient for ambient 5 N tests.

What is immediately obvious is that all the median friction coefficients are high for lubricated wear between steel contacts. Only the two lowest points in the base grease are comparable to any of the results seen in previous chapters. There is what looks like an anomalous test in the base grease surface. If that is the case then it clearly produced the lowest friction compared to the other surfaces but more tests would be needed to confirm this. Including the potentially anomalous result in ANOVA single factor analysis, the high variance meant that the base grease results were not statistically significant compared to any of the other results. The two greases containing Cu_2S did produce significantly higher friction than the Lith-Moly grease. This could be due to the reduced copper that had sintered into the surfaces. Ductile materials such as copper have strong adhesion (Hutchings and Shipway, 2017) which can lead to higher friction. The Lith-Moly grease COF improvement over the control plate was also statistically significant, this could be due to the reduced roughness in the treated surface more than any chemical differences in the respective surfaces.

The load in the TE 77 was increased to 50 N and the point contact wear tests repeated with double the initial contact pressure of the previous tests. Median friction is shown in Figure 6.4.

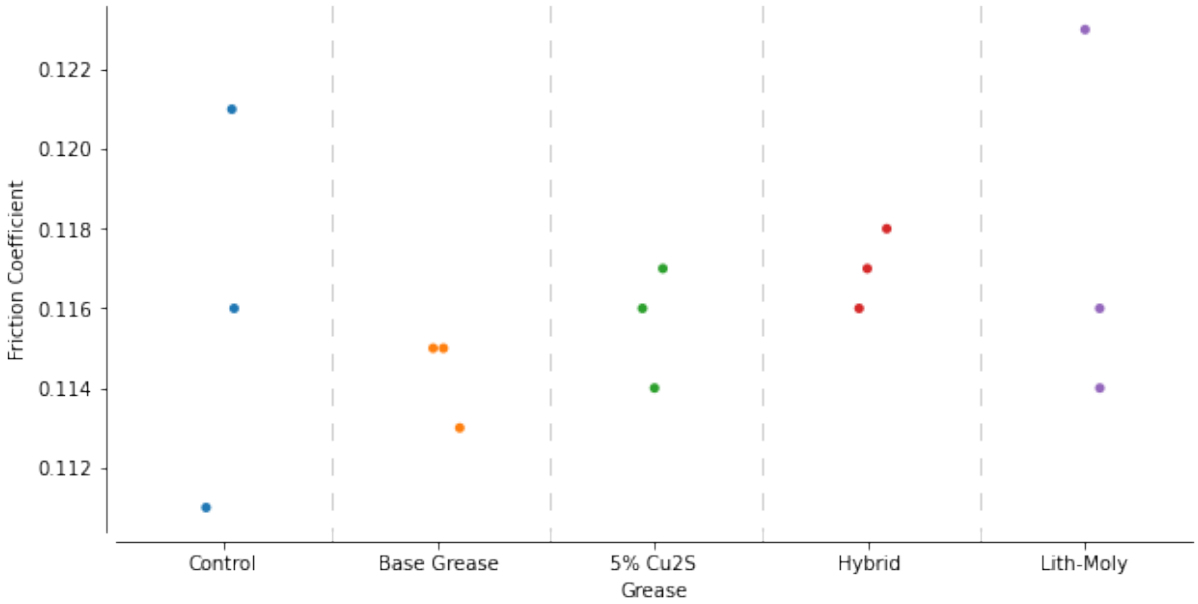

Figure 6.4: Median Friction coefficient for ambient 50 N tests.

The friction coefficient is drastically lower compared to in Figure 6.3. For the hybrid and Cu_2S worn surfaces it is around half. This is remarkable given that with the increased load and other factors remaining the same, lubricant conditions should be much more severe. Considering the Stribeck curve in Figure 2.1, the load change will have pushed the lubricant conditions further into boundary lubrication. Unfortunately this decrease is not due to any of the additives introduced with the greases as none of the produced surfaces performed significantly better than any of the others, though the control plate had high variance compared to the others.

The lower specimen wear scars were analysed using the Alicona, however, the scars were too shallow to be meaningfully differentiated from the asperities already in the material surfaces. This is another downside of all the processes performed on the surfaces acting in the same direction, when there is little wear, the asperities caused by the grinding process are more pronounced than the wear scar and as they are acting in the same direction, meaningful wear scar measurements are impossible. The upper specimens were

observed and the WSD measured using an optimal microscope in order to gain a level of comparison between the wear rates of the different lower specimen surfaces. The measured average WSDs are presented in Figure 6.5.

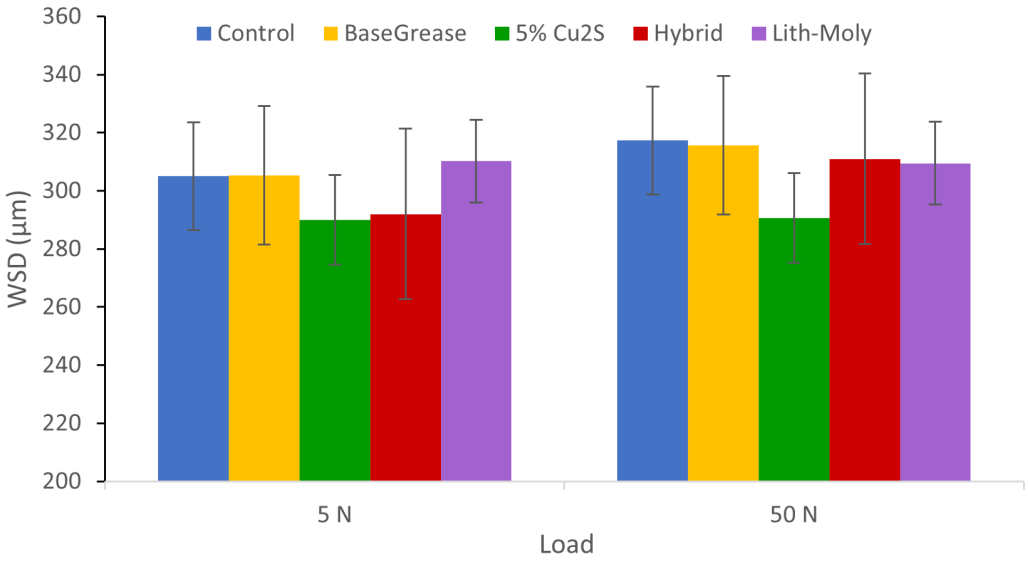

Figure 6.5: Average wear scar diameter for ambient wear tests. Error bars signify ± 1 standard deviation.

According to Equation 3.1, the initial contact area should have a diameter of 94 µm for the 5 N load and 203 µm for the 50 N load. Given that the Alicona observed minimal wear scar depth, the upper specimens' WSDs could be similar to the initial contact diameter, however, this is not the case at 5 N. The average WSD across all the surfaces is only 7 µm greater at 50 N than at the lower load (308.9 µm to 301.6 µm). The wear scars are also smallest in the 5 N load for the surfaces that had Cu_2S as a grease additive; the same surfaces that had the highest friction. In the higher load test, the Cu_2S surface continues to have the narrowest wear scar.

The high wear on the balls and the friction at 5 N are likely to be related. It is also intriguing that there is no obvious depth to the lower specimen scars. As Table 3.4 shows, before anything was done to the plates, they had a similar hardness to the upper specimen balls. Varenberg et al. (2016), found that when they only shot-peened the surface with alumina microparticles, plastic deformation caused the roughness to be reduced and the surface hardness to increase (191 HV to 250 HV). Although only one of the greases

contained Al_2O_3, the grease-wear process involved very high pressure on the plate that caused some plastic deformation as it reduced the surface roughness. It could be that the process alone dramatically increased the plates' hardness regardless of the presence of additives through strain hardening of the surface (Buckley, 1981). Unfortunately, for this hypothesis, the control plate would show very different wear results to the other surfaces, however, it is almost identical to the base grease in both tests. The upper specimen wear scar diameter may not be due to increased wear on the ball compared to the lower specimen but instead, the asperities on the rougher lower specimen surface make the apparent contact area larger than that predicted by Hertzian contact dynamics.

With regards to the great difference in COF between the two test loads, this could be due to the hardness of the materials. When the load is lower, the upper specimen is only able to elastically deform asperities in the lower specimen so there is little surface polishing taking place during wear. At high load, there is enough force going through the contact to plastically deform the asperities early in the wear, so friction is lower for the remainder of the test. Figure 6.6 shows the average COF for the first minute of the two sets of tests.

At the beginning of the lower load tests in Figure 6.6, the control, base grease and lithmoly surfaces reach the settled friction coefficient without exceeding it first and the two Cu_2S surfaces exceed it by less than 20 % before settling. For the 50 N tests in Figure 6.6, all the different surfaces exceed the final coefficient and the Cu_2S surfaces by more than 35 %. This overshoot supports the surface polishing theory for the high load surfaces. In the first 20 s to 40 s asperities are being plastically deformed, causing high friction, but after that initial period, the surface is much smoother so friction is reduced. At low load the force is never great enough to permanently deform asperities of the hard surface so friction stays high and the ball continues to get worn.

Further evidence of this hypothesis can be found by looking at the TE 77's High Speed Data (HSD) for the respective tests. In the first and last five seconds of each test, the TE 77 took 10 000 stroke position and friction force readings. This data can be used to look at how the friction changes across each cycle of movement. Figure 6.7 shows the

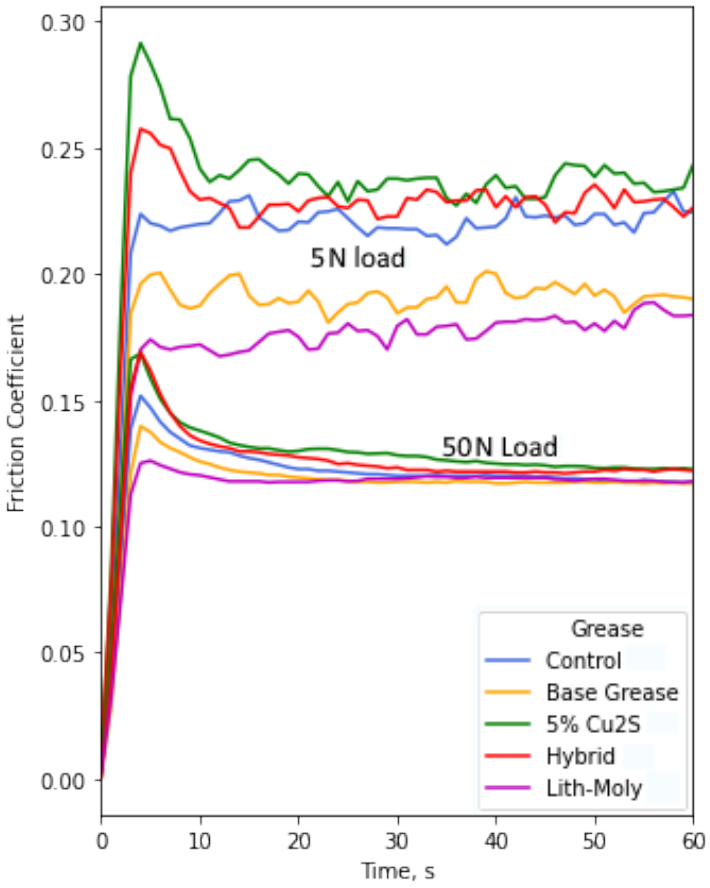

Figure 6.6: Mean friction coefficient for the first 60 s of wear for both the 5 N and 50 N loads.

HSD taken at the end of a control plate test in both loads. This is representative of the differences between the two loads for all the surfaces. The positive and negative friction coefficients represent the different directions of the stroke.

The high load tests show a smooth transition in COF across the stroke that rises as the ball slows down at the end. The low load friction fluctuates erratically throughout each cycle. This supports the hypothesis that the stresses caused by the load and sliding surfaces is insufficient to plastically deform many of the asperities in the plate but the lubricant film is thin enough for them to apply a resistance force on the sliding ball. In the high load tests, the stresses are sufficient for the asperities to be plastically deformed, smoothing out the surface so there is a much smaller resistance force that does not change dramatically across the stroke.

In an attempt to acquire wear scars that are measurable with the Alicona, the severity

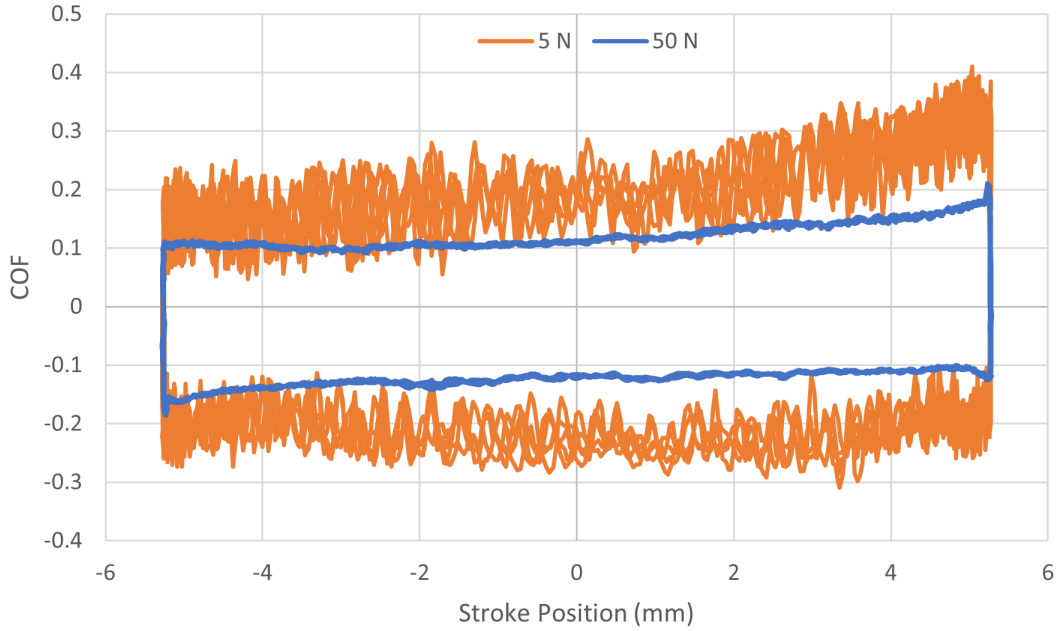

Figure 6.7: High speed data of friction across the stroke at the end of the control tests.

of the wear test was increased. The aim being to understand if there are significant differences in wear generated through the use of different additives. The runtime and reciprocating frequency were doubled to quadruple the number of cycles but stroke length was halved so that the maximum sliding velocity remained the same as in previous tests. The temperature was also increased to 50 °C so the lubricant film would be thinner. Figure 6.8 depicts the mean friction over time on the different surfaces for the more severe tests.

The initial friction bares resemblance to that of the high load ambient tests in **??** with the spike up to 35 % higher than the eventually settled coefficient. All the surfaces produced very similar COF with little variance, every individual test median was between 0.125 and 0.129. However, for the control scar, the COF consistently rises throughout the test leading to a higher mean friction. Due to the very low variance in all the tests (between 7.4×10^{-8} and 1.1×10^{-6}), this small increase was enough to make the mean statistically higher than all the other surfaces according to ANOVA single factor tests with two sample t-tests between pairs of surfaces. This small improvement shows that the high pressure grease treatment did affect all the surfaces even without the presence of

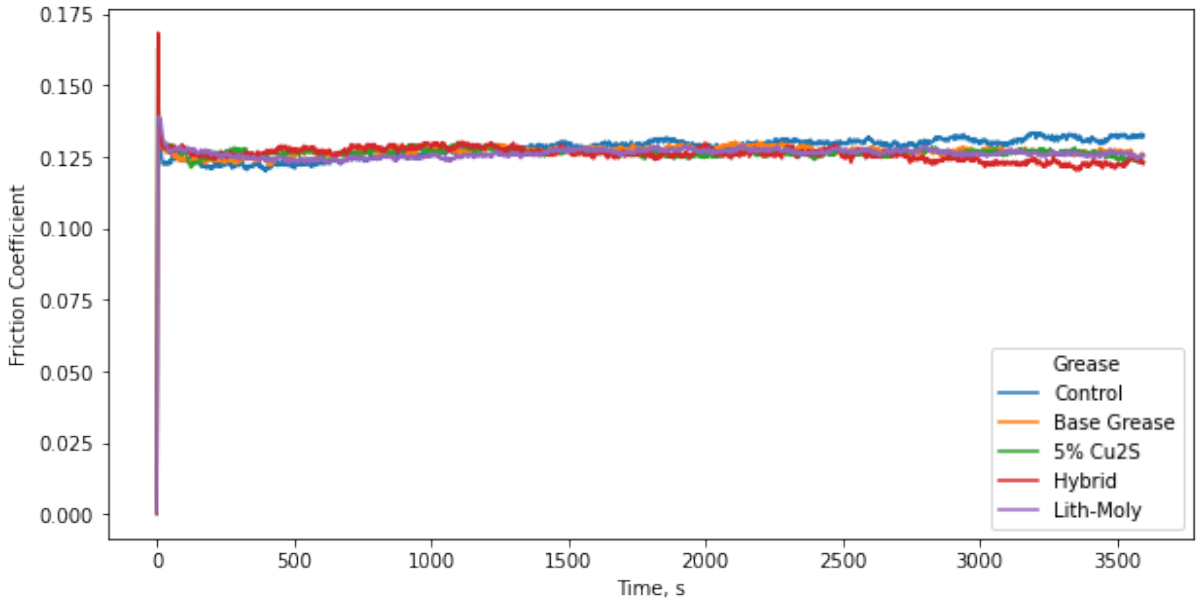

Figure 6.8: Mean friction coefficient over time for point contact 50 N load wear tests at 50 °C.

additives. The trajectory of friction for the control suggests that the longevity of the other surfaces was improved. This could be due to the work hardening hypothesis mentioned previously. The hybrid surface had the opposite trajectory to the control and the lowest overall mean friction, however, t-tests showed the difference was not significant.

As with the previous tests the upper specimens were analysed using an optical microscope and the wear scar diameter measured. The average WSDs for the different surfaces are shown in Figure 6.9.

For all except the hybrid specimens, the WSDs are very similar with the Lith-Moly average 4 µm to 9 µm lower than the control, base grease and Cu_2S scars. The hybrid scars were significantly wider (14 %) than the others even though the average friction was the lowest. The EDS of the hybrid surface did not detect any aluminium, however, very small quantities of alumina microparticles may have been embedded in the surface that increased wear on the upper specimen. The lower specimen wear scars were deep and wide enough to get meaningful 3D scans using the Alicona InfinteFocus. False colour 3D images, showing the depth of representative scars from each of the surfaces are shown in Figure 6.10.

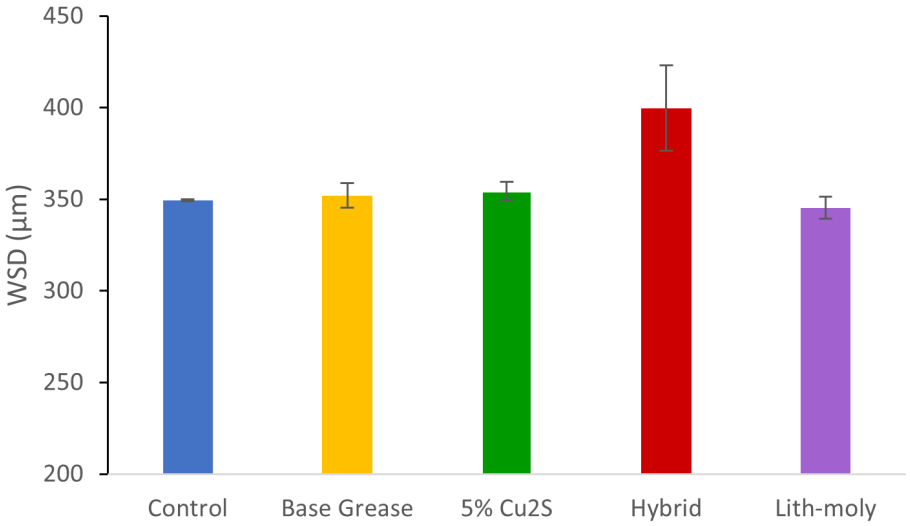

Figure 6.9: Average wear scar diameter for upper specimens from 50 °C wear tests.

The lines in the surfaces caused by honing and the grease-wear process are clearly visible outside of the wear scars. The apparent shallowness of the base grease scar in Figure 6.10b is a little misleading as the average surface height around the scar is 1 µm to 1.5 µm higher than in the hybrid and Lith-Moly scar and ≈0.5 µm higher than the Cu_2S scar. This is reflected in the colour scale bars for each image. The magnitude of the scale is identical for each but the 0 point is adjusted to be the average unworn surface height.

The base grease in Figure 6.10b produced a scar with of a depth ranging between 3 µm and 4 µm along its length with a narrow raised section in the middle around 1 µm higher than the rest of the scar either side. The control scar shown in Figure 6.10a also has a very narrow line of less wear compared to the 4 µm to 4.5 µm depth in much of the scar. In this particular case, the line continues outside the scar so it is a result of the grinding process on the plate. The Cu_2S scar in Figure 6.10c appears to be the deepest grease treated scar, with a wear depth between 4 µm and 4.5 µm towards the ends of the stroke and a little shallower in the middle where sliding speed was highest and so the lubricating regime least severe. Similarly to the base grease scar, raised sections are visible in Figure 6.10d and Figure 6.10e. The hybrid scar has inconsistent depth running through the length of it. Only 2 µm deep at one end but with areas close to 4 µm. A wide shallower section more than a third of the scar diameter is sometimes visible running through the centre. For

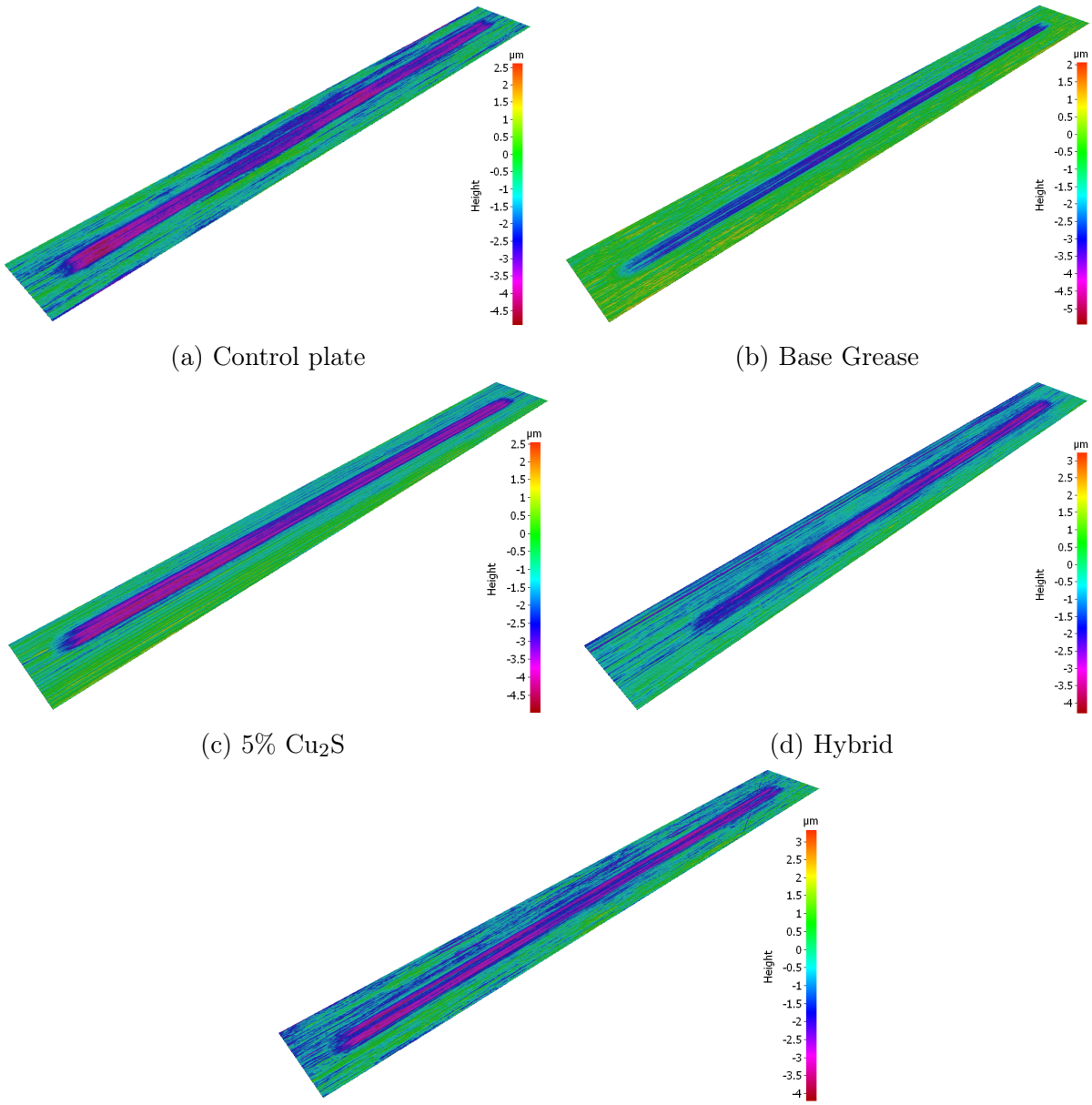

(a) Control plate

(b) Base Grease

(c) 5% Cu_2S

(d) Hybrid

(e) Lith-Moly

Figure 6.10: 3D depth images of wear scars taken using the Alicona InfinteFocus.

the Lith-Moly scar, the shallow section is sometimes 2 µm shallower than the surrounding ≈3 µm deep scar and runs the length of the scar. A true colour image of the Lith-Moly scar (see Figure 6.11) shows the middle section to be very smooth in comparison to the rest of the surface.

The hybrid and Lith-moly scars in Figure 6.10 appear to have a similar cross-sectional profile to the hybrid scar in chapter 5 that had a sulphide/sulphate tribofilm which could be the effect of the sulphide additives introduced during the grease-wear process. This

Figure 6.11: A true colour 3D image of the Lith-Moly wear scar taken in the Alicona.

does not explain the narrower, but still clearly visible line running through the middle of the base grease scar. It could be a particularly hard asperity in the original surface that wore more slowly than the surrounding area, but as it is present on all the scars then this hypothesis is unlikely.

All the scars from the 50 °C test were analysed in the TM3030 SEM to characterise the surfaces, and particularly to understand if a similar tribofilm to that seen in chapter 5 had been reproduced in any of the surfaces. Table 6.5 shows the mean atomic % within the scars of the various surfaces.

Table 6.5: Mean atomic % of elements present in the wear scars generated in the 50 °C test. The elements represented in the last row are typical additives in BO1 tool steel, i.e. manganese, silicon and chromium.

	Mean Atomic %			
	Base Grease	5% Cu_2S	Hybrid	Lith-Moly
Carbon	40.661	43.908	58.824	62.052
Iron	50.743	47.276	30.179	30.391
Oxygen	6.845	6.876	9.374	6.340
Aluminium	–	–	0.019	–
Copper	–	0.047	0.141	–
Molybdenum	–	–	–	0.003
Sulphur	0.327	0.579	0.334	0.239
Other	1.424	1.315	1.131	0.957

The earlier hypothesis that small quantities of alumina were present in the hybrid

surface causing the increased upper specimen WSD as the regime grew more severe is reflected by the trace amounts of Aluminium in the hybrid scars shown in Table 6.5 that were not detected prior to the wear tests.

Only in the Lith-Moly scar was there less sulphur present than detected prior to the wear tests in Table 6.3. The quantity of sulphur in each wear scar initial appears inversely proportional to the depth of each wear scar with the Cu_2S scar averaging > 0.2 atomic % more sulphur than any of the other surfaces and the Lith-Moly having the lowest quantity. Another curiosity is the significant presence of sulphur in the base grease scar. This appears to be inexplicable through any means other than contamination due to the lack of significant quantities of sulphur in either BO1 tool steel or AISI 52100 as well as the multipurpose grease, SN 100 base oil, or ethanol with which the specimens were cleaned. This is further mystified as the surface outside the scar was measured at the same time with EDS and no sulphur was found. At present, the source of sulphur or possible contamination of the base grease wear scars is unknown.

A couple of other factors make the data in Table 6.5 misleading. The mean atomic % was taken from various points both at the extremes and centre of the stroke. Debris pushed to the ends of the track may include sulphide particles not embedded or reacted with the surface. Indeed in one such area in the 5% Cu_2S track, 3.21 % sulphur was present which greatly affected the overall average. Interestingly, no copper was found in that same scan further suggesting that reductions had occurred with the Cu_2S microparticles. Another factor that influences Table 6.5's clarity is the varying carbon content. As discussed in chapter 5, EDS results often show high quantities of carbon, introduced by the oil or the ethanol used in cleaning. This addition could be very hard to control absolutely and probably has very little influence on the tribological results, especially as some of it is introduced after any wear tests have been performed. Hu et al. (2010), Ratoi et al. (2013) and Kalin et al. (2014) all showed X-ray Photoelectron Spectroscopy (XPS) or EDS results with greater than 30 Atomic% carbon in worn steel surfaces and where a comparison could be made, the quantity of carbon had little bearing on the friction or wear resistance of the surfaces.

In order to negate the influence of the factors mentioned above, the quantities were adjusted to ignore the carbon content. Additionally, the EDS scans were studied further, to see if the shallower patches running through the centre of most wear scars contained different quantities of sulphur to the deeper sections running either side. Figure 6.12 shows how the sulphur content differs in those areas and shows the adjusted atomic % after carbon is ignored. To highlight the wide range in results for some of the variables, the maximum and minimum % are shown in each case.

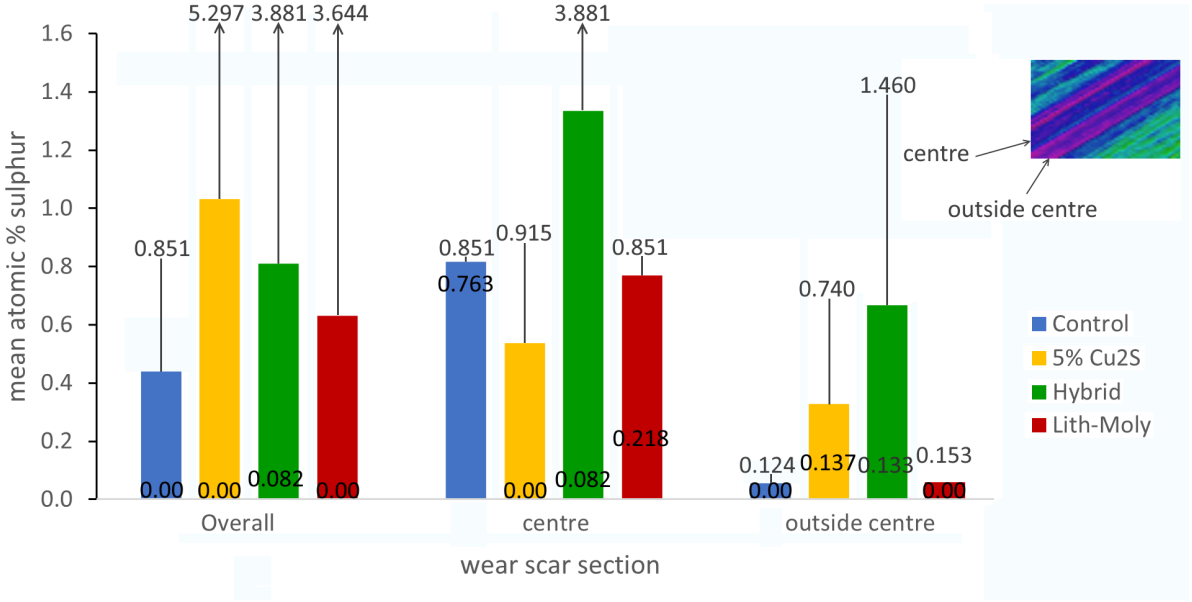

Figure 6.12: Average atomic % sulphur in different areas of the wear tracks according to EDS after carbon is ignored. The overall values include all reading taken inside the scar. The other two sets of values show only readings taken in the indicated areas. The Maximum and minimum values for each variable are shown.

The maximum and minimum values show the wide range in readings for sulphur content even in the same area of a scar. The overall values particularly, which include the ends the wear scars have a range that is far greater than that of the y-axis. This makes comparison between the three additised greases in this section is difficult, however, the overall content after the adjustment shows that the base grease scar actually had the lowest sulphur content of all the scars with both the lowest average and maximum value. This would be expected even if there was some contamination. The Cu_2S scar was unique in that it did not have greater than average sulphur content in the centre of its wear track, this was due to most of the high sulphur content being found at the ends of the stroke

and not in either of the areas represented in the other two sections of the Figure 6.12. Cu_2S was also the only one that did not show reduced wear in the centre, which suggests that sulphides were important to reducing wear in the track. What is less obvious, is how the presence of sulphides in the surfaces after the grease-wear process translated to sulphur content in the wear scar after the point contact tests. Prior to the severe wear tests, the Lith-Moly grease had introduced the most sulphur, followed by the hybrid, then the 5 % Cu_2S grease. The wear scar depth followed a similar trend between those three with the Lith-Moly surface least worn and Cu_2S most. However, the Hybrid scar had far more sulphides present in the track centres and both the surfaces treated with copper sulphide microparticles contained a higher percentage sulphur in the wear scar than the initial surface. A further observation is that prior to the point contact, surfaces treated with Cu_2S contained greater than double quantities of copper than sulphur whereas the wear scars contained significantly less than half. Similarly a much lower proportion of molybdenum to sulphur is present in the Lith-Moly scar than in the initial surface after treatment.

An explanation for the element changes between the grease-treated surfaces and the point contact wear scars is as follows: When Cu_2S interacts with the steel surface under high pressure, a reduction reaction occurs where the sulphur splits from the copper. The copper sinters into the iron forming Fe–Cu composites, similar to the Fe–Mo alloys found by (Mantovan et al., 2018). The sulphur reacts with the iron forming iron sulphides and sulphates. This process isn't 100 % efficient and it appears some sulphur is lost in the process. When surfaces are worn in a boundary lubrication regime, material is removed. The iron-copper compounds are softer and less wear resistant than the iron sulphides and sulphates meaning they are more easily removed leaving the sulphides/sulphates behind. This explains the inverse in proportion of copper and sulphur content between the initial treated surfaces and the wear scars. A similar process occurs with the MoS_2 in the Lith-Moly treated surface. As for the shallower section in the centre of the wear scars, this is where the pressure from the point contact is highest. This high pressure is sufficient to generate reduction reactions in any of the sulphide particles that the grease-treatment

failed to activate but remain embedded in the surface. Early in the wear process, a tribofilm is formed in a narrow strip made of the sulphides and sulphates generated in these reduction reactions meaning wear is heavily reduced. The same film is unable to form later on in the test as wear scar diameter increases beyond the width of the tribofilm and two tracks either side are worn more in the unprotected regions.

Five times more copper was detected in the 5% Cu_2S treated surface than sulphur prior to the wear tests. This suggests higher severity is needed to make sulphur, reduced from the microparticles, react with the steel surface than for copper to sinter into. This is supported by the higher quantity of surface sulphur found with the addition of Al_2O_3, which is as expected given the results in chapter 5 and research by Varenberg et al. (2016). Though a higher quantity of sulphur was detected in the wear scar, most of this had been pushed to the ends of the scar and was ineffective in reducing wear suggesting it had not properly bonded with the surface. The MoS_2 particles were much easier to bond with the steel surface as their 2D nature and easy separation of layers (Rabaso et al., 2014b) meant that a larger surface area to volume ratio could be in contact with the surfaces.

The use of Cu_2S as the additive in a mechanochemical finishing was perhaps called into question in the lower load tests due to copper's high adhesion (Hutchings and Shipway, 2017). At higher loads, the copper appears to have been removed early in the tests leading to only the beneficial sulphides being left behind. The high reduction potential of Cu_2S may only be useful if the copper can reliably be removed from the surface, leaving the sulphur behind. Though at the much lower pressures seen in chapter 4, the copper may have been easily smoothed into valleys in the surfaces and in less severe lubrication regimes where a lubricant film is present, the lower roughness could reduce friction as adhesion won't occur.

6.4 Summary

Three greases containing different quantities of Cu_2S and Al_2O_3 microparticles were prepared and worn against BO1 tool steel plates with a line contact and up to 920 N load.

They were compared along with a base grease and a commercial grease containing MoS_2 for their ability to improve the tribological properties of the steel plates. Surface characterisation and morphology was analysed through the use of SEM, EDS and a 3D microscope The friction and wear resistance of the plates were tested using point contact in reciprocating motion at two different loads and temperatures. The key results are summarised below:

- The commercial grease containing MoS_2 was most effective at increasing the sulphide content of the surfaces as well as the surface with the lowest average roughness. For all the additive containing greases, the elemental composition on the surfaces was highly inconsistent. The process would produce stripes of sulphides in the direction of reciprocation. This was partly because the plates had been ground in the same direction as the wear prior to purchase.

- Point contact, reciprocating motion tests with a 5 N load at ambient temperature produced a coefficient of friction around 2× that when the load was 50 N, going against the principles of the Stribeck curve. This was consistent across all of the surfaces. High speed data showed that the friction coefficient as the ball moved along the stroke in the low load tests was erratic compared to the high load tests. The reason for this was considered to be the stresses in the low load tests were insufficient to plastically deform the asperities in the rough lower specimen surface, but the lubricant film was thin enough for the same asperities to provide a resistance to sliding. At high loads the asperities were deformed early in the test leaving a much smoother surface.

- The upper specimen wear scar diameter was very high in the low load tests. The lower specimen wear scars were barely detectable in the 3D microscope. Wear scar diameter in the ball is not an indication of depth, so the increased diameter was likely due to the roughness of the lower specimen creating a higher apparent contact area than expected from Hertzian contact mechanics.

- 50 °C tests running for 4 × the number of cycles were performed with the higher load in order to get deeper wear scars in the lower specimen that would be detectable with a 3D microscope. Coefficient of friction was similar for most of the surfaces, though all the grease treated plates caused a statistically significant reduction in friction compared to the untreated surface according to ANOVA and t-test analysis. This lead to the hypothesis that high pressure in the line contact grease-wear had caused plastic deformation in the plate surface, both slightly reducing roughness and work-hardening the metal.

- The MoS_2 commercial grease produced the shallowest wear scar and the grease containing only Cu_2S produced the deepest. Both the hybrid grease and the MoS_2 grease produced a wear scar with a similar appearance to the one containing a tribofilm in chapter 5. The central shallow sections in the tracks were confirmed to contain more sulphur than the deeper regions either side, suggesting successful tribofilm formation.

- Explanations for how the reduced components from Cu_2S interacted with the steel surfaces were put forward, both in the grease treatment and point contact tests. Mechanisms for how the central tribofilm was formed in some of the wear scars were also discussed.

This chapter provided further evidence of how a mechanical process similar to honing could be used with the addition of sulphide micro or nano particles to produce tribologically superior surfaces. It appeared that the mechanical process potentially had a greater effect on the wear resistance of the material than the sulphides but some variation was noticed with different compositions in the grease and further experimentation could optimise this process.

Chapter 7

Summary discussion and limitations

This thesis has explored mechanical finishing processes that could be adapted with the use of additives to cause chemical reactions that further improved the tribological properties of metal surfaces. Additionally, research to understand the beneficial synergistic mechanisms of ceramic nanospheres and Transition Metal Dichalcogenides (TMDC) in lubricated wear was also performed. This chapter discusses the work done along with its limitations and what could have been done to improve the findings.

The first experiments undertaken adapted a simple honing process using silicon grit paper against cast iron plates. Dry Cu_2S microparticle powder was spread on the paper prior to honing. After 100 mg of additives failed to significantly affect the presence of either sulphur or copper on the surface, 1 g was used instead during honing. After the finishing process, Energy Dispersive Spectroscopy (EDS) showed a huge increase in copper, far greater than double the increase in sulphur. In combination with Scanning Electron Microscopy (SEM), EDS maps revealed that much of the sulphur was in the same regions as copper so it was unlikely that much sulphur had reacted with iron. The large excess of copper suggested a sintering process had occurred after a reduction reaction had removed sulphur from the Cu_2S. X-ray Photoelectron Spectroscopy (XPS) did show that some FeS_2 or other iron sulphides/sulphates may have formed on the honed surfaces.

Two sets of friction tests were performed on the honed plates. The first was a line contact load ramp test at 2.5 Hz and 12.5 mm stroke. The load increased by 50 N every 15 min from 50 N to 200 N. Once the load increase to 100 N a small improvement was seen in the high copper samples compared to controls honed without additives. The second set of tests was a low pressure test with a maximum initial contact pressure of 3.8 MPa. The test speed was also much higher, at 23 Hz. This put the lubrication regime seemingly into hydrodynamic territory with the friction coefficient in the region of 0.01. Again, a very small improvement was seen with the additised plates but with the number of tests performed it was not statistically significant.

In order to better understand the formation of sulphide tribofilms and discover the mechanisms through which ceramics and TMDCs exhibit synergistic behaviour, MoS_2 and SiO_2 were analysed as lubricant additives between steel contacts. High Frequency

Reciprocating Rig (HFRR) tests were performed first at ambient temperature with a variety of loads (2 N to 8 N) with 1 wt% of either SiO_2 or MoS_2 in two lubricants then a hybrid lubricant with 0.5 % of each. Friction was very similar for all the mixtures in each of the loads. The hybrid mixture provided the smallest wear scar diameter in the upper specimen up to 8 N where MoS_2 was very slightly smaller.

A second set of friction tests was performed at 50 °C and with the highest load of 8 N. The SiO_2 mixture concentration was reduced to 0.5 wt% and an additional hybrid mix was made with 1 % MoS_2 and 0.5 % SiO_2. The hybrid mixtures produced a reduced Coefficient Of Friction (COF) around 0.01 lower than all the other mixtures.

EDS maps of the hybrid surface showed a tribofilm that contained more oxygen, sulphur, molybdenum and slightly more silicon than the rest of the scar and wear profile cross-sections showed the tribofilm to have significantly reduced wear scar depth where it was present.

Hard X-Ray Photoelectron Spectroscopy (HAXPES) identified MoS_2, molybdenum oxides, iron sulphates that were likely $FeSO_4$ and iron sulphides in the tribofilm. This showed that beneficial chemical reactions had occurred in the hybrid mixture surfaces that did not when only pure MoS_2 was present. This indicated that the presence of SiO_2 increased the likelihood of beneficial tribo-chemical reactions. The hard particles being ground into the surface increased pressure and possibly localised temperatures where MoS_2 was interacting with the contacts making reduction reactions in the MoS_2 and sulphur uptake reactions to iron in the steel more likely than when SiO_2 was not present.

After showing that the HFRR produced wear scars that did not have consistent load throughout, further tests were performed in the Low Load Adapter (LLA) for the TE 77 High Frequency Friction Machine (TE 77) with a wider variety of concentrations. The LLA was not able to generate similar results to the HFRR though there was a very high variance in results between tests with constant variables. Bath geometry and the way in which the normal load was transferred to the contact were identified as possible reasons for this high variance.

An attempt to resolve the issue of inconsistent dispersion of additives was made with

the use of grease. Line contacts in the TE 77 with very high loads (up to 920 N) at 50 °C were used with grease and micro additives in a burnishing style process against steel plates. 5 wt% Cu_2S and the same concentration with 0.5 % Al_2O_3 microparticles in a base grease were compared against a commercial grease containing MoS_2.

There was a small uptake in copper and sulphur after the grease process had occurred according to EDS but nowhere near the quantities seen when using honing. Sulphur uptake in the MoS_2 grease was greater than with the Cu_2S greases but still only around 0.5 atomic% of the total surface content. All the burnished surfaces had lower roughness than the untreated surface, with MoS_2 again producing the lowest average roughness. The hybrid surface had an *Ra* 0.05 µm lower than without Al_2O_3.

Point contact tests with 5 N and 10 N loads, at 2.5 Hz with a 10 mm stroke at ambient temperature were performed on each of the surfaces lubricated by a base oil. The lower load tests produced a much higher COF than the 50 N tests. High Speed Data (HSD) indicated this was due to only elastic deformation occurring at low loads which provided resistance every stroke whereas at high loads, plastic deformation occurred in the asperities early in the wear tests resulting in smoother surfaces through the tests' remaining time producing lower friction. At low loads, the MoS_2 surface was the only one to produce significantly lower friction with none doing so at high loads.

Further wear tests at the higher load and 50 °C showed all the burnished surfaces, including without additives, producing slightly lower friction than the untreated surface. With the hybrid producing the lowest mean friction even though the upper specimen had the highest wear scar diameter. 3D wear scar analysis showed the commercial MoS_2 grease produced the shallowest wear scar with both that and the hybrid surface showing a similar tribofilm looking section to that seen in the hybrid scars from the HFRR nanolubricant tests. This section contained significantly more sulphur in the hybrid scar than elsewhere in the scars according to EDS.

While this work offers some promising initial results for developing a new mechanochemical finishing process, it is a long way off commercial viability and represents the very initial concept stage of this research. A significant amount of work is needed, particularly

on the mechanochemical processes before introducing them to component tests. The rest of this chapter will review the work done and some key points that are needed to improve upon or develop the processes and understanding of how the changes introduced affected the tribological properties of the surfaces.

In both chapter 4 and chapter 6, any improvements in tribological results observed were very small. This suggests that while the processes used have promise and are a proof of concept, a lot more optimisation would be needed before it would be worth taking tribology tests beyond simple specimen tests. The honing process in chapter 4 was very basic, spreading dry powder onto grit paper and honing the cast iron plates directly onto it by hand. This worked as a simple concept process and indeed, the surface elemental change compared to the control was far greater than in either of the other chapters, but to properly optimise it, honing paper or grinding stones with the sulphide additive incorporated into them would be far more effective in ensuring that the additives were always in the finishing contact and could not be pushed out. Attempts at creating grit paper incorporating Al_2O_3 and Cu_2S in the lab were made but it was not effective at honing.

Similarly in chapter 6, the TE 77 was used for the grease film forming process, rather than a commercial metal burnishing tool. The aim was for it to be similar to a tribofilm forming wear test, as observed in literature, that would then have subsequent wear tests performed on the tribofilm. It appears, however, that the regime was not severe enough for sufficient chemical reactions to occur for consistent tribofilm coverage.

Reciprocating tests were used throughout the thesis. There are many real world examples of reciprocating motion that lubricants need to be able to cope with and if successful reductions in friction and wear are observed using this kind of test then it is likely that the processes used to cause this improvement are more widely applicable. However, processes that affect an interaction in one area of the Stribeck curve and are ineffectual elsewhere will only result in a very small change in reciprocating wear. This is reflected by the small improvements seen throughout the thesis. A more thorough approach would have been to use linear sliding with a control surface or lubricant at a

range of loads or speeds until a visible Stribeck curve could be observed and then test the introduced variables at various points on that Stribeck curve. This would enable a better understanding of the range of regimes at which each process or additive is most effective. This process would likely require a far greater number of tests and so be much more expensive, but the beneficial changes observed in this thesis would likely be far more pronounced and the scope for where they would be most useful in the real world would be better understood.

Similarly, the point contact geometry used in chapter 5 and chapter 6 is not really representative of real world applications and was chosen for purely practical reasons. The SiO_2 nanoparticles were expensive and so to use as little as possible in each test, the HFRR was chosen as it used a tenth of the lubricant per test as the standard TE 77 bath. In chapter 6, point contacts were used for wear tests on the treated surfaces so that multiple tests could be performed on one surface generated by the line contact grease process. The downside of point contacts is that the geometry leads to very high contact pressures that are not typical of real world applications. The lowest initial maximum Hertzian contact pressure (p_o) in any test was 790 MPa when the load was 2 N. The highest p_o without point contact was the grease treatment process in chapter 6 when the load was 920 N. p_o was ≈720 MPa. This means that the lubrication regime is always going to be closer to the boundary lubrication regime than with other geometries. This resulted in the processes and additives not being given the best chance in yielding positive results at a variety of lubrication conditions. Alternative geometries would lead to regimes that are more common in most machine systems when in operation.

Finally, the end of the discussion section in chapter 6 illuded to the possible disadvantages of Cu_2S as an additive in a mechanochemical finishing process. It was selected in this thesis and by other researchers for its high reduction potential and this was clearly evident in chapter 4 where ≈15 atomic% of the surface was copper and <2 % was sulphur. Though the ductile nature of copper may help to reduce surface roughness and decrease friction when the lubricant film is thick enough that the sliding surfaces do not come into direct contact, in more severe regimes, the same ductile nature results in high adhesion,

increasing friction. When the severity is increased further, the tests in chapter 6 suggest that the copper is quickly removed leaving only beneficial sulphides, but this leaves a window in the Stribeck curve where Cu_2S is detrimental as a mechanochemical finishing additive. What may partly be down to the chemical structure of Cu_2S or simply that there are twice as many copper atoms as sulphur, it appears far more effective at producing a surface high in copper than significantly higher in sulphur.

This thesis offers a proof of concept for two mechanochemical finishing processes that have potential to be cost effective single stage operations to significantly reduce friction and wear in a wide range of applications. It also shows the synergistic potential of combining TMDCs with ceramic nanospheres in nanolubricants for better tribofilm formation. The scope for this research is vast as it applies to the majority of mechanical systems that include sliding metal contacts but a lot of work is needed to optimise the methods and understand where they would be most beneficial.

Chapter 8

Conclusions and future work

In order to evaluate the success of the research undertaken in this thesis, each of the objectives outlined in chapter 2, and their measures of success, are analysed against the work done. Below are the previously stated aim and objectives:

Aim: To begin the development of a new mechanochemical finishing process that reduces friction and wear in metal components.

Objectives:

1. Prove the concept of using a simple mechanical finishing process with sulphide additives to induce a tribofilm-like surface.

   Measures of success:

   (a) Observe new metal sulphides that were not produced without additives through use surface analysis equipment such as Energy Dispersive Spectroscopy (EDS) and X-ray Photoelectron Spectroscopy (XPS).

   (b) Determine the mechanisms by which these reactions occurred supported by experimental analysis.

   (c) Outline avenues for improving and optimising the process.

2. Understand the synergistic properties and mechanisms of nanoparticles that offer mechanical improvements working with nanoparticles that are more chemically reactive in hybrid nanofluids.

   Measures of success:

   (a) Show statistically significant improvements in friction and/or wear with hybrid nanofluids when compared to separated equivalents.

   (b) Develop a provable hypothesis for at least one synergistic mechanism that is supported by observations through a range of surface analysis techniques, including XPS, EDS and profilometry.

3. Discover if the mechanochemically generated surfaces in objective 1 offer tribological benefits over purely mechanical processes.

   Measures of success:

   (a) Observe statistically significant reductions in friction and/or wear when compared to purely mechanically finished samples.

   (b) Develop provable hypotheses for tribological mechanisms leading to any improvement or otherwise, supported by friction data and surface analysis techniques.

4. Develop a method of surface finishing that keeps additives in the contact patch.

   Measures of success:

   (a) Visual inspection of interacting surfaces during and after the finishing process shows additives in the contact area.

   (b) A consistent coverage of chemically bonded additive material with low variance in concentrations within and between specimens.

Objective 1

Using Cu_2S in the honing process in chapter 4 clearly affected the chemical content of the cast iron plates' surfaces. Chemical reactions certainly occurred due to the massive increase in copper compared to sulphur found by EDS meaning that the proposed reduction of microparticles had been successful. However, XPS could not conclusively prove that new iron sulphides had been formed by the process and it appeared that much of the sulphur had been lost in the honing with mainly the copper sintering into the surface.

Dry honing with the microparticles was much more successful at altering the chemical composition of the surfaces than burnishing them with Cu_2S in grease, even though the latter method kept the additives in the contact throughout the process. Very little wear was observed in the burnishing process so it may have been that the regime was not severe enough for many reduction reactions to occur.

Future work Further testing of the honing process and the surfaces it generates would br needed to confirm the beneficial changes observed. For both the honing and grease-burnishing processes, additional analysis of the surfaces to identify what other properties had been changed would also be useful. Some properties to test could be hardness, surface roughness and wear resistance.

The honing process itself could be improved by experimenting with the following:

- A variety compounds as the additive; preferably ones with a higher ratio of sulphur to metal and where the metal is less susceptible to adhesion when subject to wear than copper.

- Liaise with manufacturers to create bespoke grit paper or grinding stones with the desired chemically reactive additives forming part of the grit.

- A mechanical rig where the honing speed and pressure can be controlled as well as monitor the surface temperatures to allow for more control and optimising the process to maximise the likelihood of chemical reactions.

Objective 2

The lubricants in chapter 5 containing only MoS_2 or SiO_2 did not show any of the improvements that would be expected according to literature when compared to the base oil. However, this helped to show that significant improvements in both friction and wear observed with the hybrid lubricants had to be due to a synergistic interaction rather than two separate mechanisms working in tandem. EDS and XPS provided evidence for new iron sulphides formed in a tribolfilm, the formation of which was aided by the mechanical effect of the SiO_2 grinding the MoS_2 against the surface.

The unusual shape of the hybrid wear scars with a raised tribofilm running through the middle was not fully understood, neither was the lack of a tribological advantage observed with either nanoparticle when used individually.

Future work This objective was included in order to better understand mechanochemical reactions that cause tribological improvements, with the aim of using this understanding to improve the finishing process mentioned in the aim. There is scope, though, for this work to be expanded upon for improving commercial lubricants. That would require overcoming the dispersion issue found in literature for retaining the effectiveness of MoS_2 without allowing it to form large agglomerations that could be detrimental to machinery.

Understanding the perfect mixture and conditions to maximise the benefits of this synergistic behaviour would also be necessary. Thorough testing of different loads and sliding speeds using a linear motion tribo-tester would allow a complete Stribeck curve to be made for each of the nanofluids. Along with further experimentation with different concentrations and ratios, this would not only improve the understanding of the synergistic process and in which regimes it is most effective, but would also aid the identification of appropriate commercial mechanical operations to target for development of this work.

Objective 3

Both the finishing processes developed in this thesis as well as the hybrid nanolubricant produced some tribological benefits when operated on or between ferrous contacts. The addition of Cu_2S particles in chapter 4 to the honing process causes a very small but statistically significant reduction in friction compared to samples that were honed with out the additives. In chapter 6, the burnishing process causes a similarly small improvement against an un-burnished surface but none of the additives produced significantly better surfaces than the non-additised process.

For honing, the huge increase in copper on the specimen surfaces was suspected to be the reason for reduced benefit, as its tendency to adhere to contacting surfaces when the film thickness is small would cause increased friction and somewhat negate any benefit that the small increase in surface sulphides would have had. This proposed mechanism is supported by the EDS results in chapter 6 where the copper atomic % is far greater before the tribological tests than after. This indicates that more traditional additives

in tribology such as MoS_2 or WS_2 could be more effective for use in mechanochemical finishing.

Future work Whilst the mechanochemical honing process has shown some tribological benefit, considering the significant change in the surfaces' chemical composition, a greater difference in tribological performance was expected. A combination of the honing process improvements outlined in section 8 as well using linear motion tribo-testers to generate a complete Stribeck curve for the mechanochemically finished surfaces would be hugely beneficial in further understanding and improving their tribological performance as well as identifying the process's applications.

Objective 4

Intended to be an improvement on the honing process of chapter 4, the TE 77 High Frequency Friction Machine (TE 77) burnishing process of chapter 6 was observed to keep additives in the contact throughout, however it did not induce a consistent coverage of chemically bonded additive material. In fact, uptake of the additive elements to the specimen surfaces was significantly lower than that of the honing. The tribological benefits observed appeared to be more down to mechanical changes such work hardening.

Future work Further work could include a wider variety of additive concentrations as well as increased time of burnishing and higher temperatures to increase the process's severity. Analysing more physical properties of the surfaces such as hardness would also useful information about the changes made by the different grease additives and the process as a whole. Additionally, further characterisation of the surfaces through the use of XPS or other chemical species analysis could help to identify the possible tribofilms in the surfaces. Using commercial metal burnishing tools rather than a tribo-tester like the TE 77 would also likely be beneficial for improving this technique.

Alternatively, focussing on mechanochemical honing using bespoke grinding stones or grit paper with embedded reactive additives would be recommended, based on the findings

of this thesis, as a more likely direction for successful consistent coverage of chemically bonded additive material.

Novelty

As part of the research undertaken to understand mechanochemical interactions in tribology, a new hypothesis for the synergistic behaviour of hard ceramic nanospheres with chemically reactive Transition Metal Dichalcogenides (TMDC) nanoparticles as lubricant additives was proposed. Supported by tribological experiments and a variety of surface analysis techniques, this synergistic mechanism not only supports the idea of mechanochemical finishing but could also enable the development of new superior nanolubricants.

This thesis explored two methods of mechanochemical finishing and offers a proof of concept for honing with sulphide microparticles as an effective single stage operation to improve the tribological performance of interacting metal surfaces. With further developments, this research has potential to benefit a wide range of mechanical operations as it aims to introduce a cost effective method of improving metal surfaces that could reduce friction and wear in any system where there are contacting metal surfaces in relative motion.

Bibliography

Abe, H. et al. (2018). *Nanoparticle Technology Handbook*. Ed. by M. Naito, T. Yokoyama, K. Hosokawa, and K. Nogi. 3rd ed. Elsevier.

Adams, D. R. (2010). "Tribological considerations in internal combustion engines". In: *Tribology and Dynamics of Engine and Powertrain: Fundamentals, Applications and Future Trends*. Cambridge: Woodhead Publishing, pp. 251–283.

Ali, M. K. A., H. Xianjun, A. Elagouz, F. Essa, and M. A. A. Abdelkareem (2016). "Minimizing of the boundary friction coefficient in automotive engines using Al2O3 and TiO2 nanoparticles". In: *Journal of Nanoparticle Research* 18.12, p. 377.

Alves, S. M., V. S. Mello, E. A. Faria, and A. P. Camargo (2016). "Nanolubricants developed from tiny CuO nanoparticles". In: *Tribology International* 100, pp. 263–271.

Asefa, T. and V. Dubovoy (2017). "Ordered Mesoporous/Nanoporous Inorganic Materials via Self-Assembly". In: *Comprehensive Supramolecular Chemistry II* 9, pp. 157–192.

Bao, Y. Y., J. L. Sun, and L. H. Kong (2017). "Tribological properties and lubricating mechanism of SiO2 nanoparticles in water-based fluid". In: *IOP Conference Series: Materials Science and Engineering*. Vol. 182. 1, p. 012025.

Biesinger, M. C., B. P. Payne, A. P. Grosvenor, L. W. Lau, A. R. Gerson, and R. S. C. Smart (2011). "Resolving surface chemical states in XPS analysis of first row transition metals, oxides and hydroxides: Cr, Mn, Fe, Co and Ni". In: *Applied Surface Science* 257.7, pp. 2717–2730.

Buckley, D. H. (1981). *Surface effects in adhesion, friction, wear, and lubrication*. Vol. 5. Elsevier.

Calka, A., D. Wexler, B. Monaghan, A. Mosbah, and P. Balaz (2009). "Rapid reduction of copper sulfide (Cu2S) with elemental Fe and Mg using electrical discharge assisted mechanical milling (EDAMM)". In: *Journal of Alloys and Compounds* 486.1-2, pp. 492–496.

Chang, Y., S. T. Yang, J. H. Liu, E. Dong, Y. Wang, A. Cao, Y. Liu, and H. Wang (2011). "In vitro toxicity evaluation of graphene oxide on A549 cells". In: *Toxicology Letters* 200.3, pp. 201–210.

Chen, Z., Y. H. Liu, S. Gunsel, and J. B. Luo (2015). "The investigation of oleylamine as a dispersant for ball-milled MoS2 in hydrocarbon base oil". In: *2015 IFToMM World Congress Proceedings, IFToMM 2015*. Airiti Library, pp. 610–615.

Choi, Y., C. Lee, Y. Hwang, M. Park, J. Lee, C. Choi, and M. Jung (2009). "Tribological behavior of copper nanoparticles as additives in oil". In: *Current Applied Physics* 9.2 SUPPL. e124–e127.

Chou, S. S., M. De, J. Kim, S. Byun, C. Dykstra, J. Yu, J. Huang, and V. P. Dravid (2013). "Ligand conjugation of chemically exfoliated MoS2". In: *Journal of the American Chemical Society* 135.12, pp. 4584–4587.

Cressey, D. (2010). "The science of dispersants". In: *Nature*.

De Feo, M., C. Minfray, M. I. De Barros Bouchet, B. Thiebaut, and J. M. Martin (2015). "MoDTC friction modifier additive degradation: Correlation between tribological performance and chemical changes". In: *RSC Advances* 5.114, pp. 93786–93796.

Dowson, D and G. Higginson (1977). *Elasto-hydrodynamic lubrication: international series on materials science and technology*. 2nd ed. Vol. 23. Oxford: Pergamon Press Ltd.

Dreyer, D. R., S. Park, C. W. Bielawski, and R. S. Ruoff (2010). *The chemistry of graphene oxide*.

Dumcenco, D. O., K. Y. Chen, Y. P. Wang, Y. S. Huang, and K. K. Tiong (2010). "Raman study of 2H-Mo1-xWxS2 layered mixed crystals". In: *Journal of Alloys and Compounds* 506.2, pp. 940–943.

Eckold, D. G. (2016). "Spinal implants - the problems of debris". PhD thesis. Birmingham: University of Birmingham.

Egerton, R. F. (2016a). "The Scanning Electron Microscope". In: *Physical Principles of Electron Microscopy*. Cham: Springer, Cham, pp. 121–147.

— (2016b). "The Transmission Electron Microscope". In: *Physical Principles of Electron Microscopy*. Cham: Springer, Cham, pp. 55–88.

Elomaa, O., V. K. Singh, A. Iyer, T. J. Hakala, and J. Koskinen (2015). "Graphene oxide in water lubrication on diamond-like carbon vs. stainless steel high-load contacts". In: *Diamond and Related Materials* 52, pp. 43–48.

Eswaraiah, V., V. Sankaranarayanan, and S. Ramaprabhu (2011). "Graphene-based engine oil nanofluids for tribological applications". In: *ACS Applied Materials and Interfaces* 3.11, pp. 4221–4227.

Fan, Q. (2009). "Polyolefin nanocomposite fibers and films". In: *Polyolefin Fibres: Industrial and Medical Application*. Cambridge: Woodhead Publishing. Chap. 11, pp. 341–362.

Fan, X., W. Li, H. Fu, M. Zhu, L. Wang, Z. Cai, J. Liu, and H. Li (2017). "Probing the Function of Solid Nanoparticle Structure under Boundary Lubrication". In: *ACS Sustainable Chemistry and Engineering* 5.5, pp. 4223–4233.

Fang, J. H., F. S. Pan, B. S. Chen, J. Wu, and L. Dong (2011). "Friction and wear performances of magnesium alloy against steel under lubrication of rapeseed oil with S-containing additive". In: *Transactions of Nonferrous Metals Society of China (English Edition)* 21.12, pp. 2649–2653.

Fu, H., G. Yan, M. Li, H. Wang, Y. Chen, C. Yan, C. T. Lin, N. Jiang, and J. Yu (2019). "Graphene as a nanofiller for enhancing the tribological properties and thermal conductivity of base grease". In: *RSC Advances* 9.72, pp. 42481–42488.

Galda, L., J. Sep, and S. Prucnal (2016). "The effect of dimples geometry in the sliding surface on the tribological properties under starved lubrication conditions". In: *Tribology International* 99, pp. 77–84.

Gao, D. and J. Luo (2016). "Synthesis of Hyper-Dispersant Based on the Application of Nano-Lubricants". In: *Journal of Dispersion Science and Technology* 37.10, pp. 1415–1422.

Garcia, C. E., M. Ueda, H. Spikes, and J. S. Wong (2021). "Temperature dependence of molybdenum dialkyl dithiocarbamate (MoDTC) tribofilms via time-resolved Raman spectroscopy". In: *Scientific Reports* 11.1, pp. 1–13.

Gelinck, E. R. and D. J. Schipper (2000). "Calculation of Stribeck curves for line contacts". In: *Tribology International* 33.3-4, pp. 175–181.

Gray, J. E. and B. Luan (2002). *Protective coatings on magnesium and its alloys - A critical review.*

Guo, Y., X. Zhou, K. Lee, H. C. Yoon, Q. Xu, and D. Wang (2021). "Recent development in friction of 2D materials: From mechanisms to applications". In: *Nanotechnology* 32.31, p. 312002.

Gupta, P., A. Lakes, and T. Dziubla (2016). "A Free Radical Primer". In: *Oxidative Stress and Biomaterials.* Ed. by T. Dziubla and D. A. Butterfield. Academic Press, pp. 1–33.

Hamrock, B. J., S. R. Schmid, and B. O. Jacobson (2004). *Fundamentals of Fluid Film Lubrication.* 2nd ed. Boca Raton: CRC Press.

Hao, L., P. Li, A. Aljabri, H. Li, G. Liu, Z. Xie, and T. Li (2021). "Investigation on the tribological performance of functionalized nanoscale silica as an amphiphilic lubricant additive". In: *Journal of Materials Research and Technology* 15, pp. 5507–5515.

Hasan, M. N., M. Nafiujjaman, and Y. K. Lee (2019). "2D nanomaterials for gene delivery". In: *Biomedical Applications of Graphene and 2D Nanomaterials.* Elsevier, pp. 87–104.

He, X., H. Xiao, H. Choi, A. Díaz, B. Mosby, A. Clearfield, and H. Liang (2014). "α-Zirconium phosphate nanoplatelets as lubricant additives". In: *Colloids and Surfaces A: Physicochemical and Engineering Aspects* 452.1, pp. 32–38.

Hendel, S., F. Schäfers, M. Hävecker, G. Reichardt, M. Scheer, J. Bahrdt, and K. Lips (2016). "The EMIL project at BESSY II: Beamline design and performance". In: *AIP Conference Proceedings.* Vol. 1741. 1. AIP Publishing LLCAIP Publishing, p. 030038.

Hersey, M. D. (1914). "The laws of lubrication of horizontal journal bearings". In: *Journal of the Washington Academy of Sciences* 4.August, pp. 542–552.

Holmberg, K. and A. Erdemir (2015). "Global impact of friction on energy consumption, economy and environment". In: *FME Transactions* 43.3, pp. 181–185.

Honeywell Specialty (Apr. 2017). *Aluminium Oxide 342688-100G*. CID 9989226. Ver. 1.1. Seelze, Germany.

Howard, K. (2014). "Advanced engine oils to improve the performance of modern internal combustion engines". In: *Alternative Fuels and Advanced Vehicle Technologies for Improved Environmental Performance: Towards Zero Carbon Transportation*. Woodhead Publishing, pp. 138–164.

Hu, K. H., X. G. Hu, Y. F. Xu, F. Huang, and J. S. Liu (2010). "The effect of morphology on the tribological properties of MoS2 in liquid paraffin". In: *Tribology Letters* 40.1, pp. 155–165.

Hutchings, I. and P. Shipway (2017). "Tribology: Friction and wear of engineering materials: Second Edition". In: *Tribology: Friction and Wear of Engineering Materials: Second Edition*. 2nd. Oxford: Elsevier Ltd., pp. 1–388.

Hutchings, I. M. (2016). "Leonardo da Vinci's studies of friction". In: *Wear* 360-361, pp. 51–66.

Ibrahim, R. (2001). "Liquid Sloshing". In: *Encyclopedia of Vibration*. Elsevier. Chap. Liquid Slo, pp. 726–740.

Institution of Mechanical Engineers, T. G. (2014). *Tribological Design Guide Part 5 - Wear*.

Jääskeläinen, H. (2006). "Fuel Property Testing : Sulfur". In: *DieselNet Technology Guide - What is Diesel Fuel*, pp. 1–10.

Johnson, K. L., J. A. Greenwood, and S. Y. Poon (1972). "A simple theory of asperity contact in elastohydro-dynamic lubrication". In: *Wear* 19.1, pp. 91–108.

Jost, H (1966). *Lubrication (tribology) : education and research : a report on the present position and industry's needs*. London: HMSO.

Kalha, C. et al. (2021). *Hard x-ray photoelectron spectroscopy: A snapshot of the state-of-the-art in 2020*.

Kalin, M., J. Kogovšek, J. Kovač, and M. Remškar (2014). "The Formation of Tribofilms of MoS2 Nanotubes on Steel and DLC-Coated Surfaces". In: *Tribology Letters* 55.3, pp. 381–391.

Kalin, M, J Kogovšek, and M Remškar (2012). "Mechanisms and improvements in the friction and wear behavior using MoS 2 nanotubes as potential oil additives". In: *Wear* 280-281, pp. 36–45.

Kamps, T. J., J. C. Walker, R. J. Wood, P. M. Lee, and A. G. Plint (2015). "Reproducing automotive engine scuffing using a lubricated reciprocating contact". In: *Wear* 332-333, pp. 1193–1199.

Kinoshita, H., Y. Nishina, A. A. Alias, and M. Fujii (2014). *Tribological properties of monolayer graphene oxide sheets as water-based lubricant additives.*

Kotia, A., G. K. Ghosh, I. Srivastava, P. Deval, and S. K. Ghosh (2019). "Mechanism for improvement of friction/wear by using Al2O3 and SiO2/Gear oil nanolubricants". In: *Journal of Alloys and Compounds* 782, pp. 592–599.

Krishnan, U., M. Kaur, K. Singh, M. Kumar, and A. Kumar (2019). "A synoptic review of MoS2: Synthesis to applications". In: *Superlattices and Microstructures* 128, pp. 274–297.

Lahouij, I., B. Vacher, and F. Dassenoy (2014). "Direct observation by in situ transmission electron microscopy of the behaviour of IF-MoS2 nanoparticles during sliding tests: Influence of the crystal structure". In: *Lubrication Science* 26.3, pp. 163–173.

Lee, I. and I. Park (2006). "Solid lubrication coating of FeS layer on the surface of SKD 61 steel produced by plasma sulfnitriding". In: *Surface and Coatings Technology* 200.11, pp. 3540–3543.

Liu, X., N. Xu, W. Li, M. Zhang, L. Chen, W. Lou, and X. Wang (2017). "Exploring the effect of nanoparticle size on the tribological properties of SiO2 / polyalkylene glycol nanofluid under different lubrication conditions". In: *Tribology International* 109, pp. 467–472.

Lu, L. and O. Ishiyama (2015). "Iron ore sintering". In: *Iron Ore: Mineralogy, Processing and Environmental Sustainability.* Woodhead Publishing, pp. 395–433.

Luo, Q. (2013). "Tribofilms in Solid Lubricants". In: *Encyclopedia of Tribology.* Springer US, pp. 3760–3767.

Luo, T., X. Wei, X. Huang, L. Huang, and F. Yang (2014). "Tribological properties of Al2O3 nanoparticles as lubricating oil additives". In: *Ceramics International* 40.5, pp. 7143–7149.

M. A. Delgado, C. Valencia, M. C. Sánchez, J. M. Franco, and C. Gallegos (2006). "Influence of Soap Concentration and Oil Viscosity on the Rheology and Microstructure of Lubricating Greases". In: *Industrial and Engineering Chemistry Research* 45.6, pp. 1902–1910.

Mantovan, R., Y. Matveyev, G. Vinai, C. Martella, P. Torelli, A. Molle, S. Zarubin, Y. Lebedinskii, and A. Zenkevich (2018). "Bonding Character and Magnetism at the Interface Between Fe and MoS ₂ Nanosheets". In: *physica status solidi (a)* 215.13, p. 1800015.

Meng, Y., J. Sun, J. He, F. Yang, and P. Wu (2021). "Interfacial interaction induced synergistic lubricating performance of MoS2 and SiO2 composite nanofluid". In: *Colloids and Surfaces A: Physicochemical and Engineering Aspects* 626, p. 126999.

Moore, C. et al. (2017). "Industrial grade 2D molybdenum disulphide (MoS2): An in vitro exploration of the impact on cellular uptake, cytotoxicity, and inflammation". In: *2D Materials* 4.2, p. 025065.

Oberdörster, G., E. Oberdörster, and J. Oberdörster (2005). *Nanotoxicology: An emerging discipline evolving from studies of ultrafine particles*.

Parvez, K. (2019). "Two-dimensional nanomaterials: Crystal structure and synthesis". In: *Biomedical Applications of Graphene and 2D Nanomaterials*. Elsevier, pp. 1–25.

Pei, S. and H. M. Cheng (2012). "The reduction of graphene oxide". In: *Carbon* 50.9, pp. 3210–3228.

Peña-Parás, L., J. Taha-Tijerina, L. Garza, D. Maldonado-Cortés, R. Michalczewski, and C. Lapray (2015). "Effect of CuO and Al2O3 nanoparticle additives on the tribological behavior of fully formulated oils". In: *Wear* 332-333, pp. 1256–1261.

Peng, D. X., C. H. Chen, Y. Kang, Y. P. Chang, and S. Y. Chang (2010). "Size effects of SiO2 nanoparticles as oil additives on tribology of lubricant". In: *Industrial Lubrication and Tribology* 62.2, pp. 111–120.

Peres, N. M. and R. M. Ribeiro (2009). "Focus on graphene". In: *New Journal of Physics* 11.9, p. 095002.

Piątkowska, A., M. Romaniec, D. Grzybek, M. Możdżonek, A. Rojek, and R. Diduszko (2018). "A study on antiwear properties of graphene water-based lubricant and its contact with metallic materials". In: *Tribologia* 281.5, pp. 71–81.

Plint, G. (2010). *Comparison-TE 80 and PCS HFFR*. Tech. rep. Kingsclere: Phoenix Tribology Ltd.

Popova, E. and V. L. Popov (2015). "The research works of Coulomb and Amontons and generalized laws of friction". In: *Friction* 3.2, pp. 183–190.

Qi, Y., V. Nguyen, S. Melkote, and M. Varenberg (2019). "Mechano-chemical surface modification of high-speed steel cutting tools". In: *Journal of Manufacturing Science and Engineering, Transactions of the ASME* 141.4.

Rabaso, P., F. Dassenoy, F. Ville, M. Diaby, B. Vacher, T. Le Mogne, M. Belin, and J. Cavoret (2014a). "An investigation on the reduced ability of IF-MoS2 nanoparticles to reduce friction and wear in the presence of dispersants". In: *Tribology Letters* 55.3, pp. 503–516.

Rabaso, P., F. Ville, F. Dassenoy, M. Diaby, P. Afanasiev, J. Cavoret, B. Vacher, and T. Le Mogne (2014b). "Boundary lubrication: Influence of the size and structure of inorganic fullerene-like MoS2 nanoparticles on friction and wear reduction". In: *Wear* 320.1, pp. 161–178.

Rapoport, L., N. Fleischer, and R. Tenne (2005). "Applications of WS2(MoS2) inorganic nanotubes and fullerene-like nanoparticles for solid lubrication and for structural nanocomposites". In: *Journal of Materials Chemistry* 15.18, p. 1782.

Ratoi, M., V. B. Niste, J. Walker, and J. Zekonyte (2013). "Mechanism of action of WS2 lubricant nanoadditives in high-pressure contacts". In: *Tribology Letters* 52.1, pp. 81–91.

Rawat, S. S., A. P. Harsha, D. P. Agarwal, S. Kumari, and O. P. Khatri (2019). "Pristine and Alkylated MoS2 Nanosheets for Enhancement of Tribological Performance of Paraffin Grease under Boundary Lubrication Regime". In: *Journal of Tribology* 141.7.

Regoutz, A., M. Mascheck, T. Wiell, S. K. Eriksson, C. Liljenberg, K. Tetzner, B. A. Williamson, D. O. Scanlon, and P. Palmgren (2018). "A novel laboratory-based hard X-ray photoelectron spectroscopy system". In: *Review of Scientific Instruments* 89.7, p. 073105.

Rosentsveig, R., A. Gorodnev, N. Feuerstein, H. Friedman, A. Zak, N. Fleischer, J. Tannous, F. Dassenoy, and R. Tenne (2009). "Fullerene-like MoS 2 nanoparticles and their tribological behavior". In: *Tribology Letters* 36.2, pp. 175–182.

Sato, T., Y. Hirai, T. Fukui, and H. Usami (2016). "Tribological properties of bronze containing micro sized sulfide-application of atomic force microscopy". In: *Tribology Online*. Vol. 11. 2. Japanese Society of Tribologists, pp. 195–202.

Sayuti, M., O. M. Erh, A. A. Sarhan, and M. Hamdi (2014). "Investigation on the morphology of the machined surface in end milling of aerospace AL6061-T6 for novel uses of SiO2 nanolubrication system". In: *Journal of Cleaner Production* 66, pp. 655–663.

Seyedzavvar, M., H. Abbasi, M. Kiyasatfar, and R. N. Ilkhchi (2020). "Investigation on tribological performance of CuO vegetable-oil based nanofluids for grinding operations". In: *Advances in Manufacturing 2020 8:3* 8.3, pp. 344–360.

Sifuentes, E. T., O. V. Kharissova, D. Maldonado-Cortés, L. Peña-Parás, R. Michalczewski, and B. I. Kharisov (2021). "A comparison of tribological properties of nanolubricants containing carbon nanotori and additional additives". In: *Materials Chemistry and Physics* 272, p. 124973.

Sigma-Aldrich (May 2017a). *Copper(I) sulfide - powder, –325 mesh*. SID 24851068. Ver. 5. Saint Louis, MO, USA.

— (May 2017b). *Molybdenum(IV) sulfide - nanopowder, 90 nm diameter (APS), 99% trace metals basis*. SID 329768848. Ver. 2. Saint Louis, MO, USA.

— (June 2020). *Silica nanosphers - 50 nm avg. part. size (TEM), 10 %(w/v) in ethanol*. Product No. 803073. Ver. 6.2. Saint Louis, MO, USA.

Singh, J., D. Kumar, and N. Tandon (2018). "Tribological and Vibration Studies on Newly Developed Nanocomposite Greases Under Boundary Lubrication Regime". In: *Journal of Tribology* 140.3.

Singh, P. N., A. Saxena, and S. Gangwar (2021). "Tribological Aspect of Nano-lubricant Based on Carbon Nanotubes (CNTs) and Graphene—A Review". In: *Lecture Notes in Mechanical Engineering*. Springer, Singapore, pp. 257–267.

Song, H. J. and N. Li (2011). "Frictional behavior of oxide graphene nanosheets as water-base lubricant additive". In: *Applied Physics A: Materials Science and Processing* 105.4, pp. 827–832.

Stav, O., H. Kasem, R. Akhvlediani, A. Hoffman, Y. Kligerman, and I. Etsion (2019). "Simultaneous Shot-Peening of hard and soft particles for friction reduction in reciprocal sliding". In: *Tribology International* 130, pp. 19–26.

Stribeck, R. (1902). "Die wesentlichen Eigenschaften der Gleit- und Rollenlager (Characteristics of Plain and Roller Bearings)". In: *Zeitschrift des VDI* 46, pp. 1341–1348.

Sutton, M., J. A. Kocsis, and I. Nakagawa (2007). "Improved friction modifiers to aid in future fuel economy targets". In: *SAE Technical Papers*.

Tannous, J., F. Dassenoy, I. Lahouij, T. Le Mogne, B. Vacher, A. Bruhács, and W. Tremel (2011). "Understanding the tribochemical mechanisms of IF-MoS 2 nanoparticles under boundary lubrication". In: *Tribology Letters* 41.1, pp. 55–64.

Tao, C., B. Wang, G. C. Barber, J. D. Schall, and H. Lan (2018). "Tribological behaviour of SnO2 nanoparticles as an oil additive on brass". In: *Lubrication Science* 30.5, pp. 247–255.

Telegdi, J., A. Shaban, and G. Vastag (2018). "Biocorrosion-steel". In: *Encyclopedia of Interfacial Chemistry: Surface Science and Electrochemistry*. Elsevier, pp. 28–42.

Tougaard, S. (2013). "SURFACE ANALYSIS | X-ray Photoelectron Spectroscopy". In: *Encyclopedia of Analytical Science*. 3rd ed. Academic Press, pp. 400–409.

Ueda, S., Y. Katsuya, M. Tanaka, H. Yoshikawa, Y. Yamashita, S. Ishimaru, Y. Matsushita, and K. Kobayashi (2010). "Present status of the NIMS contract beamline BL15XU at SPring-8". In: *AIP Conference Proceedings*. Vol. 1234. 1. American Institute of PhysicsAIP, pp. 403–406.

Uzoma, P. C., H. Hu, M. Khadem, and O. V. Penkov (2020). *Tribology of 2D nanomaterials: A review*.

Vaitkunaite, G., C. Espejo, B. Thiebaut, A. Neville, and A. Morina (2022). "Low friction tribofilm formation and distribution on an engine cylinder tested with MoDTC-containing low viscosity engine lubricants". In: *Tribology International* 171, p. 107551.

Vanossi, A., D. Dietzel, A. Schirmeisen, E. Meyer, R. Pawlak, T. Glatzel, M. Kisiel, S. Kawai, and N. Manini (2018). "Recent highlights in nanoscale and mesoscale friction". In: *Beilstein Journal of Nanotechnology* 9.1, pp. 1995–2014.

Vanýsek, P. (2010). *Standard Redox Potential Table*.

Varenberg, M., G. Ryk, A. Yakhnis, Y. Kligerman, N. Kondekar, and M. T. McDowell (2016). "Mechano-Chemical Surface Modification with Cu2S: Inducing Superior Lubricity". In: *Tribology Letters* 64.2, p. 28.

Wan, Q., Y. Jin, P. Sun, and Y. Ding (2014). "Rheological and tribological behaviour of lubricating oils containing platelet MoS2 nanoparticles". In: *Journal of Nanoparticle Research* 16.5, p. 2386.

Wang, B., F. Qiu, G. C. Barber, Q. Zou, J. Wang, S. Guo, Y. Yuan, and Q. Jiang (2022). "Role of nano-sized materials as lubricant additives in friction and wear reduction: A review". In: *Wear* 490-491, p. 204206.

Wang, L., L. Wang, and G. Li (2013). "Analysis of engine oil containing MoDTC on the thermo-oxidation engine oil simulation test (TEOST 33C)". In: *Lecture Notes in Electrical Engineering*. Vol. 189 LNEE. VOL. 1, pp. 475–482.

Wang, Y. and Q. J. Wang (2013). "Stribeck Curves". In: *Encyclopedia of Tribology*. Springer, Boston, MA, pp. 3365–3370.

Wang, Y., Y. Du, J. Deng, and Z. Wang (2019). "Friction reduction of water based lubricant with highly dispersed functional MoS2 nanosheets". In: *Colloids and Surfaces A: Physicochemical and Engineering Aspects* 562, pp. 321–328.

Webster, G. A. and A. N. Ezeilo (2001). "Residual stress distributions and their influence on fatigue lifetimes". In: *International Journal of Fatigue* 23.SUPPL. 1, pp. 375–383.

Williams, D. B. and C. B. Carter (2009). "Scattering and Diffraction". In: *Transmission Electron Microscopy*. Springer, Boston, MA, pp. 23–38.

Wu, H., L. Qin, G. Dong, M. Hua, S. Yang, and J. Zhang (2017). "An investigation on the lubrication mechanism of MoS2 nano sheet in point contact: The manner of particle entering the contact area". In: *Tribology International* 107, pp. 48–55.

Wu, L., Y. Zhang, G. Yang, S. Zhang, L. Yu, and P. Zhang (2016). "Tribological properties of oleic acid-modified zinc oxide nanoparticles as the lubricant additive in poly-alpha olefin and diisooctyl sebacate base oils". In: *RSC Advances* 6.74, pp. 69836–69844.

Wu, X., K. Gong, G. Zhao, W. Lou, X. Wang, and W. Liu (2018). "MoS2/WS2 Quantum Dots as High-Performance Lubricant Additive in Polyalkylene Glycol for Steel/Steel Contact at Elevated Temperature". In: *Advanced Materials Interfaces* 5.1, p. 1700859.

Xie, H. M., B. Jiang, Q. H. Wang, X. S. Xia, and F. S. Pan (2016a). "Effects of combined additions of SiO2 and MoS2 nanoparticles as lubricant additive on the tribological properties of AZ31 magnesium alloy". In: *Science China Technological Sciences* 59.5, pp. 689–698.

Xie, H., B. Jiang, J. He, X. Xia, and F. Pan (2016b). "Lubrication performance of MoS2 and SiO2 nanoparticles as lubricant additives in magnesium alloy-steel contacts". In: *Tribology International* 93, pp. 63–70.

Xie, H., B. Jiang, X. Hu, C. Peng, H. Guo, and F. Pan (2017). "Synergistic effect of MoS2 and SiO2 nanoparticles as lubricant additives for magnesium alloy–steel contacts". In: *Nanomaterials* 7.7, p. 154.

Xu, Y., J. Geng, Y. Peng, Z. Liu, J. Yu, and X. Hu (2018). "Lubricating mechanism of Fe3O4@MoS2 core-shell nanocomposites as oil additives for steel/steel contact". In: *Tribology International* 121, pp. 241–251.

Xu, Y., Y. Peng, K. D. Dearn, X. Zheng, L. Yao, and X. Hu (2015). "Synergistic lubricating behaviors of graphene and MoS2 dispersed in esterified bio-oil for steel/steel contact". In: *Wear* 342-343, pp. 297–309.

Zhai, W., N. Srikanth, L. B. Kong, and K. Zhou (2017). *Carbon nanomaterials in tribology.*

Zhao, G., Q. Zhao, W. Li, X. Wang, and W. Liu (2014). "Tribological properties of nano-calcium borate as lithium grease additive". In: *Lubrication Science* 26.1, pp. 43–53.

Zhao, Y., Z. Geng, D. Li, L. Wang, Z. Lu, and G. Zhang (2021). "An investigation on the tribological properties of graphene and ZDDP as additives in PAO4 oil". In: *Diamond and Related Materials* 120, p. 108635.

Zheng, D., Z. bing Cai, M. xue Shen, Z. yang Li, and M. hao Zhu (2016). "Investigation of the tribology behaviour of the graphene nanosheets as oil additives on textured alloy cast iron surface". In: *Applied Surface Science* 387, pp. 66–75.

Zhmud, B. (2012). "Triboconditioning: In-manufacture running-in process for improving tribological properties of mechanical parts made of steel or cast iron". In: *Society of Tribologists and Lubrication Engineers Annual Meeting and Exhibition 2012*, pp. 353–360.

Zhmud, B., E. Tomanik, W. Grabon, D. Schorr, and B. Brodmann (2020). "Optimizing the Piston/Bore Tribology: The Role of Surface Specifications, Ring Pack, and Lubricant". In: *SAE Technical Papers*. 2020. SAE International.

Zhmud, B., E. Tomanik, and F. A. Xavier (2014). "Tribology, surface chemistry and morphology of WS2 tribofilms generated by the ANS triboconditioning process". In: *Lubrication Science*. Vol. 26. 5. Wiley-Blackwell, pp. 277–282.